



ARIC

**ATHEROSCLEROSIS RISK
IN COMMUNITIES STUDY**

Manual 6B

**Ultrasound Assessment: Ultrasound
Reading Procedures for Visit 2**

The National Heart, Lung, and Blood Institute
of the National Institutes of Health

ATHEROSCLEROSIS RISK IN COMMUNITIES STUDY PROTOCOL

Manual 6B

ULTRASOUND ASSESSMENT: ULTRASOUND READING PROCEDURES FOR VISIT 2

**For Copies, Please Contact
ARIC Coordinating Center
Suite 203, NCNB Plaza
137 E. Franklin St.
Chapel Hill, NC 27514**

Version 2.0: February, 1991

TABLE OF CONTENTS

1.	Introduction.....	1
2.	Summary of Data Flow Within the URC.....	1
3.	Reader Training and Monitoring.....	3
4.	Reader Work Station Instrumentation.....	3
4.1	General Description.....	3
4.2	Operation of Instrumentation.....	6
5.	Operation of the Reader Station.....	7
5.1	Equipment Start-up and Login.....	7
5.2	Transfer of Participant Files from Central Computer.....	7
5.3	The ARIC Image Measurement System.....	7
5.4	The Optical Disk Player Control Menu.....	8
5.5	The Calibration Frame.....	9
5.6	Measuring B-Mode Images.....	9
5.7	The ARIC Database Screen.....	11
5.8	Ending the Reading Session.....	12
6.	Reading of Ultrasonic B-Mode Images.....	13
6.1	Orientation to the Biosound B-Mode Image.....	13
6.2	Arterial Sites to be Examined.....	13
6.3	Definition of Important Tissue Interfaces Within the Normal Arterial Wall.....	18
6.4	Physical Principles of the B-Mode Image Formation.....	20
6.5	Identification of Principal Boundaries from the B-Mode Images.....	28
6.6	Calibration of Image Pixel Size.....	68
6.7	Selection of Image Frames.....	68
6.8	Placement of Crosshairs on Principal Boundaries.....	68
6.9	Subjective Comments on the B-Mode Image Frames.....	71
6.10	Procedure for Reporting Alert Values.....	71
7.	References	74
8.	Appendices	
	1. Reprints of Publications.....	A-1

LIST OF FIGURES

- 2.A Ultrasound Reading Center Flow Chart
- 4.2.3.A Front Panel of Computer
- 4.2.3.B Rear Panel of Computer
- 4.2.4.A Front Panel of Optical Disc Player
- 4.2.4.B Rear Panel of Optical Disc Player
- 6.1.A Geometry of the B-Mode Image
- 6.2.1.A Diagram of the Arterial Tree
- 6.2.1.B Simplified Diagrams of the B-mode Images to be Read
- 6.3.1.A Diagram of the Arterial Wall
- 6.4.A Idealized B-mode Image of a Single Boundary
- 6.4.B Idealized B-mode Image of Two Boundaries
- 6.4.C Idealized B-mode Image of Boundaries Simulating Arterial Walls
- 6.4.D Idealized B-mode Image of Boundaries Simulating Arterial Walls
- 6.5.A(1) B-mode Image of Right Common Carotid
- 6.5.A(2) B-mode Image of Right Common Carotid: Detail of B-Mode Image
- 6.5.B(1) B-mode Image of Right Common Carotid
- 6.5.B(2) B-mode Image of Right Common Carotid: Detail of B-Mode Image
- 6.5.C(1) B-mode Image of Right Common Carotid
- 6.5.C(2) B-mode Image of Right Common Carotid: Detail of B-Mode Image
- 6.5.D(1) B-mode Image of Right Common Carotid
- 6.5.D(2) B-mode Image of Right Common Carotid: Detail of B-Mode Image
- 6.5.E(1) B-mode Image of Right Common Carotid
- 6.5.E(2) B-mode Image of Right Common Carotid: Detail of B-Mode Image
- 6.5.F(1) B-mode Image of Right Common Carotid
- 6.5.F(2) B-mode Image of Right Common Carotid: Detail of B-Mode Image
- 6.5.G(1) B-mode Image of Right Common Carotid
- 6.5.G(2) B-mode Image of Right Common Carotid: Detail of B-Mode Image
- 6.5.H(1) B-mode Image of Right Internal Carotid
- 6.5.H(2) B-mode Image of Right Internal Carotid: Detail of B-Mode Image
- 6.5.I(1) B-mode Image of Left Common Carotid-Posterior
- 6.5.I(2) B-mode Image of Left Common Carotid-Posterior: Detail of B-Mode
Image
- 6.5.J(1) B-mode Image of Left Common Carotid-Optimal
- 6.5.J(2) B-mode Image of Left Common Carotid-Optimal: Detail of B-Mode
Image
- 6.5.K(1) B-mode Image of Left Carotid Bulb
- 6.5.K(2) B-mode Image of Left Carotid Bulb: Detail of B-Mode Image
- 6.5.L(1) B-mode Image of Left Carotid Bulb
- 6.5.L(2) B-mode Image of Left Carotid Bulb: Detail of B-Mode Image
- 6.5.M(1) B-mode Image of Left Internal Carotid
- 6.5.M(2) B-mode Image of Left Internal Carotid: Detail of B-Mode Image
- 6.6.A Biosound Calibration Frame for Determination of Image Pixel Size
- 6.8.A Placement of Crosshairs on B-mode Image Boundaries
- 6.9.A B-Mode Image Data Stored in Computer

1. INTRODUCTION

The participant data acquired at the ultrasound area work station within each ARIC field center are analyzed at a central reading facility located at the Ultrasound Reading Center (URC) in Winston-Salem, North Carolina. The data include B-mode images and arterial distensibility waveforms. The data are forwarded to the URC from each field center at weekly intervals in the form of 3/4" video cassette tapes and 5" floppy disks. After analyses, data summaries are sent from the URC to the ARIC Coordinating Center in Chapel Hill, North Carolina.

This protocol describes the detailed procedures used in reading the ultrasound B-mode images at the URC. Figures referred to in each section are numbered to correspond with sections in which they are cited.

2. SUMMARY OF DATA FLOW WITHIN THE URC

Data flow within the URC is summarized in Figure 2A. The video cassettes (VC) and floppy disks (FD) received from each of the four Field Centers are checked in upon their arrival at the URC, with verification of package contents. The video cassettes containing the participant ultrasound scans and the floppy disks containing participant identification information and arterial distensibility data are then logged into the computer.

When this has been completed, the floppy disks and the video cassettes are routed to the transcription station. Video cassette B-mode images are transcribed onto the optical disks which are used at the reading stations. Once the cassettes are transcribed, they are stored at the transcription station temporarily where they are readily accessible for additional viewing by the URC staff. Following temporary storage at the transcription station, the video cassettes are transferred to long-term storage.

Each optical disk can store 24,000 B-mode image frames. The number of participant studies on each disk to maintain daily availability to readers and to ensure that each reader receives approximately the same number of studies to read are regulated. Approximately one-half of the total space on each optical disk is used during the initial session at the transcription station. The disks are then sent to the reader station where they are read by an assigned reader. Once read, the optical disks are returned to the transcription station to store additional participant studies on the unused space of the disk. The disks are again sent to the reader station where the newly added material is read. Each optical disk cycles through the transcription station and the reader station twice. All ultrasound studies on the disk will have been read by this time, and the optical disks are then assigned to long-term storage.

On occasion it will be necessary to review data on a stored video cassette or optical disk. The cassettes, optical and floppy disks in long-term storage are available for review and can be checked out for additional studies by authorized personnel.

3. READER TRAINING AND MONITORING

All readers receive intensive training from the URC staff in order to become certified to perform ultrasound readings in ARIC. This training includes lectures and work station activities which cover the following topics: arterial anatomy, pathology of atherosclerosis, gross dissection (cadaver), acoustical physics, ultrasonic instrumentation, ultrasonic scanning, problems associated with B-mode image acquisition, common artifacts arising in B-mode images, operation of work station instrumentation, and detailed performance of the ultrasound reading protocol. Each reader establishes his own intra-observer reliability statistics to use as a baseline for assessing future performance by performing blinded repeat readings on randomly selected studies. Inter-observer statistics are also developed for the entire group of readers to determine achievable and acceptable criteria for certification. After completion of the training program, each reader is examined by a member of the URC staff to assess satisfactory performance of the reader protocol from the perspectives of proficiency and efficiency of performance.

Inter- and intra-observer measurement statistics are reviewed quarterly to monitor the performance of individual readers as well as the entire reader group. Trends suggesting a deterioration in performance levels are promptly discussed with the individuals concerned in order to correct deficiencies as soon as possible. Sustained high performance levels during the studies are recognized and commendation and incentives provided to the individuals involved.

4. READER WORK STATION INSTRUMENTATION

4.1 General Description

The instrumentation provided at each B-mode image analysis work station includes a personal computer (PC) (Leading Edge Model M, IBM-XT equivalent) with computer monitor, a frame grabber card, a color TV monitor and an optical disk player (ODP). The reader selects specific image frames from an optical disk provided by the chief reader and acquires these image frames using the PC. The detailed reader protocol for making measurements is completed on these frames, and a data file on each participant is stored on the 20 Mb hard disk of the PC. After participant data have been stored on the PC hard disk, these data are transmitted to the URC central computer for storage, analyses, and preparation of data summaries which are forwarded to the ARIC Coordinating Center in Chapel Hill.

4.2 Operation of Instrumentation

4.2.1 Color TV Monitor Cabling and Adjustments

The switch positions on the front control panel of the color TV monitor are as follows:

<u>Switch</u>	<u>Position</u>
Line A	Out
Line B	Out
VTR	Out
RGB	In
CMPTR	Out
Power	On

The BRIGHT and PICTURE controls are used to adjust image brightness during reading. Cable hook-ups for the color monitor are located in the rear.

<u>Color Coded Cable</u>	<u>Connector</u>	<u>Position 75 OHM</u>
Red	R	Up
Green	G	Up
Blue	B	Up
Black	Ext Sync	Up

4.2.2 Computer Monitor Cabling and Switches

The switches and controls located in the front and rear of the computer monitor are listed below with their correct settings.

<u>Located in Front</u>	<u>Correct Setting</u>
Power switch	ON
Color & brightness controls	adjusted to preference
<u>Located in Rear</u>	<u>Correct Setting</u>
Mode I/Mode II Switch	Mode II position
Input labeled "SIGNAL IN"	Large cable connects here

4.2.3 Computer Cabling

For a diagram and explanation, see figures 4.2.3.A and 4.2.3.B.

4.2.4 Optical Disc Player Control Panel and Rear Panel Terminals

For a diagram and explanation see figures 4.2.4.A and 4.2.4.B

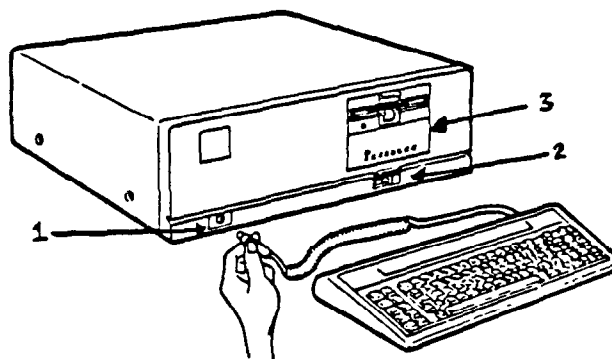
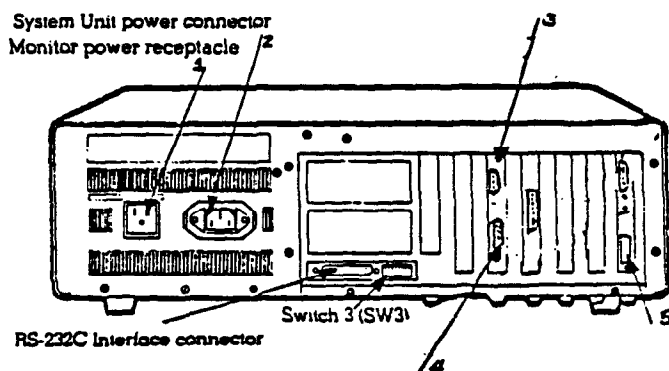


Figure 4.2.3.A - Front Panel of Computer

1. Keyboard connector - IN
2. Power switch - ON
3. Hard Drive

The figure below shows the switch and the possible connections you may have already present in your System Unit. Depending upon your selection of options, your rear panel may be configured in a different way.



1. Monitor cord - cables to large monitor
2. Power cord - to electric source
3. Targa Board Connector - cables to optical disc player allowing operator to "grab" frames to read
4. RGB (4 wire cable) - cables to back of large color monitor
5. Video Out - cables to small computer monitor and sends video signals out to be viewed on the small monitor

Figure 4.2.3.B Rear Panel of Computer

NOMENCLATURE AND FUNCTIONS of the CONTROL PANEL.

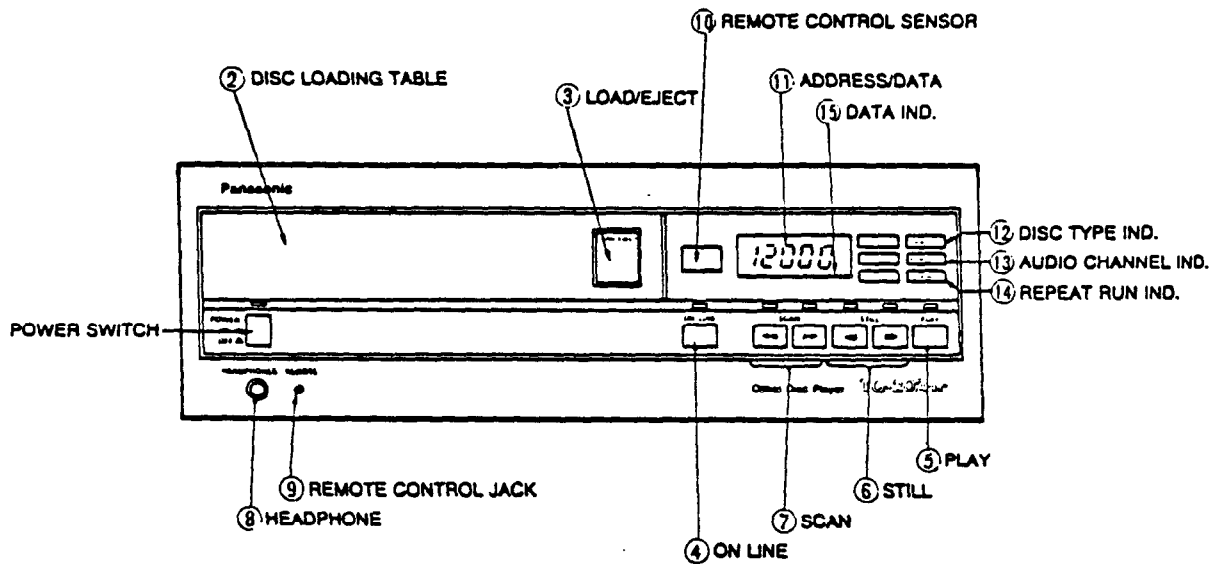


Figure 4.2.4.A - Front Panel of the Optical Disc Player

1. Power switch - DOWN
2. Load/Eject - located on drawer for disc
3. Play

REAR PANEL TERMINALS

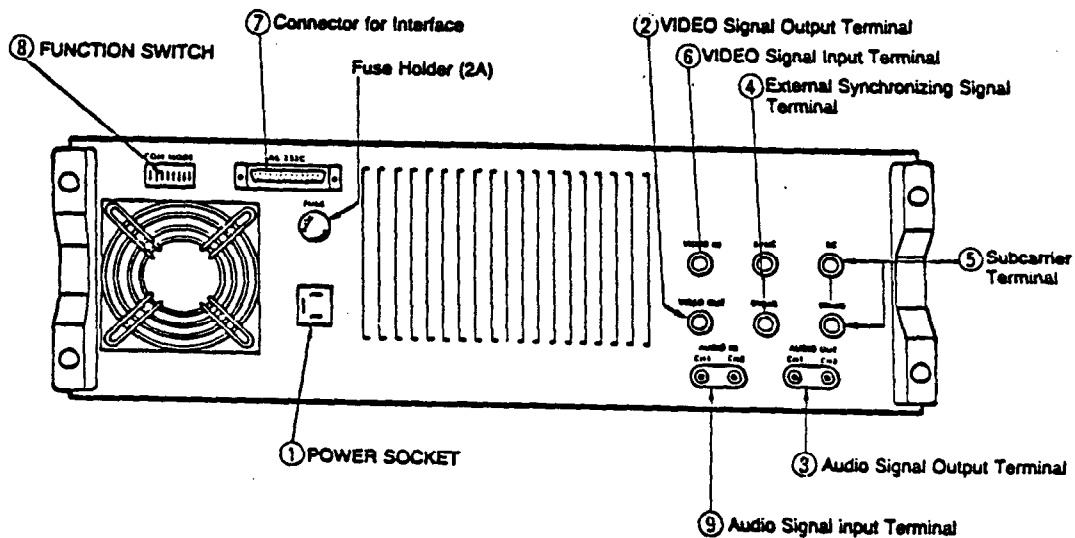


Figure 4.2.4.B - Rear Panel of the Optical Disc Player

1. Power Source - to electric source
2. Video Signal Output Terminal - cabled to Target Board on the computer

5. OPERATION OF THE READER STATION

5.1 EQUIPMENT START-UP AND LOGIN

1. Turn on the optical disk player (ODP), Sony TV monitor, computer monitor and computer in that order. Peripheral devices should be turned on first to prevent a power surge to the personal computer.
2. Follow the instructions on the computer monitor. Use either upper or lower case:
 - a) Type in the date: month-day-year <enter>. Example: "12-5-88".
 - b) Type the hours and minutes in military time <enter>. Add zeros when there is only one digit. Hours equal 24 per day: 7:30 a.m. is 07:30; 1:30 p.m. is 13:30. When figuring military time, add 12 to your hours after 12 Noon. The minutes are always 01-60 preceded by a colon.
3. Log-in with the central URC Computer:

The procedure for this step is on file at the Ultrasound Reading Center.

5.2 Transfer of Participant Files from the Central Computer

The reader obtains a study code sheet from the chief reader for each participant study that will be done during the reading session. The average number of participant studies read during a reading session is four; therefore, a reader would transfer at least four participant studies from the central computer to the reader station PC before beginning the reading session. The participant ID # is located in the upper right hand corner of the study code sheet.

The file transfer procedure is on file at the Ultrasound Reading Center.

Files do not have to be retrieved again from the central computer if readers do not read them that same day. They will remain on the computer's hard disk until the reader deletes them. They are deleted when the chief reader notifies the readers to do so.

5.3 The ARIC Image Measurement System

Access the ARIC image measurement system program as follows:

- a. At C> type CPS <enter> (Upper or lower case).
- b. The Main Menu appears.
- c. Move the highlighted box on the Main Menu with the arrow keys to ACQUIRE <enter>.
- d. Move the highlighted box on the Main Menu with the arrow keys to CAMERA <enter>.
- e. A blue screen will appear on the computer monitor with instructions to enter the participant number identifying the study to be read.

- f. Select a participant number from one of the study code sheets. Type in that six digit participant number excluding non-numeric characters and <enter>.
- g. The computer monitor will prompt the reader with the message, "Put optical disk#..... in optical disk holder.
- h. Carefully load the optical disk listed in this message. This disk contains B-mode images for the participant number chosen.
- i. When "DISK IN" message appears on the Sony TV monitor, <enter>.
- j. Wait for the ODP to initialize, at which time a B-mode image OR a calibration frame will appear on the Sony TV screen. <enter>.
- k. The Optical Disk Player Control Menu is present on the computer monitor.

5.4 The Optical Disk Player Control Menu

A brief explanation of each command follows:

NC: Move to the next study code.
 PC: Move to the previous study code.
 SR#: Return to a selected frame number.**
 FR#: Play forward from the present frame to a selected frame and then return to present frame.**
 TF: Move forward one frame.
 RETURN: By pressing the RETURN or <enter> key, any command on the command line will be repeated.

**NOTE: To use this command, a specific frame number must be entered.
 This frame number must be within limits of the selected study code.
 (EXAMPLE: SR1234 or FR2811)

The upper left corner displays the participant ID#. The left side of the menu displays each study code with its corresponding start and stop frames.

There will be three asterisks (***) beside the stop frame of the code which the optical disk player is presently displaying on the Sony TV screen. At the bottom of the screen is a rectangular box displaying a blinking cursor where menu commands are entered. On the right side of the screen is a list of optical disk player commands. Each time an "NC" and <enter> is typed at the blinking cursor, the three asterisks move down to the next study code, and the Sony TV monitor displays the first frame of that particular study code. The "NC" and <enter> command is used to move from study code to study code after each site has been read.

Movement through this menu with its commands allows the reader to view frames, choose frames to be captured, and to get an overall view of the study codes present on the participant scan.

5.5 The Calibration Frame

The calibration frame is usually the first frame measured. (See Figure 6.6.A). If a calibration frame is present on the participant study, and the asterisks are in place next to this calibration study code, do the following:

- a. Enter Q at the Optical Disk Player Control Menu blinking cursor command box <enter>.
- b. The calibration frame appears inside a colored border on the Sony TV monitor. It is "captured" by the computer and measurements can be made.
- c. The Main Menu is present on the computer monitor.
- d. Using the arrow keys, move the highlighted box to MEASURE <enter>.
- e. The Measurements Screen appears. Use any arrow key until POINT appears and is highlighted at AOI TYPE in the upper left corner and <enter>. The crosshair appears on the Sony TV image.
- f. "DO YOU WISH TO CALIBRATE" appears in the lower portion of the Measurements Screen. Answer Y and <enter>.
- g. To measure the calibration line, use the arrow keys to move the crosshair up or down, right or left until the vertical leg of the crosshair touches (1) the start of the calibration line; press <enter> and then (2) the end of the calibration line; press <enter>. The ODP Menu will return when the second crosshair is entered.

5.5.1 No Calibration Code

When a calibration code is not present, the first valid code listed on the ODP Control Menu will be a B-mode image, which will also be displayed on the Sony TV screen. Using the ODP Menu and the TF command, view the frames of the first study code, and choose the best systolic frame to be measured. (See Section 6.7). Do the following when the first site present is anything other than a calibration code.

- a. Enter Q to capture this frame; it will appear on the Sony TV monitor.
- b. The Main Menu is present on the computer monitor.
- c. Use the arrow key to move the highlighted box to MEASURE <enter>.
- d. The Measurements Screen appears. Use any arrow key until POINT appears and is highlighted at AOI TYPE in the upper left corner and <enter>. The crosshair appears on the Sony TV image.
- e. "DO YOU WISH TO CALIBRATE?" appears in the lower portion of the Measurements Screen. Answer N and <enter>. Proceed to measure the B-mode image.

5.6 Measuring B-Mode Images

5.6.1 Carotid Artery Study Codes

After choosing the best systolic frame for measuring, capture it by entering Q at the blinking cursor command box. If a command is already present in the command box, and if the cursor is in the first space at the command box, that command may be overwritten, and extra letters do not have to be deleted.

If this is the first code for this participant, the Main Menu appears on the computer monitor. See Section 5.5.1 for appropriate steps when no calibration code is present.

If a calibration code was present: when Q is entered, the Measurements Screen appears on the computer monitor, and the chosen frame with a crosshair appears inside a colored border on the Sony TV screen.

- a. "LOCATE AND ENTER CURSOR" appears at the bottom center of the Measurements Screen.
- b. When a cursor is present: using any arrow key to move left, right, up or down, move the crosshair to the point where the horizontal crossbar touches the cursor and <enter>.
- c. When a cursor is not present, or if in the reader's judgment it is placed in error: locate the appropriate anatomical reference for that study code and <enter>. (Section 6.5).
- d. Proceed to measure the boundaries, which can be measured in any order. Move the crosshair with the left or right arrow keys, taking care to place the center of the crosshair on the boundary edge, to the first boundary to be measured and <enter>. Each time <enter> is pressed, a crosshair remains at that site, and the X and Y coordinates for that boundary are registered in a temporary file. Another crosshair will appear 15 pixels up or down at the next Y coordinate.
- e. Move each crosshair with the left or right arrow keys along the selected boundary and <enter> at each measurement point until that interface can no longer be recognized. A maximum of 11 points are possible, and they may or may not be continuous.
- f. When eleven measurements on a boundary are registered, the crosshair automatically returns to the beginning measurement area. Press <F4> to register information for interface 2, <F5> for interface 3, <F6> for interface 4, or <F7> for interface 5.
- g. Measure the remaining three boundaries in a similar manner.
- h. Press <F9>, which brings up the ARIC DATABASE SCREEN on the computer monitor and stores measurements to the hard disk.

5.6.2 Measuring Study Codes with Unrecognizable Points

It is possible to measure a maximum of eleven points on each boundary. When the first of these possible eleven points is not recognizable, use the up or down arrow and, watching the Y coordinate measurement in the upper right hand corner of the computer monitor, move the crosshair 15 pixels. (This adds or subtracts a value of 15 to that number). Determine if a boundary can be measured at that point. If it can, measure it and <enter>. A crosshair remains at this point, and another crosshair appears 15 pixels down. Move along the interface and measure each recognizable boundary. (Step d. in Section 5.6.1).

5.6.2.1 The <Home> Key

If the first point was measured, but the second point is not measurable, use the <Home> key to move up or down to the next potential point. No crosshair remains at the second point, but a crosshair appears at this next potential

measuring point. If that point is recognizable, measure the boundary using the left or right arrow keys to move the crosshair, and <enter>. A crosshair remains at the measured point, and another crosshair appears 15 pixels above or below. If that point is not measurable, use the <Home> key; if it is measurable, measure it and use the <enter> key.

Continue to move along the boundary using either the <Home> key or the <enter> key until the interface can no longer be recognized. When all possible points are registered, the crosshair automatically returns to the beginning measurement area. Press <F4> to register information for interface 2, <F5> for interface 3, <F6> for interface 4, or <F7> for interface 5.

In some instances, all eleven sites may be unacceptable, and no points are measured. Press the appropriate "F" key for that boundary, and all measurements will be registered as "000". This can be qualified by viewing the printout of coordinates, which appear after the Comment Screen. (Section 5.7).

5.6.3 The <F8> Key

The <F8> key is used to escape the reading process after an image has been captured. It may ONLY be used before the measurements are stored to the hard disk using the <F9> key. Use the <F8> key:

- a. to choose a systolic frame other than the current captured frame;
- b. to look at arterial motion in other frames to determine a boundary location.

When the <F8> key is pressed, data for all boundaries that have been read on a chosen frame are erased. The reading process for that site MUST be started over, beginning with choosing a systolic frame and capturing that image (Refer to Section 5.6.1). When the <F8> key is pressed, the ODP Menu appears on the computer screen.

5.6.4 The Toggle Key

While measuring boundaries, crosshairs from previous measurements may interfere with your line of sight. Use the <F3> key to toggle previous crosshairs from your vision.

5.7 The ARIC Database Screen

The ARIC Database screen on the computer monitor is a list of questions concerning the frame which the reader has just read. Appropriate answers are entered with the keyboard. The last question asks if all the questions were answered correctly. If it is answered Y, these data are stored along with the coordinate data in the computer. If the last question is answered N, any information on the ARIC Database screen may be corrected. Shown below is the Database Screen.

ARIC DATABASE SCREEN

Reader Number
 Lesion? Y or N Shadow? Y or N
 Alert Value? Y or N
 Quality of Interfaces:
 Correct? Y or N

Explanation:

Alert Value - lumen diameter may be 2 mm or less
 Quality of each interface (A total of 4 must be entered).

- 0 - not readable
- 1 - poor
- 2 - fair
- 3 - good
- 4 - excellent

Upon completion of these questions, a printout of coordinates and responses appears for the current study code. Check for obvious errors, such as Lesion or Alert. If no measurements for any boundary were entered, check for "000" on that boundary. If anything is incorrect, the site must be read again. When the last question on this menu is answered Y, the Optical Disk Player Menu appears on the computer screen and the asterisks are still at the image just read. Type "NC", <enter> in the command box to move the asterisks to the next code to be read. View the frames in this code with the TF <enter> command to choose the best frame. Capture that frame, and make the appropriate measurements. The reading process will repeat until all sites are read.

5.8. Ending the Reading Session

After all sites have been successfully read, the reading session for one participant is complete. To end the reading session after each participant study:

- a. Enter Q at the command line on the ODP Menu and <enter>.
- b. Press <F1> several times until the C> prompt appears. (The Main Menu will appear before you come to the C> prompt.) Be certain to push ONLY the <F1> key and no others. If you hit any other key, you may erase the file you have created.
- c. Data on each participant should be sent to the central computer upon completion of the reading process.

5.8.1 Sending Data to the Central Computer

Computed readings are transferred to the URC central computer. The procedure for sending these completed readings is on file at the Ultrasound Reading Center.

5.8.2 Log Out

When reading is complete for the day, the reader logs off the central computer. This procedure is on file at the Ultrasound Reading Center.

Turn off computer, and then peripheral devices in order to prevent a power surge to the PC. Turning off the computer will also mean that you are logged out.

6. READING OF ULTRASONIC B-MODE IMAGES

6.1 Orientation to the Biosound B-Mode Image

The B-mode image appearing on the Biosound video screen shows a rectangular segment of the tissues at and below the skin surface having the dimensions shown in Fig. 6.1.A. The transducer in contact with the skin surface is located along the left side of the rectangle. Deeper structures are located at successively greater distances from left to right across the image. The deepest structures which can be imaged are located 4 cm from the skin surface. The width of the tissue segment visible is 2 cm.

6.2 Arterial Sites to be Examined

6.2.1 Introduction

B-mode images are obtained at three anatomical sites (the distal common, the bulb, and the internal carotid) in each of the left and right carotid arteries in the neck. Simplified diagrams of the anatomical sites and the various images which are obtained on each participant are shown in figures 6.2.1.A and 6.2.1.B.

When possible, each distal common carotid artery is scanned at three different transducer angles defined as follows:

1. Optimal Angle - orientation of transducer handle at which the two principal anatomical landmarks (the origin of the bulb and the most superior portion of the arc of the flow divider as shown in Fig. 6.2.1.A) are visualized. This angle is normally between 10-20 degrees above the horizontal in a supine subject.
2. Anterior angle - orientation of the transducer handle at 55 degrees above the horizontal.
3. Posterior angle - orientation of the transducer handle at 10 degrees below the horizontal.

6.2.2 Carotid Arteries (Frames 1-10 in Figure 6.2.1.B)

The right and left carotid arteries are located between the clavicle and the base of the skull on each side of the neck. The common carotid normally bifurcates (divides) into two arteries (the internal carotid and external carotid) at or near the level of the larynx.

6.2.2.1 The Right Common Carotid Artery (Frames 1-3 in Figure 6.2.1.B)

When the right common carotid image is obtained, the three transducer angles defined in Section 6.2.1 will be used to interrogate the vessel and obtain

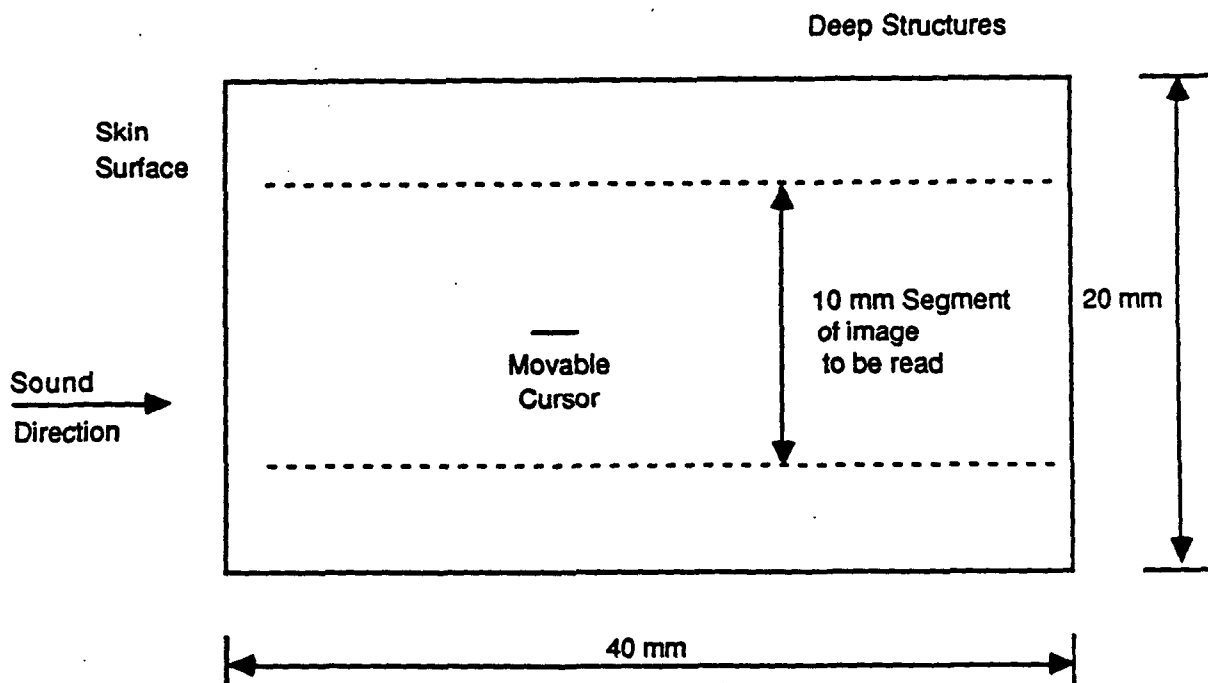


Figure 6.1.A Geometry of the B-Mode Image

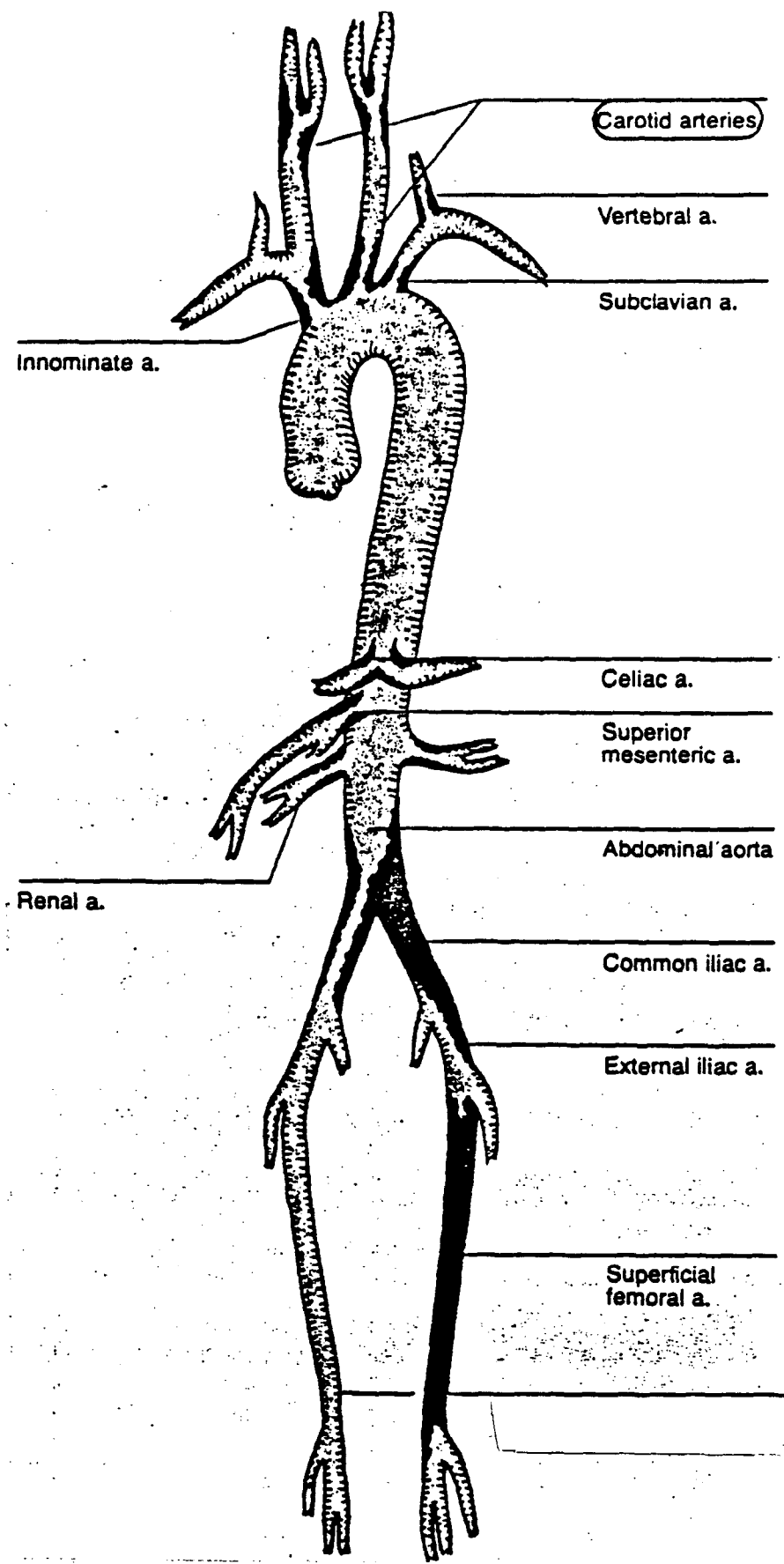


Figure 6.2.1.A Diagram of the Arterial Tree

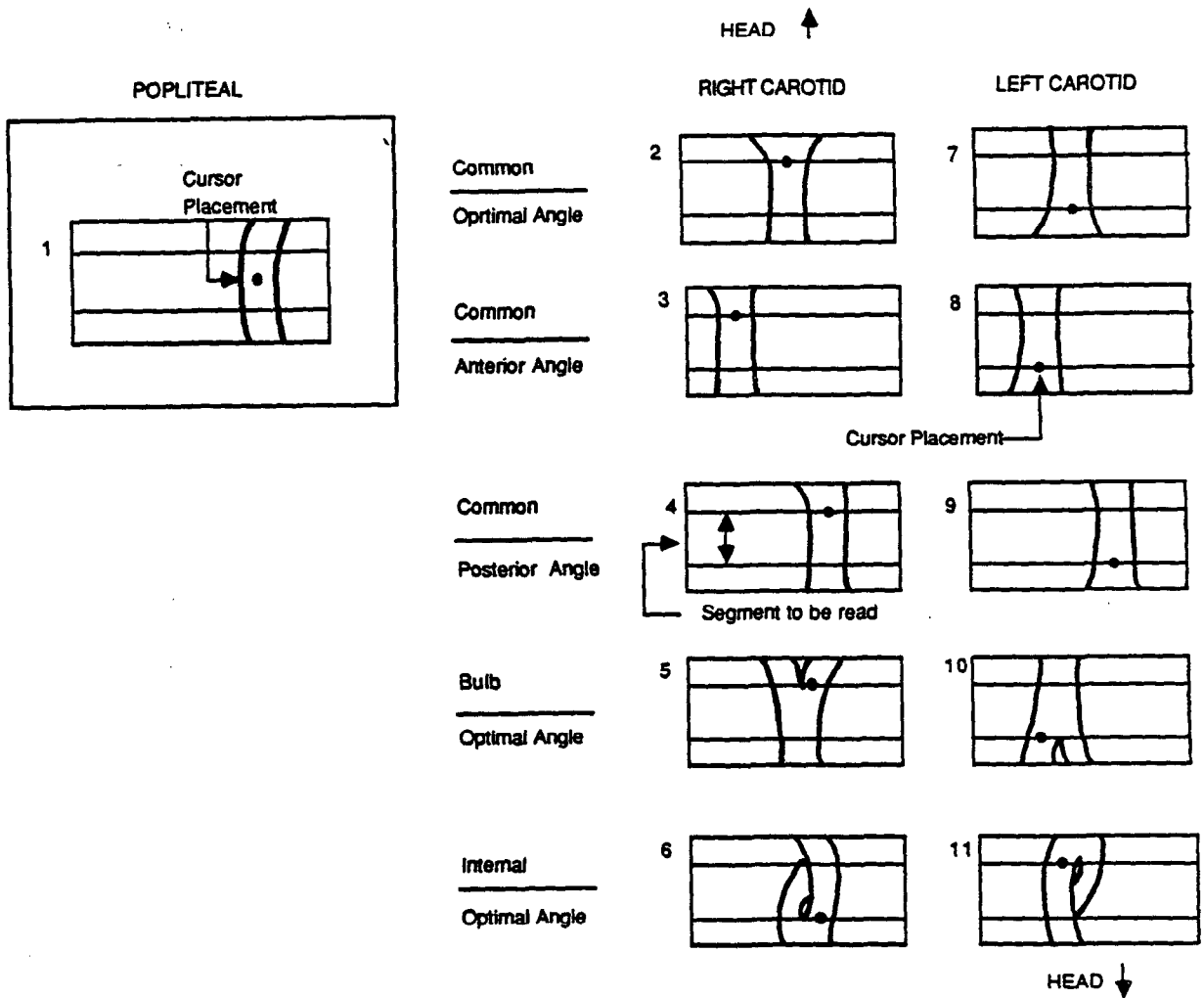


Figure 6.2.1.B Simplified Diagrams of the B-Mode Images to be Read

separate images. The origin of the crest of the bulb is the principal anatomical landmark to be identified. The cursor should always be placed at the level of the origin of the bulb by the sonographer who is able to define this point, even when the origin cannot be seen on the reader's image. Measurements are made on the 10mm segment of the common carotid artery immediately below this landmark on the image. This arterial segment is usually located between 2 cm and 3 cm below the skin surface and is generally shallowest when imaged from the anterior angle and deepest when imaged from the posterior angle.

6.2.2.2 The Right Carotid Artery Bulb (Frame 4 in Figure 6.2.1.B)

The next image acquired is that of the right carotid bulb, using only the optimal transducer angle. The superior arc of the flow divider separating the internal and external carotid arteries is the principal anatomical landmark to be identified in the image. The cursor should be located by the sonographer at this position in the image also. Measurements are made on the 10 mm segment of the bulb directly below this landmark on the image. The segment is generally located about 2cm - 3cm below the skin surface.

6.2.2.3 The Right Internal Carotid Artery (Frame 5 in Figure 6.2.1.B)

The next image acquired is that of the right internal carotid artery, using only the optimal transducer angle. The superior arc of the flow divider is again the principal anatomical landmark identified and marked with the cursor. Measurements will be made on the 10mm segment of the internal carotid directly above this landmark on the image. The segment is usually nearer to the skin surface than the external carotid and has a larger diameter.

6.2.2.4 The Right Carotid Artery Bulb - Far Wall Only (Frame 4 in Figure 6.2.1.B)

The next image acquired is that of the far wall only of the right carotid bulb. The method is identical to that described in 6.2.2.2 except that the primary objective is to acquire very high quality images of far wall boundaries only.

6.2.2.5 The Right Carotid Artery Bulb - Near Wall Only (Frame 4 in Figure 6.2.1.B)

The next image acquired is that of the near wall only of the right carotid bulb. The method is identical to that described in 6.2.2.2 except that the primary objective is to acquire very high quality images of the near wall boundaries only.

6.2.2.6 The Left Common Carotid Artery (Frames 7-9 in Figure 6.2.1.B)

The left common carotid is studied in a manner identical to that of the right common carotid. The image is inverted compared to the right side, with the participant's head located at the bottom of the image. Measurements are made on the 10 mm segment of the artery above the origin of the crest of the bulb, as seen on the image monitor.

6.2.2.7 The Left Carotid Artery Bulb (Frame 10 in Figure 6.2.1.B)

The left carotid bulb is studied in a manner identical to that of the right carotid bulb. Again, the image is inverted compared to the right side, with the participant's head located at the bottom of the image. Measurements are made on the 10 mm segment of the bulb directly above the origin of the flow divider as seen on the image monitor.

6.2.2.8 The Left Internal Carotid Artery (Frame 11 in Figure 6.2.1.B)

The left internal carotid artery is studied in a manner identical to that of the right internal carotid. This image is also inverted compared to the right side, as discussed in 6.2.2.4 and 6.2.2.5. Measurements are made on the 10 mm segment of the artery directly below the superior arc of the flow divider as seen on the image monitor.

6.2.2.9 The Left Carotid Artery Bulb - Far Wall Only (Frame 10 in Figure 6.2.1.B)

The next image acquired is that of the far wall only of the left carotid bulb. The method is identical to that described in 6.2.2.7 except that the primary objective is to acquire very high quality images of far wall boundaries only.

6.2.2.10 The Left Carotid Artery Bulb - Near Wall only (Frame 10 in Figure 6.2.1.B)

The next image acquired is that of the near wall only of the left carotid bulb. The method is identical to that described in 6.2.2.7 except that the primary objective is to acquire very high quality images of the near wall boundaries only.

6.3 Definition of Important Tissue Interfaces Within the Normal Arterial Wall

6.3.1 Tissue Layers Within the Normal Artery Wall

Three distinct anatomic layers are identified in the walls of normal arteries: the tunica intima, tunica media and tunica adventitia. A simplified diagram of these layers is shown in Fig. 6.3.1.A for a normal arterial wall.

The innermost of the three layers which is directly adjacent to the blood is the intima. In a normal artery, this is a relatively thin region measuring less than 0.10 mm. This is less than one-tenth of the total arterial wall thickness. With the development of lesions, this layer may expand greatly and become the thickest layer within the artery wall. Generally, over 90% of the normal intima plus media thickness is composed of the media. The media varies widely in thickness, depending on the arterial segment, and in composition, depending on whether the components are primarily characterized by elastic tissue, smooth muscle cells, or a combination of these tissues. With the development of lesions, the intima may involve the media and significantly modify its thickness and characteristics.

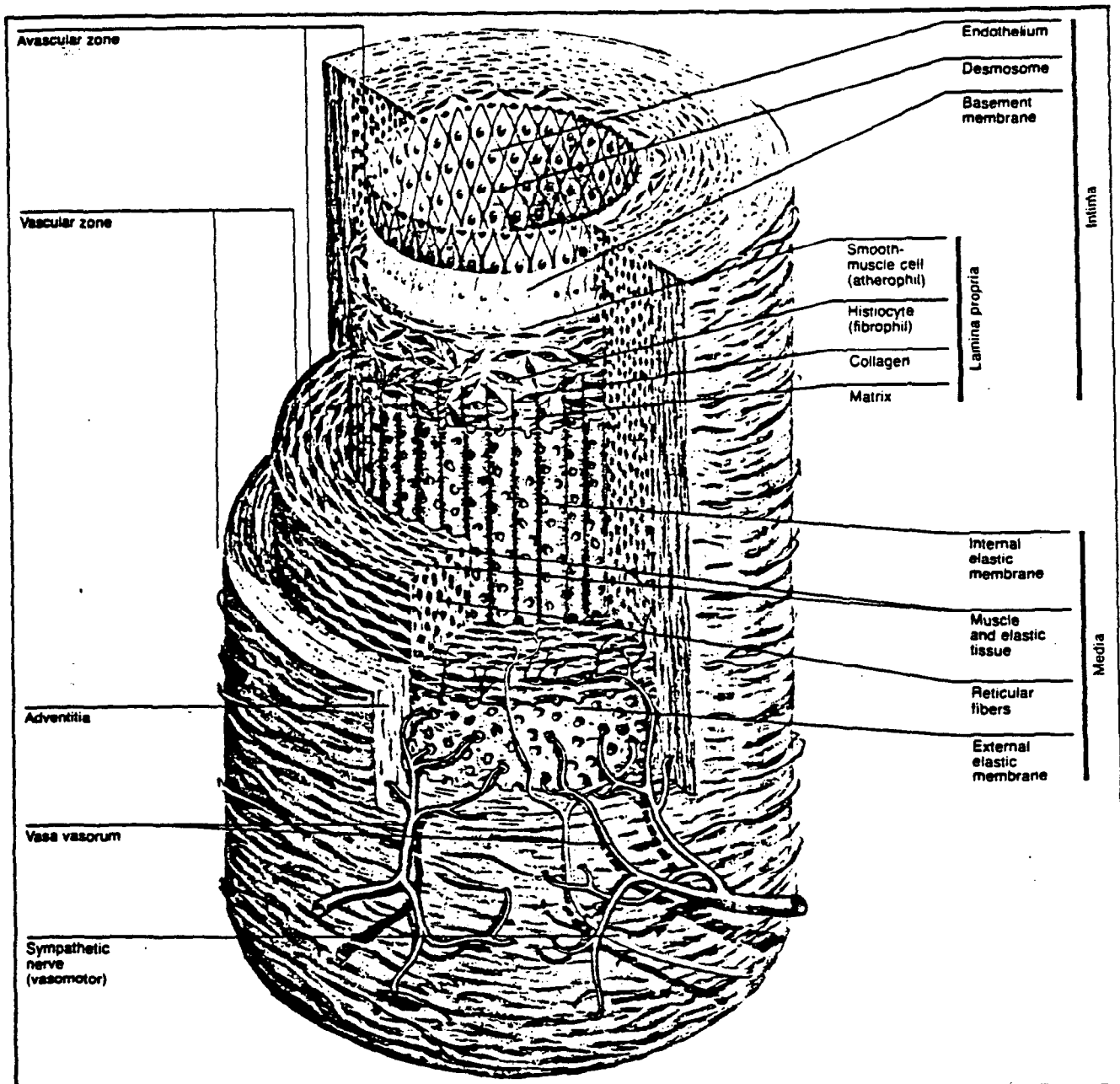


Figure 6.3.1.A Diagram of the Arterial Wall Layers

The outermost portion of the arterial wall is the adventitia. The adventitia begins at the outermost region of the media, defined anatomically as the external elastic lamina, and is composed principally of collagen, a dense form of connective tissue, with small nerve fibers, vessels and elastic fibers also being present. The thickness of the adventitia varies, depending on the particular artery segment and its location within the cardiovascular system. The outermost portion of the adventitia is bounded by periadventitial adipose tissue which may vary in thickness. It gradually merges into the surrounding tissue (periadventitial tissue). Its outer boundary is not generally well-defined. With severe disease present, plaque may protrude into and involve the adventitia.

6.3.2 Tissue Boundaries Associated With the Normal Artery Wall

The ARIC ultrasound study uses the four interfaces marked with a (*) below, that serve as boundaries and which are most easily identified in straight segments of longitudinal B-mode ultrasound arterial images. The overall goals of the ultrasound component of ARIC are the valid and reliable measurement of distances between these interfaces, including lumen diameter and (intima + media) thicknesses, as well as other linear and area measurements.

- 1 - Boundary between the periadventitia and adventitia of the near wall
- *2 - Boundary between the adventitia and media of the near wall
- *3 - Boundary between the intima of the near wall and the blood
- *4 - Boundary between blood and intima of the far wall
- *5 - Boundary between media and adventitia of the far wall
- 6 - Boundary between adventitia and periadventitia of the far wall

The following sections discuss procedures for identifying these boundaries from B-mode images and measuring their locations. Pay particular attention to the difference in the interpretation of boundary 2 relative to boundaries 3, 4 and 5, in terms of the physical principles involved in obtaining B-mode images of closely spaced interfaces.

6.4 Physical Principles of B-Mode Image Formation

6.4.1 The Pulse-Echo Principle

Ultrasonic B-mode images are obtained by sending out short, narrow bursts of acoustical energy and receiving echoes which arise from the environment. The energy is assumed to travel in a straight line until encountering a reflecting object. Echoes received are assumed to originate from reflectors located in a specific direction defined by the direction of the ultrasonic beam. After echoes arrive, the time between the transmission and reception is electronically measured and assumed to be proportional to the distance of the reflector from the source of the energy. Assuming an average sound velocity along the propagation path, an absolute distance to the target can be calculated. After converting the acoustical echoes into electrical signals, the amplitudes of these signals are used to modulate the brightness of an electron beam on a video display. This process produces an image of the plane through which the sound transducer scans. This image is referred to as a

B-mode (Brightness mode) image. Figures labeled with 6.5 (A-M) are examples of B-mode images.

6.4.2 The Origin of Echoes

Reflections originate, in general, whenever an acoustic wave passes from one material into another. If the mechanical properties (stiffness x mass density) of the two materials differ greatly, a strong reflection occurs at the boundary and only a small amount of energy passes through. If the mechanical properties are very similar, a very weak reflection occurs and most of the energy passes through. It is possible for rather different materials to have very similar mechanical properties so that the amplitude of the reflection is negligible. In such a case, a pulse-echo system would not detect the presence of the boundary. Consequently, B-mode images may fail to visualize certain boundaries located within the scan plane.

An optical analogy exists. When a first quality plate glass window is very clean, it is difficult to see its surfaces even when bright daylight is available to be reflected from these surfaces. This situation has on rare occasion resulted in a person injuring himself attempting to walk through such a plate. The mechanical properties of glass and air are very different but the factors producing optical reflection are such that the surfaces are invisible to the eye. Interpretation of anatomical information contained on B-mode images should be approached with a similar healthy skepticism.

6.4.3 Reflection From Smooth, Flat Boundaries

When a narrow beam of energy strikes a smooth flat boundary perpendicular to its path, it returns along the same path. In a pulse-echo imaging system, an echo is received from such a boundary, assuming that the mechanical properties across the boundary are sufficiently different. However, if the angle of incidence differs by only a few degrees from being perpendicular, the reflection may be missed. Consequently, the slightly oblique or curvilinear smooth boundary may not be seen on the image even though it is present.

6.4.4 Reflection From Rough Boundaries

When a ray of energy strikes a rough boundary from almost any direction, energy is scattered over a broad range of angles. Such a boundary is normally visualized on pulse-echo images since the source is likely to receive at least a small portion of the scattered energy. Rough boundaries are relatively insensitive to slight changes in ultrasonic propagation angle.

6.4.5 Imaging of Arterial Wall Boundaries

A boundary is located on a B-mode image as a dark to bright transition going from shallow to deep structures. This transition identifies the BEGINNING of the return echo and its position is relatively insensitive to the echo strength or instrument gain setting. The bright to dark transition at the end of the echo is determined by other factors including the echo strength and system gain settings. This is discussed in detail in section 6.4.8.

When sound is traveling from the center (lumen) of a normal artery outward through a wall, it passes through several principal boundaries: the blood-intima boundary; the intima-media boundary; the media-adventitia - boundary, and the adventitia-periadventitia boundary. In the absence of disease, the blood-intima boundary is rather smooth. Thus reflections are very angle dependent. In addition, the mechanical properties of the media are quite similar and the reflections are relatively weak. Consequently, it is not uncommon for the blood-intima boundary to be very faint or nearly invisible on pulse-echo images.

As the surface becomes irregular (rougher) due to disease development, the sensitivity to angle diminishes. Also, the mechanical properties of lesions may become significantly different from the blood and therefore result in larger amplitude echoes. Consequently, this boundary is more likely to be visible on the image after disease develops. Inability to visualize the boundary tends to suggest a normal artery if considerable effort has been made by the sonographer to visualize the boundary.

Since the normal intima is generally considerably thinner than 0.10 mm, the echoes from the blood-intima and intima-media interfaces tend to overlap when they are present. Consequently, the location of the intima-media boundary cannot usually be resolved in normal artery walls. As the intima thickens as a result of disease, the location of the intima-media boundary may be visualized. Generally this occurs when thickness is greater than 0.20 mm; although, should the mechanical properties of the intima and adjacent media be very similar, this interface may still not be seen.

The normal media in the carotid arteries is between 0.6-1.0 mm in thickness, and the media-adventitia boundary can generally be resolved with a high resolution ultrasound system. This boundary is usually rougher, produces strong reflections and is readily visualized on pulse-echo images.

The adventitial tissue is generally heterogeneous, containing collagen, nerve fibers, vessels, etc., and normally in the order of 0.2mm thick. Many relatively rough boundaries are present within this region and consequently the adventitia-periadventitia boundary may be difficult to resolve. Echoes from within the adventitia overlap echoes which arise at this boundary on the far wall. The location of the adventitia-periadventitia boundary can on occasion be estimated by observing the apparent end of the echoes arising from this interface and then subtracting an echo pulse length from it.

In summary, when imaging from the blood outward, i.e., far wall, in normal vessels, the normal blood-intima (boundary 4) and media-adventitia (boundary 5) interfaces are seen with clarity and are generally resolvable. The former is often nearly invisible in young, normal subjects, whereas the latter is usually seen. With the development of disease, both tend to be readily visualized.

If we now consider the boundaries encountered by a sound pulse as it enters an artery from the outside, we can expect the following differences. The periadventitia-adventitia interface on the near wall appears highly reflective, and therefore can on occasion be demonstrated in B-mode images

even when gain settings are relatively low. The easiest angle for reliably identifying this boundary is anterior. As the angle of interrogation becomes more lateral, the internal jugular vein is seen in front of the carotid artery, with the far wall of the vein adjacent to the near wall of the artery. When this vein-artery relationship is present, it is often difficult to reliably identify the arterial periadventitial-adventitial interface. Strong echoes from the adventitia tend to overlap the adventitia-media boundary. The boundary which is relatively easy to identify in the normal near wall is the media-intima interface. Because the normal intima is very thin, this is an excellent approximation of the intima-blood boundary. The media-intima boundary is again relatively smooth in the normal vessel and often invisible or nearly so due to a sensitivity to sound interrogation angle. Also, the mechanical properties across the boundary are similar, resulting in weak echoes.

One can get an estimate of the location of the adventitia-media boundary by observing the end of the echoes from this boundary and subtracting an approximate echo pulse length, although this depends on echo strength and system gain setting. As disease develops, and the intima thickens, it may be possible to see a rougher media-intima interface, and the actual intima-blood interface, if the echoes from within the intima are not particularly strong. With significant lesions present, a close estimate of the intima-blood boundary can be made by marking the end of the echoes from this boundary and again subtracting the echo duration.

In summary, when sound travels from outside to inside of the arterial wall, only the intima-lumen boundary (boundary 3) is well defined although it may often be invisible or nearly so due to similar mechanical properties across the boundary and sensitivity to angle. With disease, it is more readily seen and inability to visualize tends to suggest absence of disease. With significant disease, the intima-blood boundary may be approximated by identifying the bright-dark transition after this echo. Similarly, the adventitia-media boundary (boundary 2) may be approximated by identifying the correct bright-dark transition.

6.4.6 Effects of Arterial Geometry

6.4.6.1 Transverse Cross-Section.

The transverse cross-section of a vessel segment which is nonbranching is normally considered to be nearly circular. However, the high sensitivity to interrogation angle of boundaries 3 and 4 in B-mode images can result in a high frequency of invisible boundaries when opposite sides of the artery differ only a few degrees from being parallel. For example, if the blood-intima boundary on the far wall is visualized, there is a good chance that the intima-blood boundary on the near wall will be invisible and vice versa. Rough boundaries, such as the media-adventitia boundary on the far wall (boundary 5) and the adventitia-media boundary on the near wall (boundary 2), are relatively insensitive to these deviations from circular cross-section and are more often visualized.

6.4.6.2 Longitudinal Cross-Section (Curvature)

In a similar manner, if the artery curves within the scan plane, or bends outside of the scan plane, there may be only a small segment of (smooth-weak) boundaries which satisfy the sound angle requirement at one time. Consequently, unless a segment is very straight, only a small portion of a boundary such as the far wall blood-intima boundary will be visible. The rougher boundaries are not as sensitive to curvature, and are visualized more frequently.

6.4.7 Effects of Blood Flow and Respiration

Arterial geometry may be altered during both the cardiac and respiratory cycles by the regular changes in blood pressure during systole, diastole and respiration. Some interfaces may be visualized during part of the cardiac cycle and not at others, particularly smooth-straight-weak interfaces. Capturing such frames at systole or diastole must contend with these problems. Careful attention should be paid to wall motion in attempting to identify the several boundaries.

6.4.8 Simple Arterial Models

An ultrasonic B-mode image of an artery differs significantly from an optical image of the same vessel. A significant amount of artifact (false or misleading information) is present in the B-mode image, and a reader must be aware of the fundamental limitations inherent in interpreting such images. In this section, several simple idealized models are discussed to help identify some of these situations. Readers should also refer to recent papers entitled, "Artifacts in Ultrasound Imaging" by Dr. F. W. Kremkau and "Intimal plus medial thickness of the arterial wall: a direct measurement with ultrasound imaging" by Dr. P. Pignoli. Copies of these articles are included in Appendix II.

In Figure 6.4.A.(Real Boundary), a sound pulse traveling from left to right and encountering a single boundary is considered. If the acoustic impedances of the two media are different, an echo arises and is received by the sending transducer. In Figure 6.4.A.(High Gain), the appearance of this single boundary on the B-mode image is illustrated when the ultrasound system gain is high. A "literal" interpretation of this B-mode image would lead one to believe that a thin "layer" (the bright region) of material was present in the path of the ultrasound beam; however, in reality only one boundary is present. The apparent thin "layer" arises because of the finite time duration of the ultrasound pulse which is launched from the transducer. The apparent thickness of this "layer" has no physical relationship to the dimensions of the boundary. The real information presented in this image is the location of the boundary on the left side of the thin "layer".

In Figure 6.4.A.(Low Gain), the appearance of this single boundary model on a B-mode image is illustrated when the ultrasound system gain is low. Note that the thin "layer" is now less thick than in Figure 6.4.A.(High Gain). The left side, i.e. the location of the boundary, of this thin "layer" is essentially at the same location, whereas the right side has moved substantially,

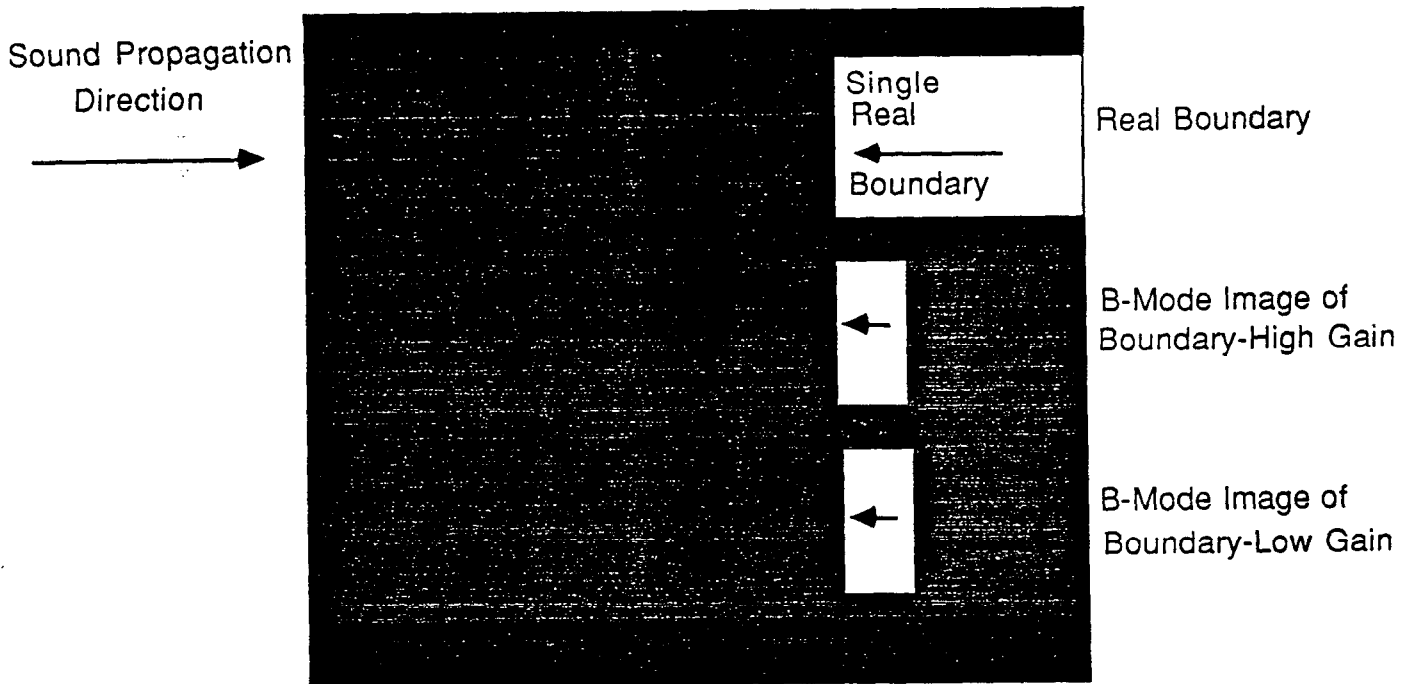


Figure 6.4.A Idealized B-mode Image of a Single Boundary

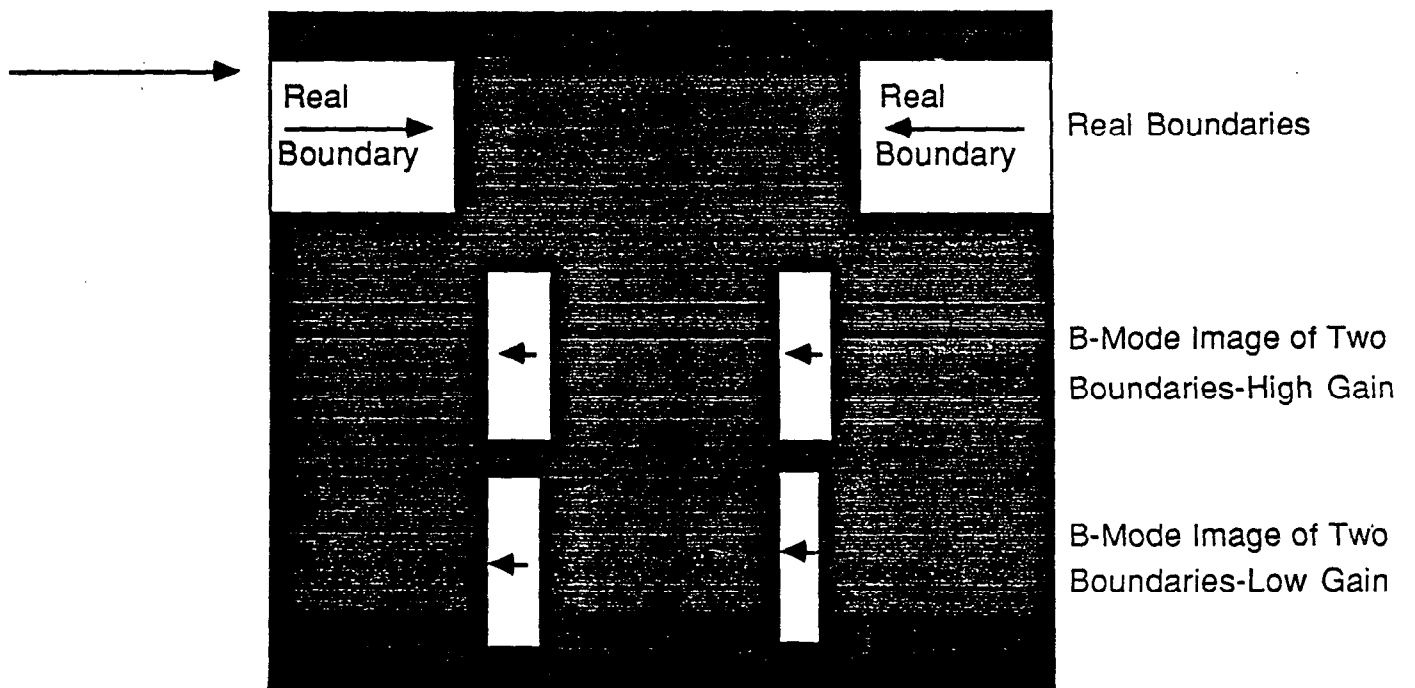


Figure 6.4.B Idealized B-mode Image of Two Boundaries

suggesting an apparent decrease in thickness of this boundary, when in fact, the boundary has not changed. Thus gain settings do affect the ultrasound echo duration significantly, but do not alter position of the left boundary in the B-mode image. Measurements made on the left side of a boundary are essentially gain (brightness) independent.

Figure 6.4.B. (Real Boundaries) shows a sound pulse again moving from left to right, now through two simple boundaries. With high gain setting, the B-mode image arising from each of these boundaries is shown in Figure 6.4.B. (High Gain). If the relative strength of the echoes at the two boundaries is different, the effective differences in pulse durations will make the corresponding thin "layers" appear to have different apparent thicknesses. To measure the distance between the boundaries on the B-mode image, the left side of each thin "layer" is located and the measurement of the distance is made between those two lines. As seen in Figure 6.4.B. (Low Gain), the distance between these two lines is essentially unchanged when the system gain is lowered even though the apparent thicknesses of the thin "layers" has been reduced. Consequently, separation distances between real boundaries measured from B-mode images are essentially independent of system gain.

In Figure 6.4.C. (Real Boundaries), two sets of three boundaries are shown to simulate a simple interface model of two normal "arterial walls" consisting of a relatively thick "media", a relatively thin "intima" and a homogeneous "adventitia".

With high gain, the corresponding B-mode image is shown in Figure 6.4.C. (High Gain). Note that the interfaces of the "intima" are so close that the pulse length of the ultrasound system prevents them from being resolved. The greater thickness of the dark region, i.e. "media", however, permits this region to be identified in this interface model of the left wall.

On the right wall, the distance between the "intimal" boundary and the "media-adventitia" boundary is clearly delineated, and the thickness defined by these interfaces is readily measured on this wall. When the gain is lowered, these two distances are not significantly altered as shown in Figure 6.4.C. (Low Gain).

If we add to this simple interface model a relatively homogeneous "adventitia", the boundary between the "adventitia" and "media" on the left wall is obscured by echoes arising within the "adventitia", adjacent to the "media" boundary. This is illustrated in Figure 6.4.D. When this occurs, direct measurements of the "media" thickness on the left side are no longer possible. The "intima plus media thickness" on the right side can however be measured as shown previously in Figure 6.4.C (Low Gain).

In general, echoes arising within the adventitial tissues are relatively strong and remain bright when the system gain (brightness) is dramatically reduced.

THE SPECIFIC BOUNDARIES, LABELED BY 2, 3, 4 and 5 ON FIGURE 6.4.D. (High Gain) ARE THE ONES TO BE IDENTIFIED AND MEASURED ON EACH OF THE IMAGE FRAMES SELECTED.

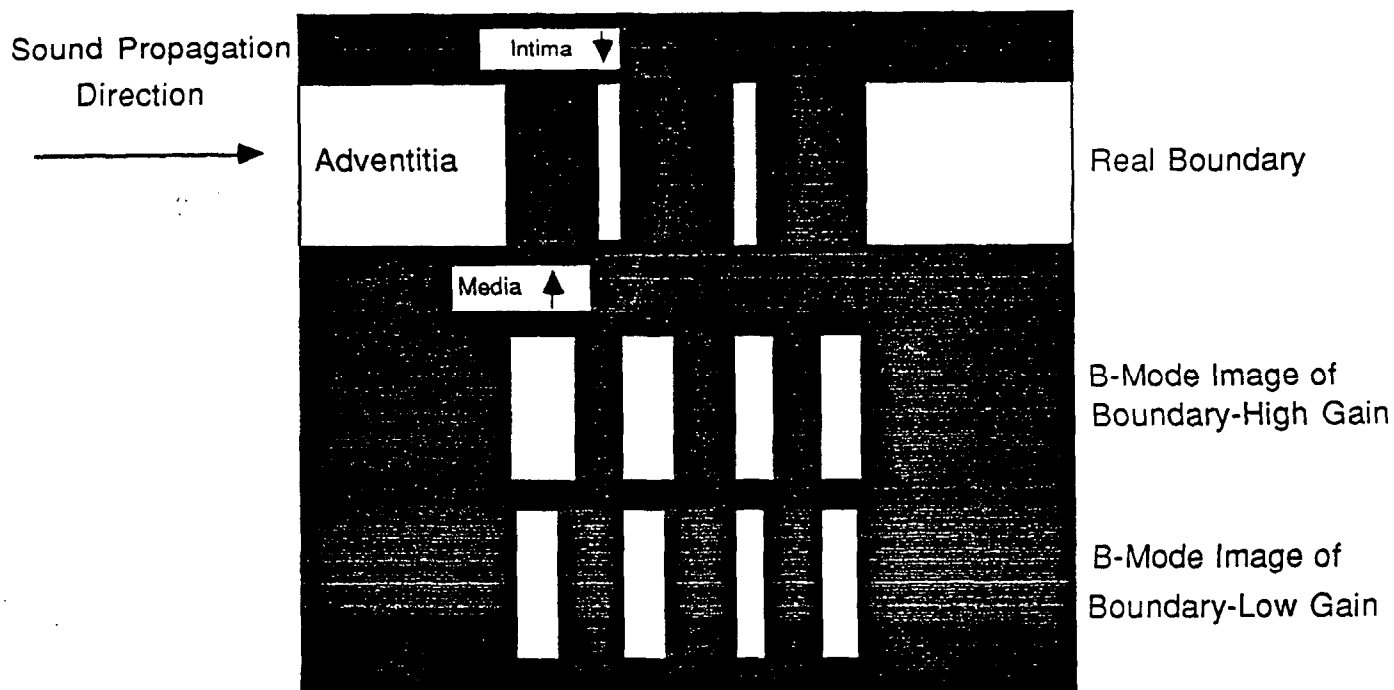


Figure 6.4.C Idealized B-mode Image of Boundaries Simulating Arterial Walls

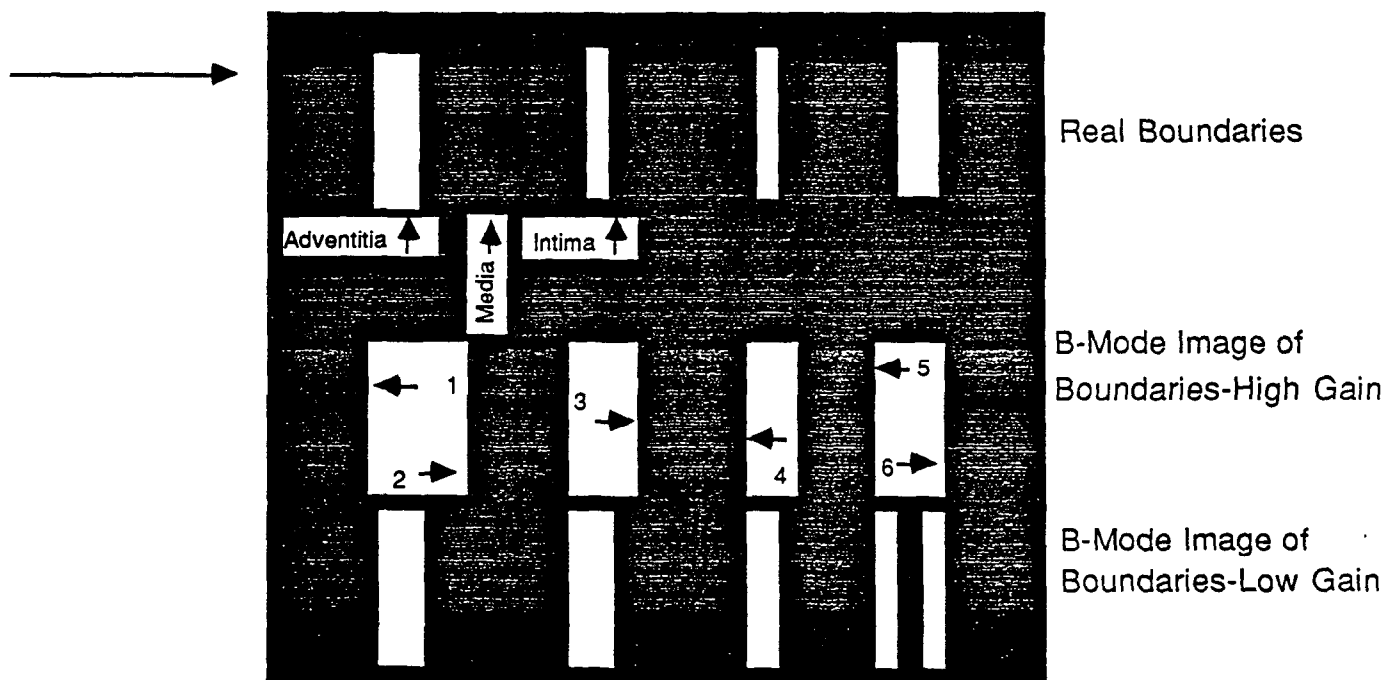


Figure 6.4.D Idealized B-mode Image of Boundaries Simulating Arterial Walls

Please note that while boundary 3 is actually located at the dark-to-bright (left side) transition of the echo shown, the bright-to-dark (right side) transition marked 3, permits a better determination of the near wall (intima plus media) thickness for a wide range of arterial conditions.

6.5 Identification of Principal Boundaries from the B-mode Images

Representative B-mode images of the carotid arteries are shown in the figures labeled by the section 6.5. (A-M). The location (or estimate) of each of the four boundaries (2,3,4 and 5) within the middle 10 mm of the image is sketched in the enlarged second image of each pair. This is the segment which is read and which has the least geometric image distortion.

Beginning readers should carefully study these figures before beginning the reading process. Particular attention should be paid to the identification of these boundaries when lesions are present. Wall motion is an important tool which should be routinely used to identify the important wall boundaries. Individual image frames recorded between diastole and systole should be carefully analyzed to clearly distinguish between vein wall and artery wall, to select the frame closest to systole and to identify artifacts which are clearly not associated with the principal boundaries being read. Images having unusual features (e.g. boundaries which are difficult to identify and possible artifacts) should be discussed with the chief reader before performing the measurements. If the reader deems it necessary, he/she may review the video cassette tape after reading an image.

6.5.1 Exercise for Reading B-Mode Image of Right Common Carotid:
Figures 6.5.A(1) and 6.5.A(2)

Site: Right Common Carotid Artery

Anterior Wall Depth: X = 1.2cm

Posterior Wall Depth: X = 2.2cm

Cursor: The cursor is correctly placed at $y = +0.3\text{cm}$. This is the origin of the bulb.

Anatomical Landmark: The origin of the bulb is clearly visible at $y = +0.3\text{cm}$. This is the correct vertical placement of the image since it positions the area of measurement in the vertical center of the screen.

Posterior Wall: B4 is clearly visible from $y = -0.3\text{cm}$ to $y = +0.1\text{cm}$ and then again at $y = +0.2\text{cm}$. This interface is fairly distinct and continuous except for the gap which appears between $y = +0.1\text{cm}$ and $y = +0.2\text{cm}$. B5 is also fairly distinct and continuous and is identified with relative confidence from $y = -0.8\text{cm}$ to $y = +0.3\text{cm}$. Although there are some diffuse echoes immediately to the left of B5, a "dark" to bright transition can be seen and indicates the location of B5. These diffuse echoes also indicate the presence of non-homogeneous tissue located within the media.

Anterior Wall: B3 is visible in the range of $y = -0.4\text{cm}$ to $y = +0.3\text{cm}$. Although it is not as smooth and distinct as B4, it can be identified with a fair amount of confidence. The bright to dark transition characteristic of B2 is clearly visible from $y = -0.6\text{cm}$ to $y = +0.3\text{cm}$ and B2 can be easily identified in this range.

Significant Artifact: There is an apparent gap in B4 located at approximately $y = +0.3\text{cm}$. This does not represent discontinuity of the interface but is an artifact which may be caused by a number of phenomena. For example the characteristics of this image suggests that the gap may be due to mild shadowing arising from strong reflectors or scatterers located on the anterior wall.

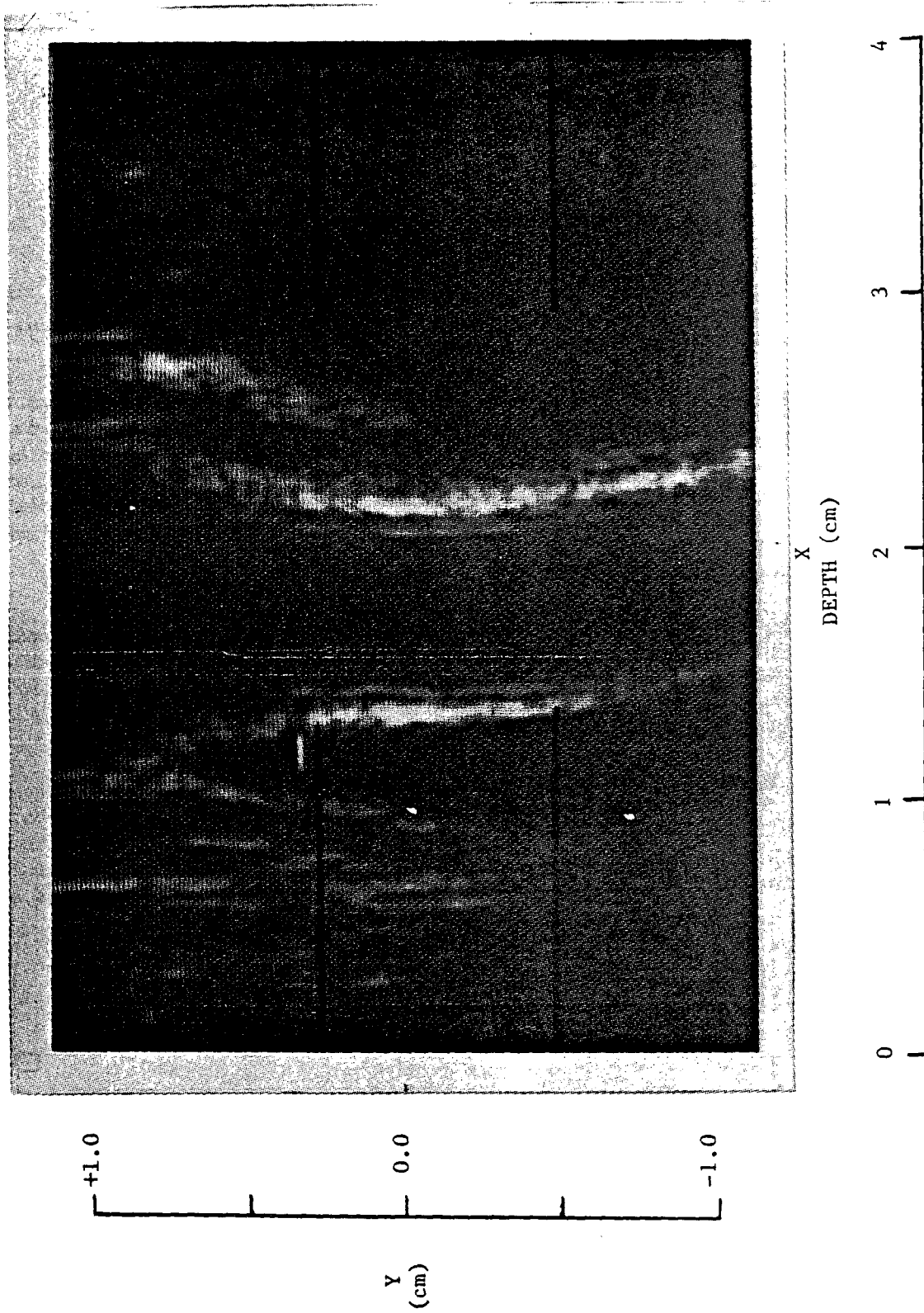
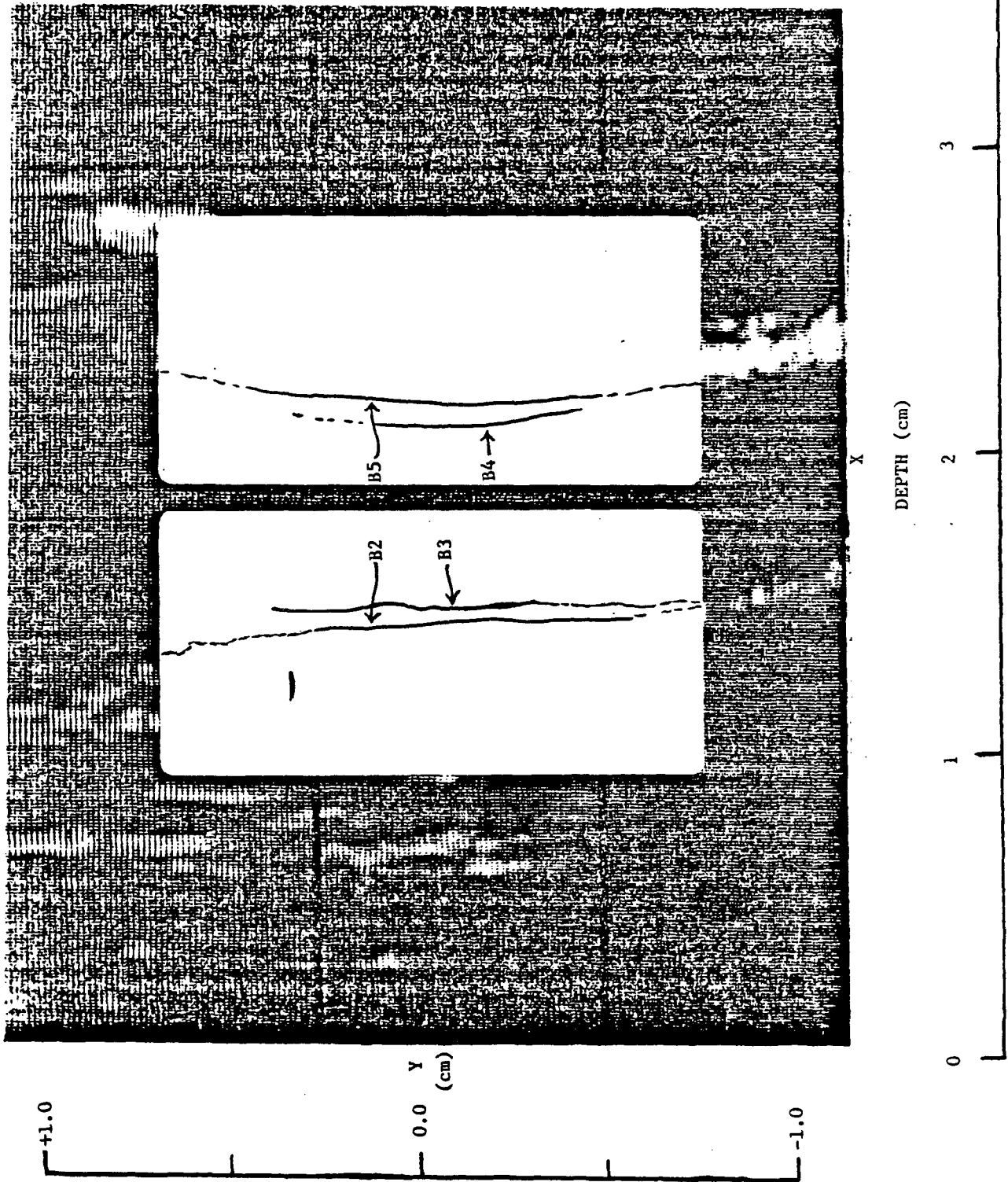


Figure 6.5.A(1) B-mode Image of Right Common Carotid

Figure 6.5.A(2) B-mode Image of Right Common Carotid: Detail of B-mode Image



6.5.2 Exercise for Reading B-Mode Image of Right Common Carotid:
Figures 6.5.B(1) and 6.5.B(2)

Site: Right Common Carotid Artery

Anterior Wall Depth: X = 1.4cm

Posterior Wall Depth: X = 2.7cm

Cursor: The cursor is correctly positioned at y = +0.4cm.

Anatomical Landmark: The origin of the bulb is visible in this image at the location of the cursor on the posterior wall. (The origin of the bulb can not be seen as well on the anterior wall.) The origin of the bulb is properly positioned so that the common carotid is in the middle third of the screen.

Posterior Wall: B5 is clearly visible from y = -1.0cm to y = +0.3cm. The thin, dark band to the left of B5 provides for a smooth, distinct interface, and measurements of this boundary can be made with relative confidence. B4 is also easily identified from y = -1.0cm to y = +0.3cm. This boundary is distinct and continuous, and measurements of B4 may confidently be made. In between B4 and B5 there appears to be some non-homogeneous structure which is producing echoes in this area. These echoes which appear within the media (which is most often echo-free) suggests that the instrument gain may have been relatively high. Another possibility is that the intima is beginning to thicken.

Anterior Wall: B2 is clearly visible from y = -1.0cm to y = +1.0cm, the entire length of the artery. This is a very good interface since rarely will a boundary be so clear and continuous. The absence of a dark band to the right of B2 makes it difficult to make confident measurements of B3. However, by turning down the monitor brightness B3 may be identified in the range from y = -1.0cm to y = -0.1cm. The most confident area of measurement would be at y = -0.2cm where B3 appears the brightest. The diffuse echoes which appear within the media in the lower half of the image are similar to those in the posterior wall media and may be explained in a like manner (for explanation see Posterior Wall).

Significant Artifact: B3 only appears in the lower half of the image which might suggest that there is no intima-lumen interface in the region above y = -0.1cm. B3 is probably in that portion of the artery even though it doesn't appear on the image. The "missing" interface may be the result of a slight artery curvature which would cause echoes to be bounced off the boundary in many different directions and missed by the signal receiving transducer.

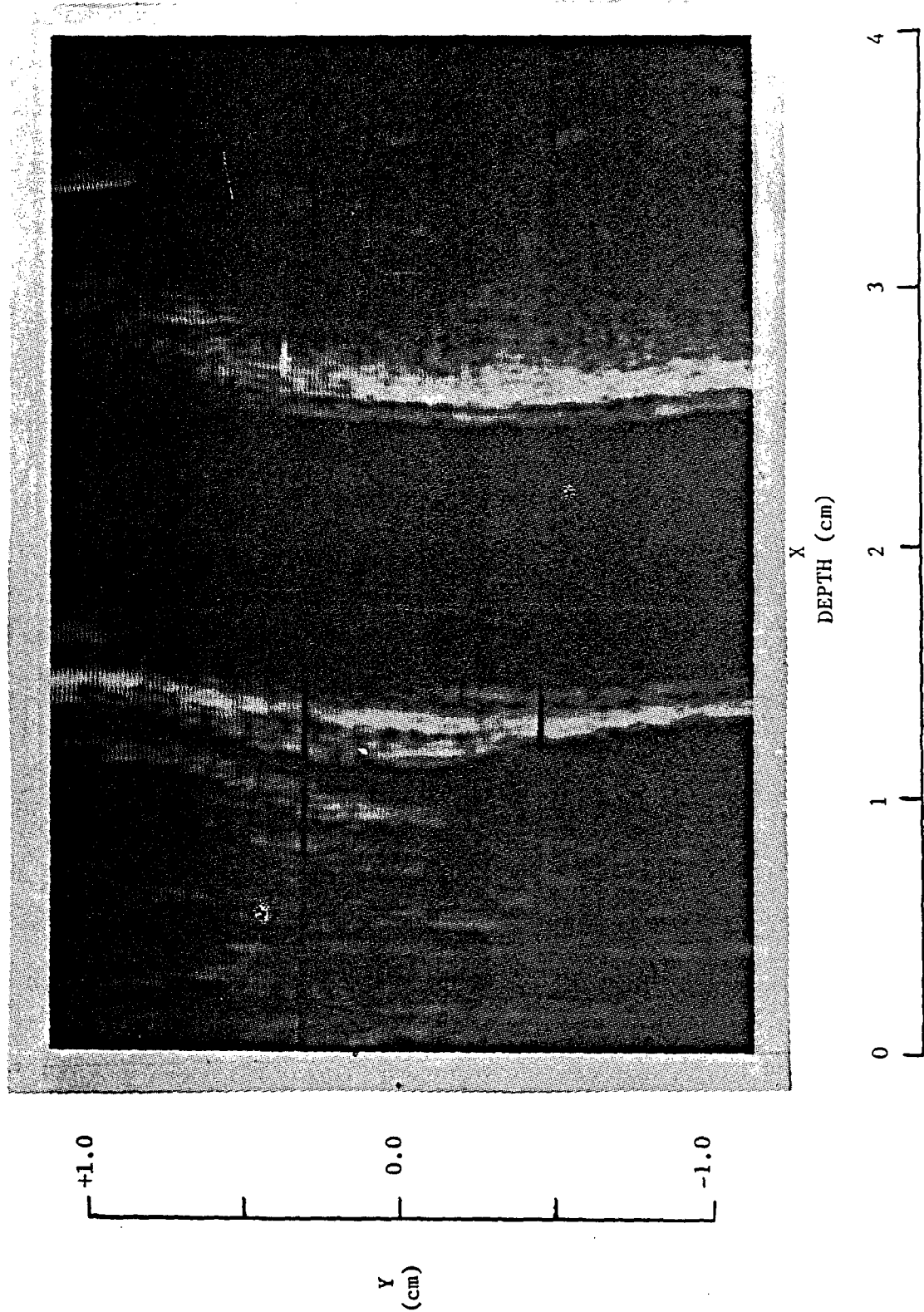
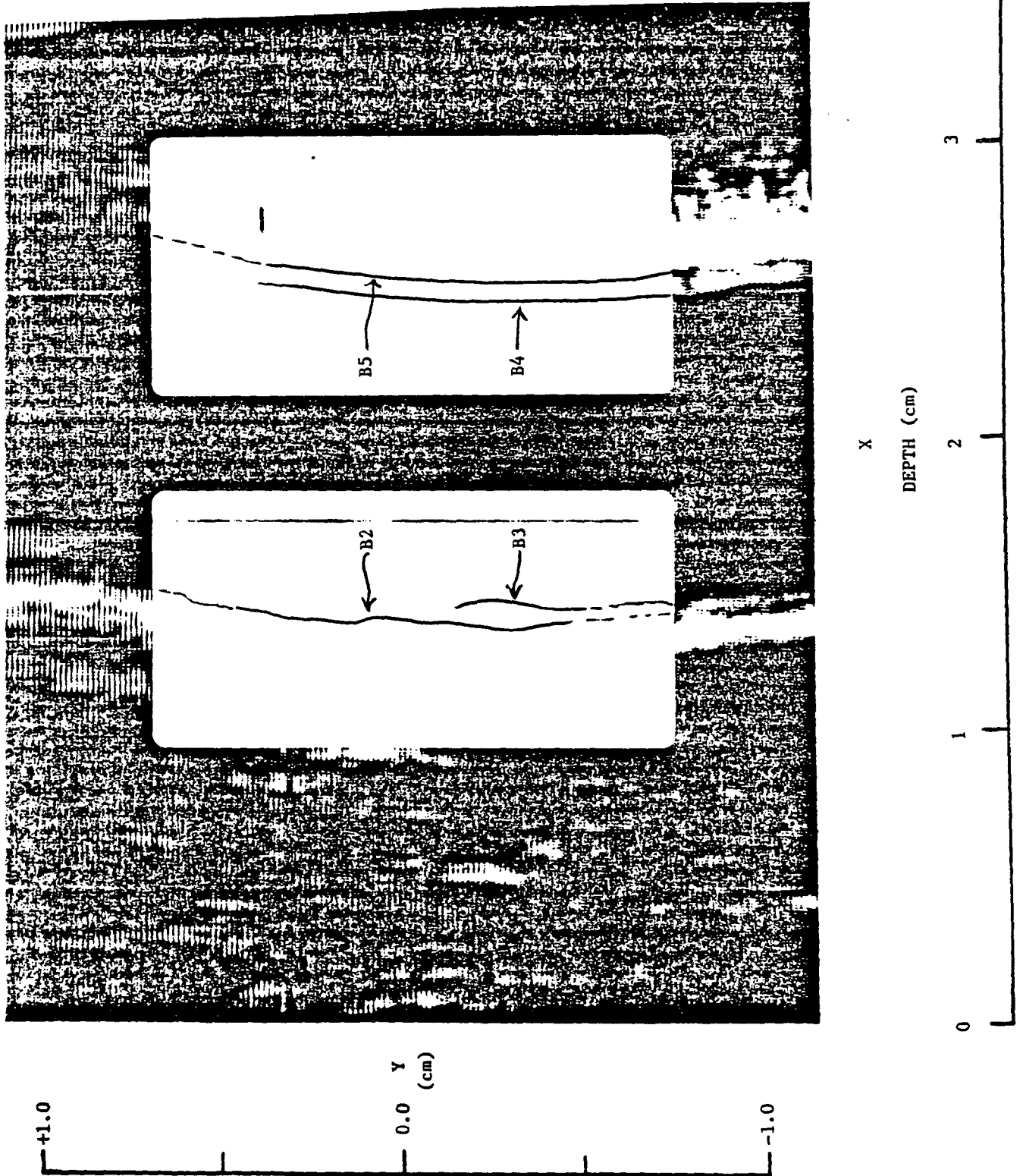


Figure 6.5.B(1) B-mode Image of Right Common Carotid

Figure 6.5.B(2) B-mode Image of Right Common Carotid: Detail of B-mode Image



6.5.3 Exercise for Reading B-Mode Image of Right Common Carotid:
Figures 6.5.C(1) and 6.5.C(2)

Site: Right Common Carotid Artery

Anterior Wall Depth: X = 1.0cm

Posterior Wall Depth: X = 2.2cm

Anatomical Landmark: The origin of the bulb is not easily identified on the image. It should have been placed adjacent to the cursor at $y = +0.5\text{cm}$.

Posterior Wall: Lesion appears to be present. B4 is clearly identifiable over $y = -0.5\text{cm}$ to $y = +0.5\text{cm}$. The lesion occupying the region to the right of B4 contains much speckle texture. B5 is preceded by a dark band from $y = -0.2\text{cm}$ to $y = +0.5\text{cm}$ and readily identified over this range. Reduction in brightness may help in identifying a more distinct dark to bright transition characteristic of B5.

Anterior Wall: B3 is not readily identifiable, probably due to improper alignment of the anterior wall with the ultrasound beam. B2 is fairly clear and should be marked with reduced brightness on the monitor. The structures appearing within the lumen are discussed below.

Significant Artifacts: The diffuse echoes appearing within the lumen to the right of B2 may be reflections from the lateral walls due to misalignment of the ultrasound or significant disease as suggested by the lesion on the posterior wall. Careful viewing of adjacent frames in the cardiac cycle is necessary to confirm an interpretation.

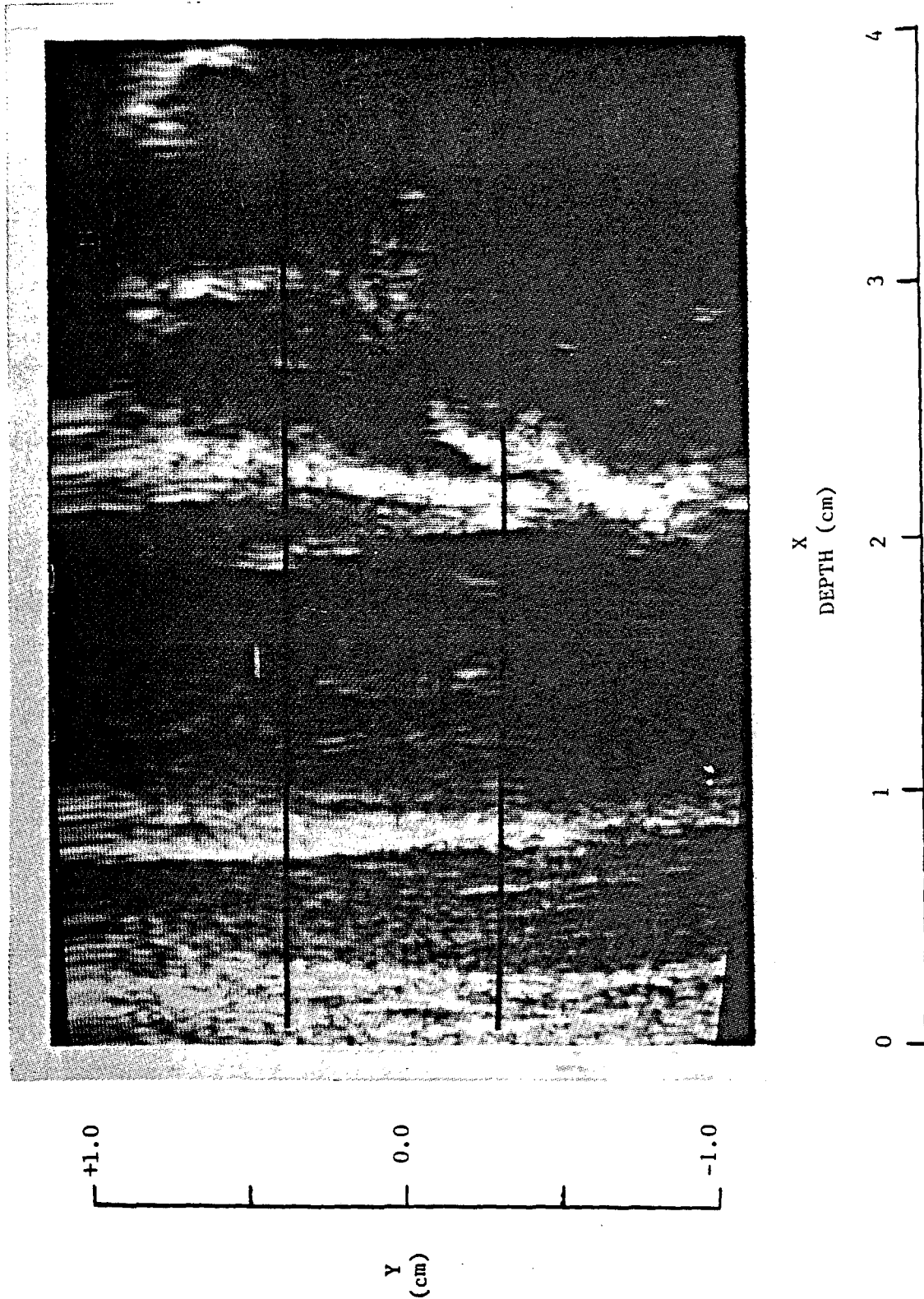
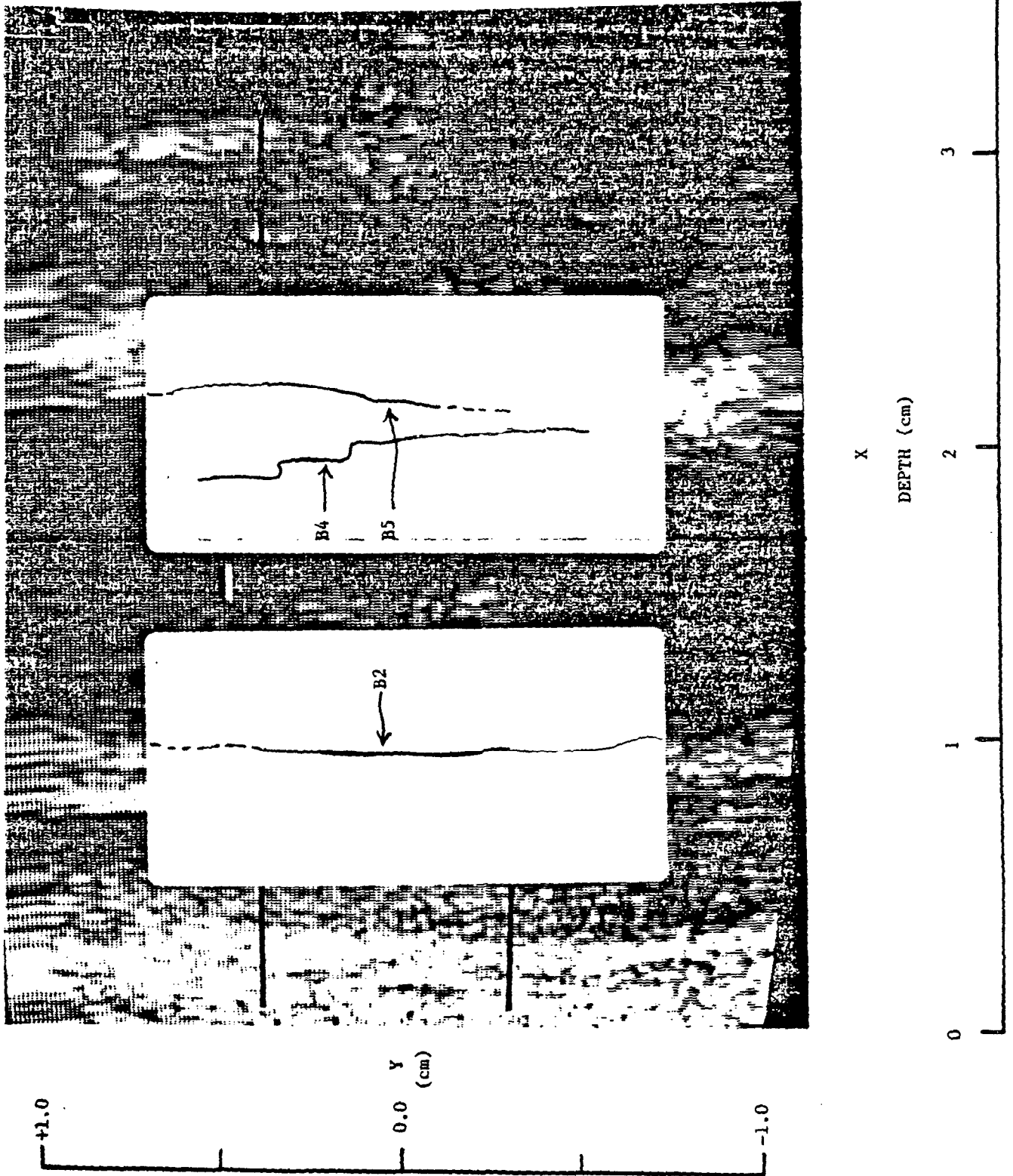


Figure 6.5.C(1) B-mode Image of Right Common Carotid

Figure 6.5.C(2) B-mode Image of Right Common Carotid: Detail of B-mode Image



6.5.4 Exercise for Reading B-Mode Image of Right Common Carotid:
Figures 6.5.D(1) and 6.5.D(2)

Site: Right Common Carotid Artery

Anterior Wall Depth: X = 1.5cm

Posterior Wall Depth: X = 2.8cm

Cursor: In this image the cursor is placed almost in the vertical center of the screen at X = 1.2cm. This is an incorrect placement. The cursor should be placed at the origin of the bulb which appears to be located at y = +0.3cm.

Anatomical Landmark: The origin of the bulb is visible and is located at approximately y = +0.3cm. This is an ideal vertical placement as it positions the area of measurement in the middle third of the screen.

Posterior Wall: B4 is identifiable from y = -0.1cm to y = +0.2cm and is fairly smooth and continuous except for the gap which is present in the middle third of the screen. B5 is not quite as smooth and distinct as B4 but can still be identified with relative confidence from y = -0.7cm to y = +0.3cm. Turning down monitor brightness can help in identifying a more distinct dark to bright transition characteristic of B5.

Anterior Wall: The anterior wall is not very clear, and the measurements taken there will not have a high quality rating. Because of the diffuse patches of echoes preceding B3 there is no dark, echo-free band, and identification of B3 and B2 is difficult. Nevertheless, B3 may be identified in two regions along the anterior wall from y = -1.0cm to y = -0.3cm and from y = +0.2cm to y = +0.4cm. There is a slightly visible bright to "dark" transition in the area of B2, thus this boundary may be identified from y = -1.0cm to y = +0.7cm. Lowering of the monitor brightness may eliminate a significant amount of the diffuse echoes between B2 and B3 and make identification of these interfaces easier.

Significant Artifact: Speckle adds apparent texture to both walls, particularly the posterior wall in the area of B5. The "gap" in B4 is either a result of transducer misalignment or shadowing from strong reflectors on the anterior wall. The echoes in the region between B2 and B3 seem to indicate heterogeneous tissue in the media, however, the echoes are probably the result of ultrasound beam-arterial wall misalignment.

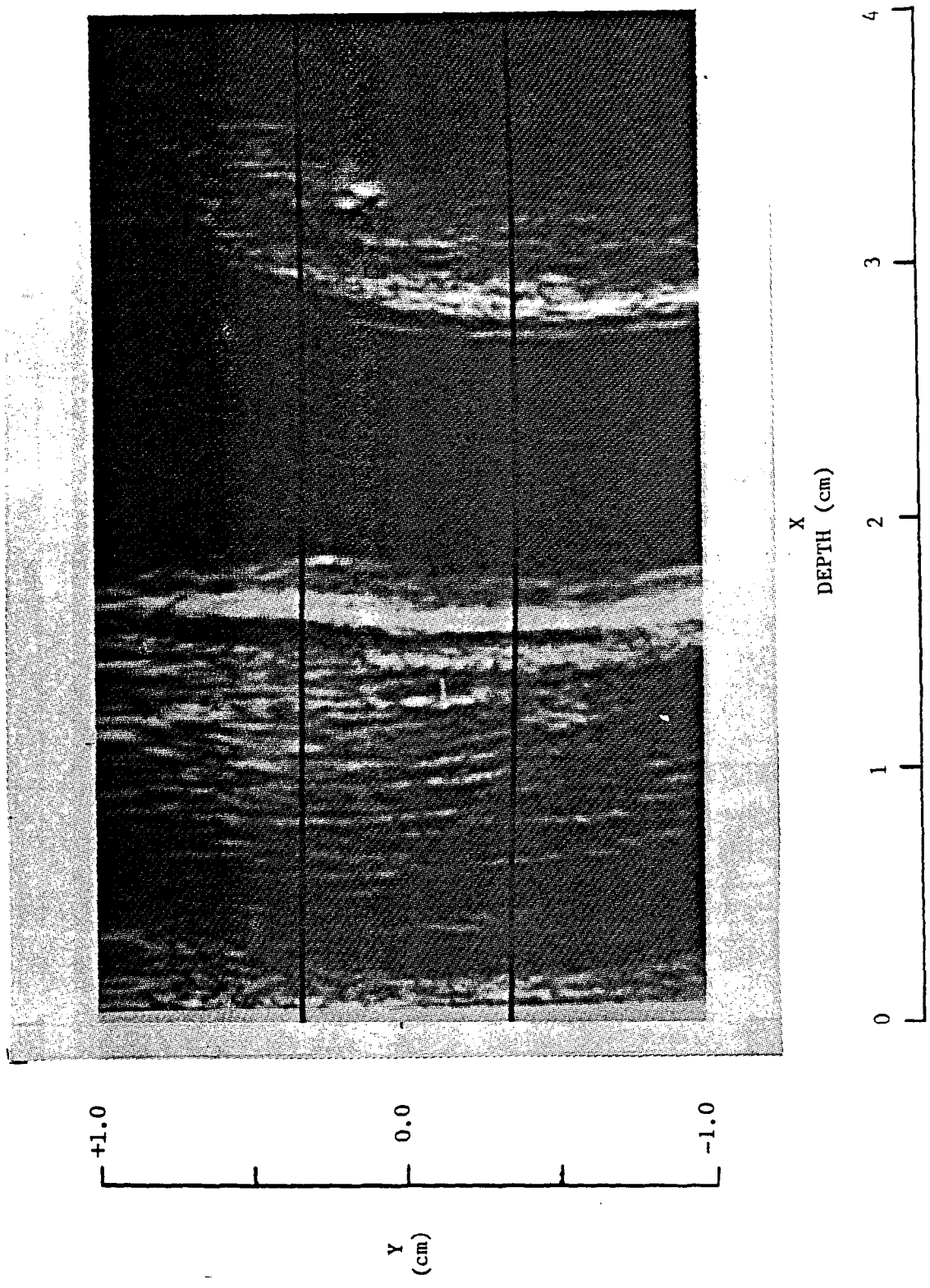
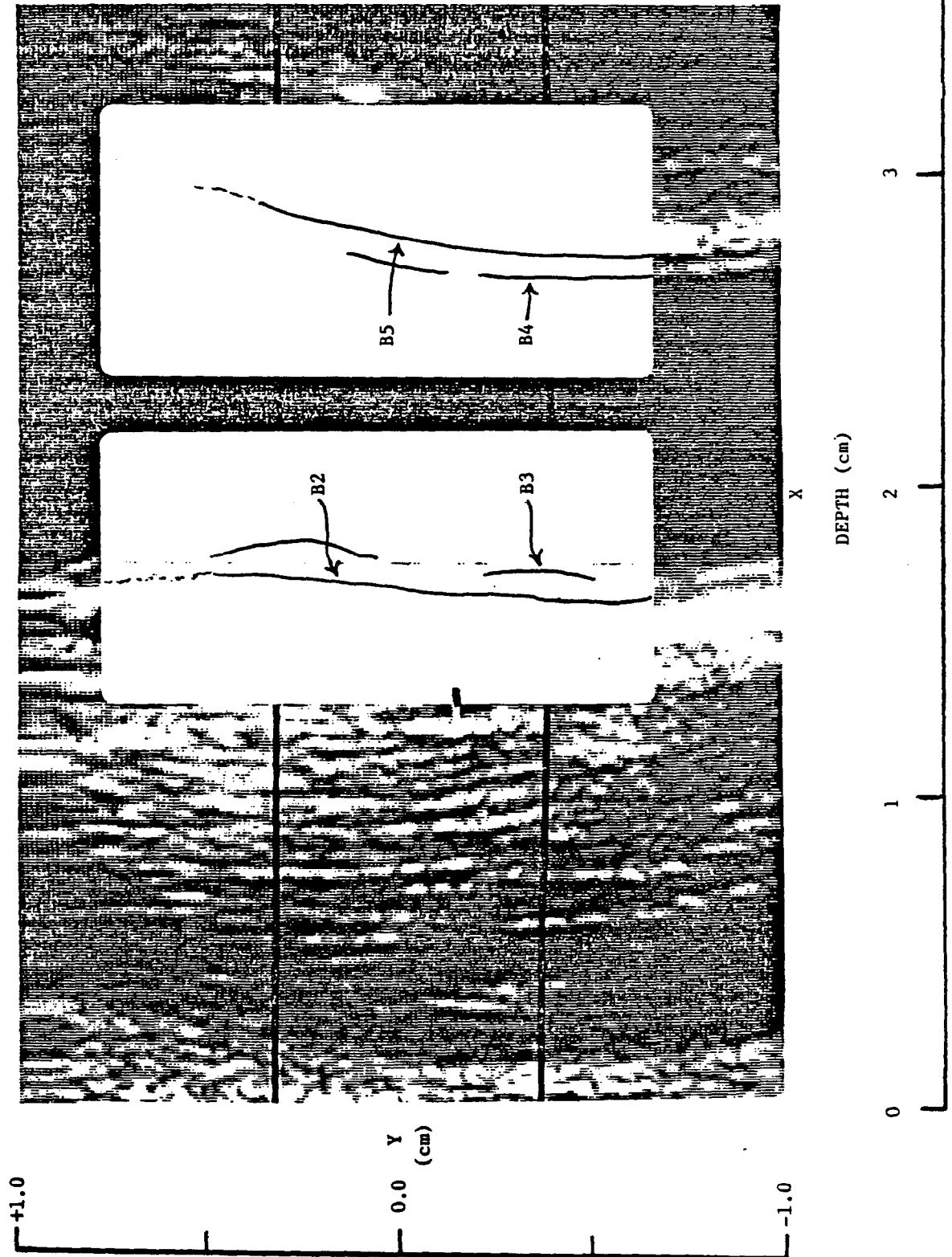


Figure 6.5.D(1) B-mode Image of Right Common Carotid

Figure 6.5.D(2) B-mode Image of Right Common Carotid: Detail of B-mode Image



6.5.5 Exercise for Reading B-Mode Image of Right Common Carotid:
Figures 6.5.E(1) and 6.5.E(2)

Site: Right Common Carotid Artery

Anterior Wall Depth: X = 2.0cm

Posterior Wall Depth: X = 2.9cm

Cursor: Improperly placed. It should be located at the origin of the bulb located at $y = +0.5\text{cm}$.

Anatomical Landmark: The origin of the bulb is located at $y = +0.5\text{cm}$. This is the proper vertical screen placement.

Posterior Wall: B4 can be easily identified from $y = -0.5\text{cm}$ to $y = 0.0\text{cm}$. There is a smooth, distinct dark to bright transition in these ranges. In the interval from $y = 0.0\text{cm}$ to $y = +0.4\text{cm}$ the dark to bright transition is not as distinct. In this range B4 appears to have a few gaps in it; however, measurements could still be made with a fair confidence. Along the interval $y = -0.2\text{cm}$ to $y = +0.4\text{cm}$, B5 is easily identified by the continuous dark band following B4 and the distinct dark to bright transition.

Anterior Wall: B3 can be identified from $y = -0.5\text{cm}$ to $y = 0.0\text{cm}$. Along this interval, there are diffuse bright patches within the dark band preceding B3, but this interface may be identified with confidence by lowering the monitor gain. B3 may be identified along the interval $y = 0.0\text{cm}$ to $y = +0.3\text{cm}$, although the dark to bright transition is not as distinct. B2 can be identified from $y = -0.5\text{cm}$ to $y = +0.8\text{cm}$ with a fair amount of confidence and with the aid of low gain. Although the bright to dark transition in this range is not as distinct, it is adequately visible.

Significant Artifact: The diffuse patches within the lumen from X = 2.0cm to X = 2.5cm are the result of reverberations from the bright reflectors to the left of this area. The apparent gaps in B4 at $y = 0.0\text{cm}$ to $y = +0.4\text{cm}$ probably do not represent actual "holes" in the interface but are probably the result of a misaligned transducer. Gain settings could be considerably lower and if so, would probably reduce the multiple reverberations present within the lumen.

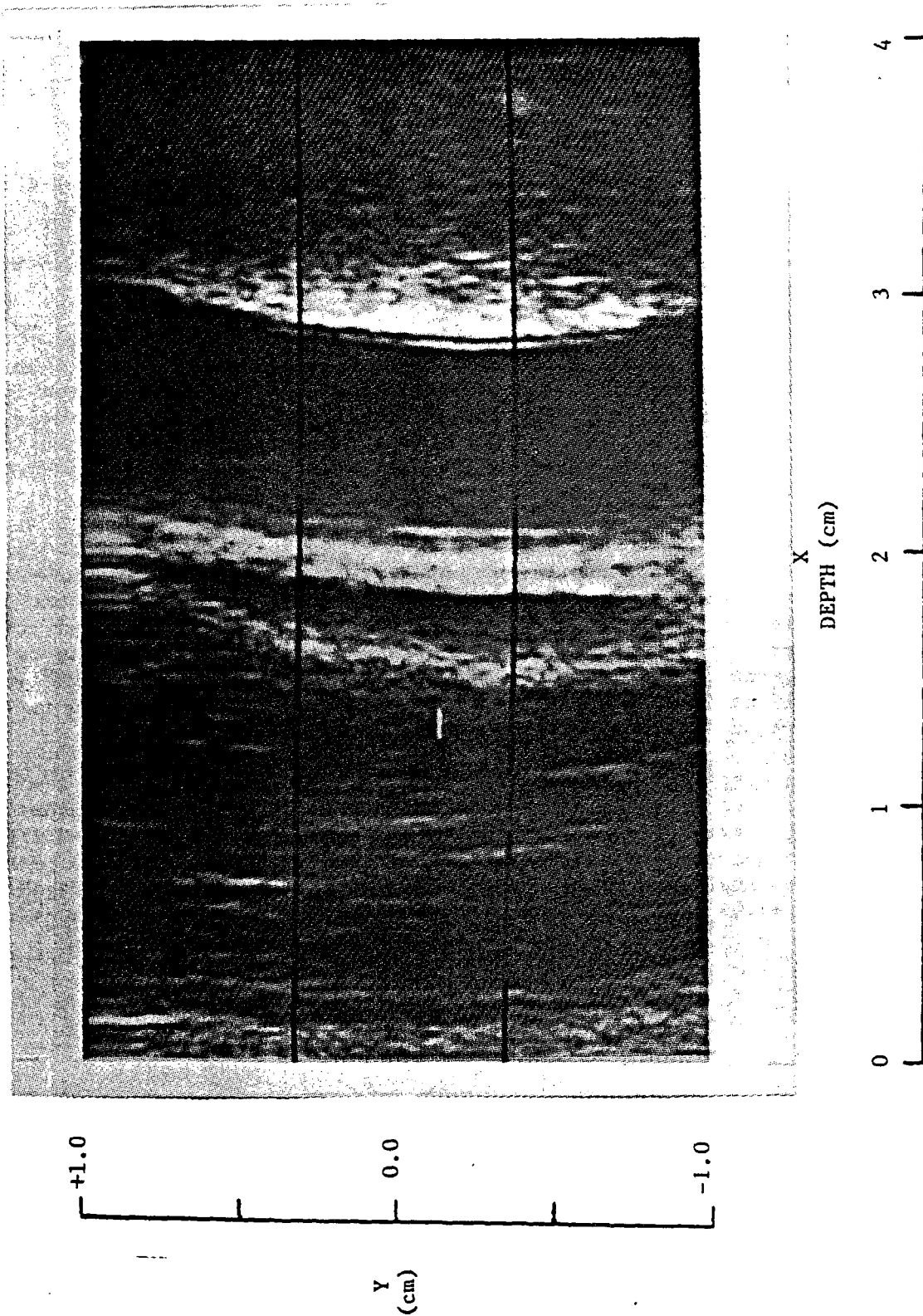
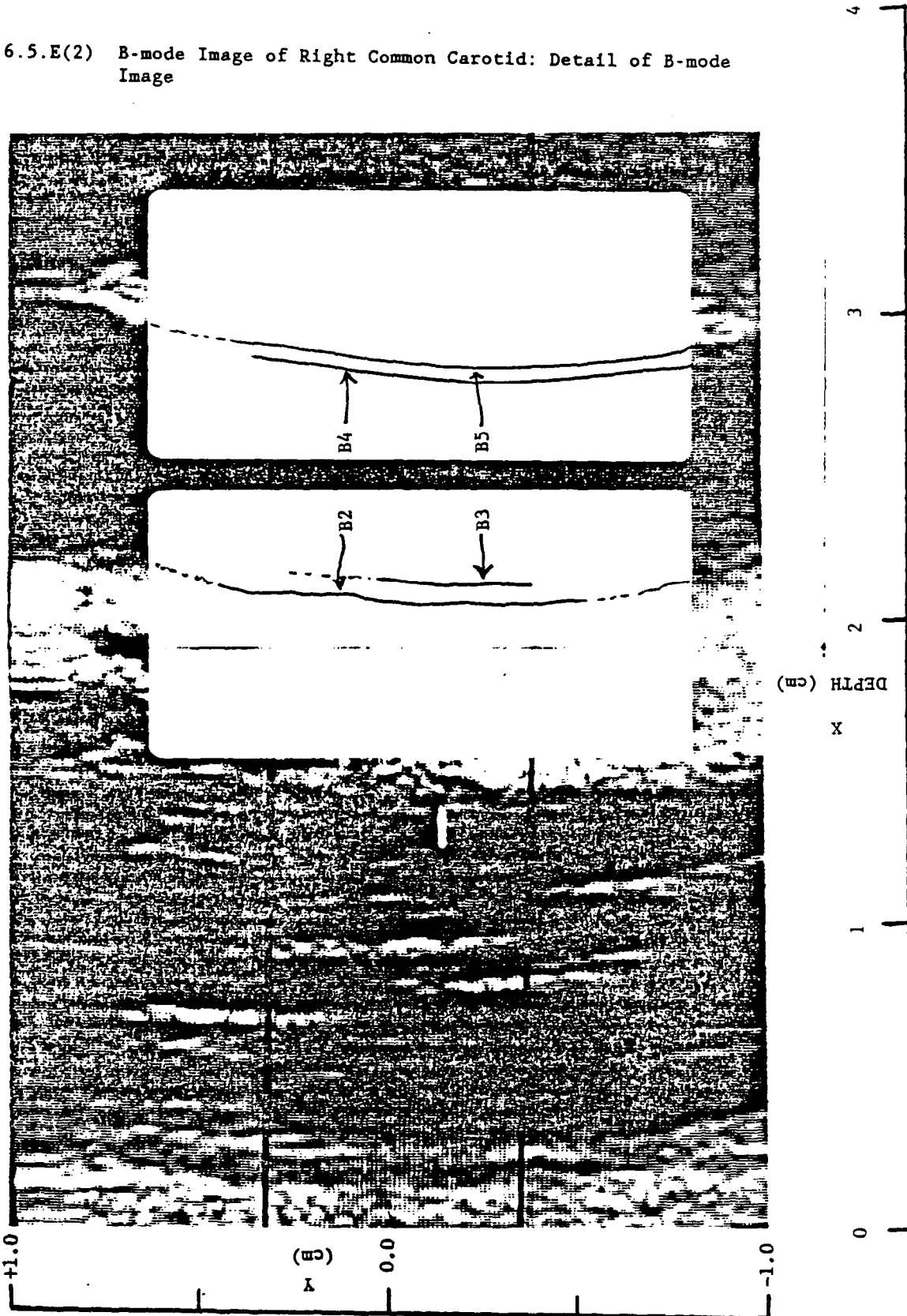


Figure 6.5.E(1) B-mode Image of Right Common Carotid

Figure 6.5.E(2) B-mode Image of Right Common Carotid: Detail of B-mode Image



6.5.6 Exercise for Reading B-Mode Image of Right Common Carotid:
Figures 6.5.F(1) and 6.5.F(2)

Site: Right Common Carotid Artery

Anterior Wall Depth: X = 1.2cm

Posterior Wall Depth: X = 2.0cm

Cursor Placement: The cursor should be located at $y = +0.5\text{cm}$ rather than $y = +0.8\text{cm}$.

Anatomical Landmark: Origin of the bulb is not identifiable. This suggests an interrogation angle other than the optimal (anatomical) angle, most probably the anterior angle. Origin of bulb should be located at $y = +0.5\text{cm}$ and marked at this vertical location by the sonographer.

Posterior Wall: B4 is well visualized from $y = -0.5\text{cm}$ to $y = +0.5\text{cm}$. The dark band to the right of B4 is moderately good and permits B5 to be easily identified over this interval. By reducing the brightness of the image monitor when marking B5, this boundary will be more clearly delineated. Sonographer alignment is excellent for the posterior wall.

Anterior Wall: B3 is well visualized from $y = -0.5\text{cm}$ to $y = 0.0$. Above this segment, reasonable estimates of the location of B3 can also be made. The dark band which frequently appears to the left of B3 is fairly clear from $y = -0.5\text{cm}$ to $y = 0.0\text{cm}$ but becomes diffuse when moving upward. B2 can be approximated fairly well from $y = -0.5\text{cm}$ to $y = 0.0$ but becomes less certain as one moves upward. Anterior wall appears to be considerably thicker than the posterior wall.

Significant Artifacts: Diffuse bright regions located within the lumen between $y = 0.0$ and $y = +0.8\text{cm}$ and near $y = -1.0\text{cm}$ are due to weak reflections of side lobes of the ultrasound beam from the lateral walls of the vessel.

Speckle adds apparent texture to both the posterior and anterior walls.

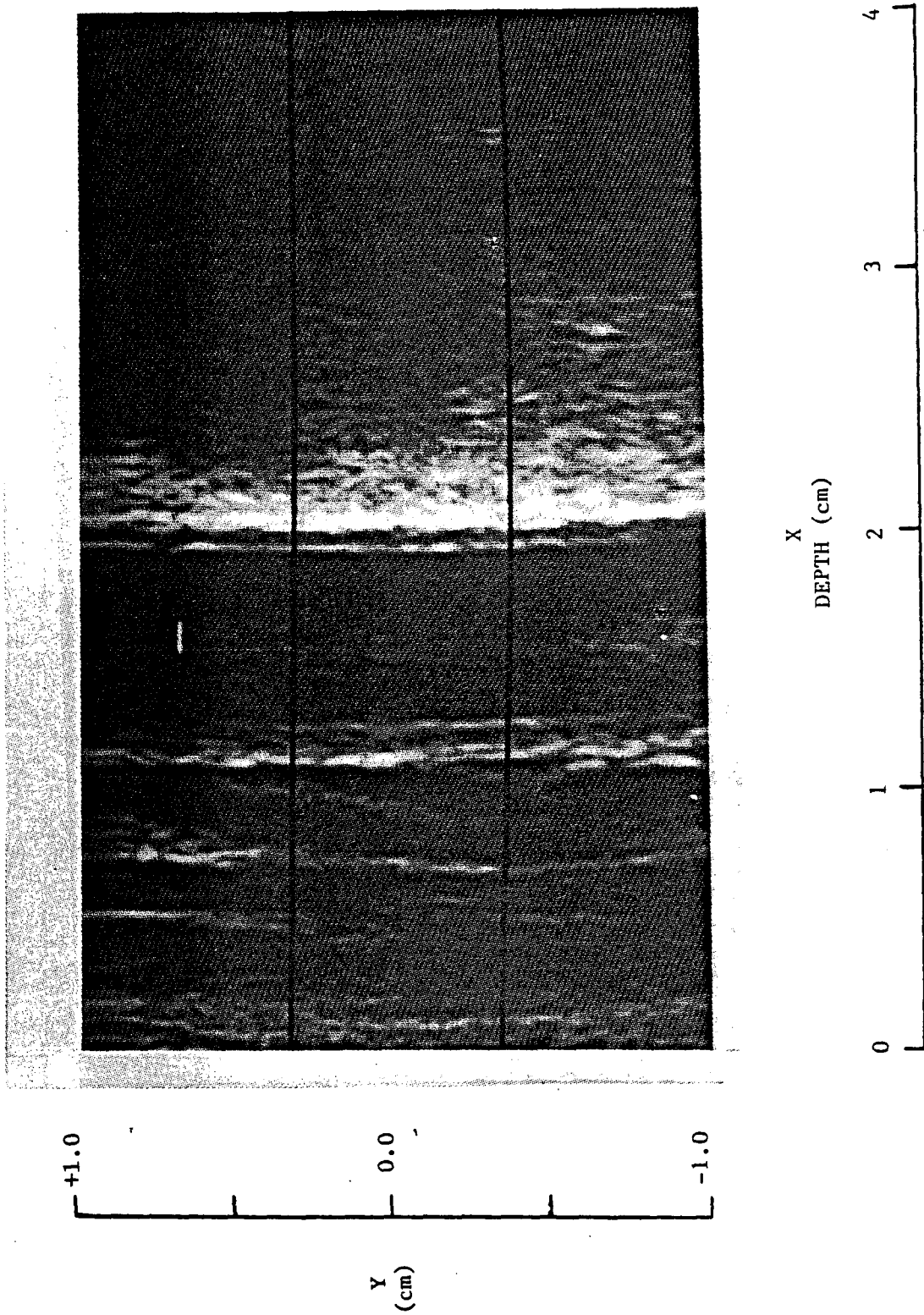
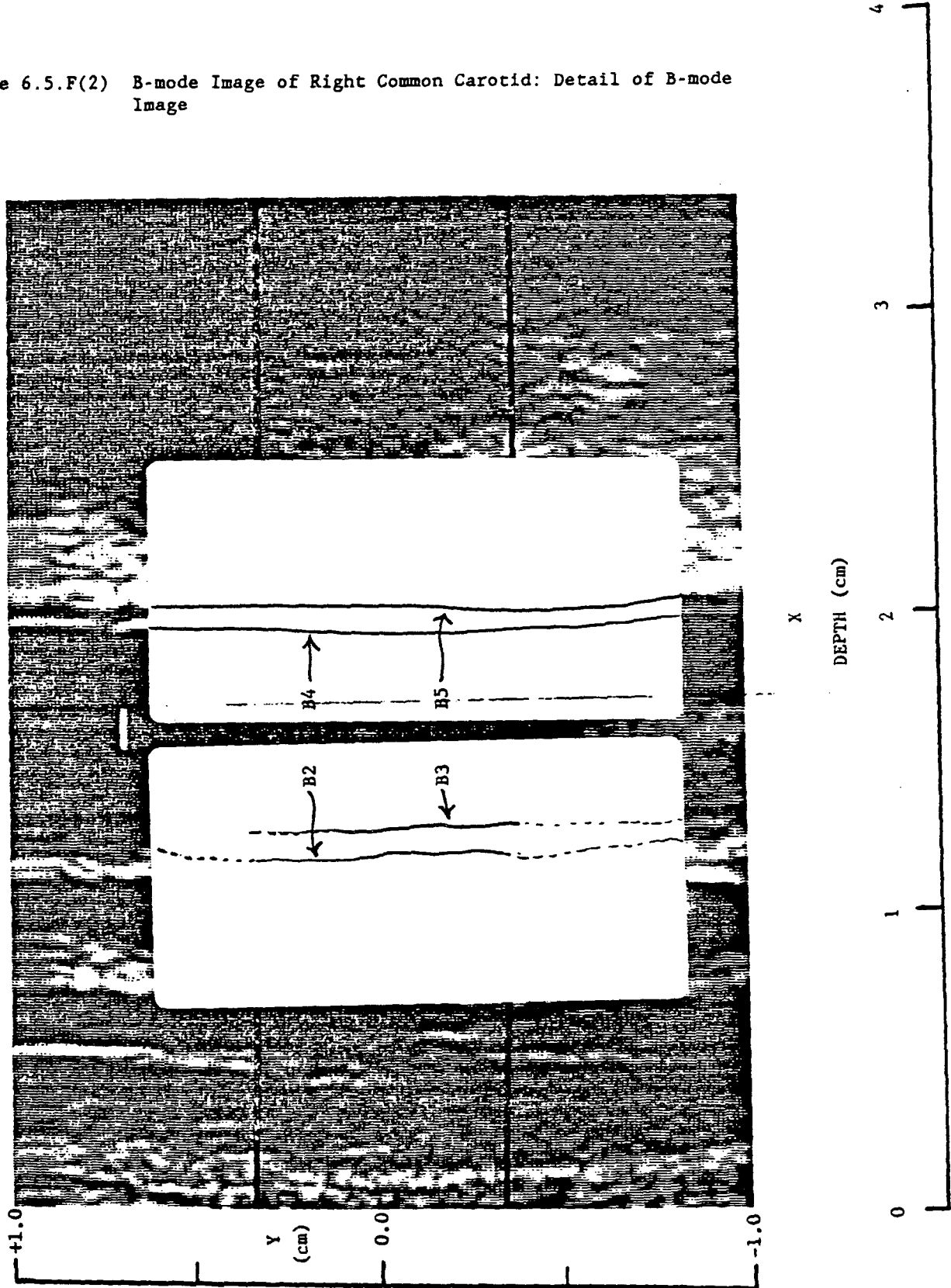


Figure 6.5.F(1) B-mode Image of Right Common Carotid

Figure 6.5.F(2) B-mode Image of Right Common Carotid: Detail of B-mode Image



6.5.7 Exercise for Reading B-Mode Image of Right Common Carotid:
Figures 6.5.G(1) and 6.5.G(2)

Site: Right Common Carotid Artery

Anterior Wall Depth: X = 2.5cm

Posterior Wall Depth: X = 3.5cm

Cursor Placement: The cursor is correctly positioned at Y = +0.5cm.

Anatomical Landmark: The origin of the bulb in this image is not distinct, but it appears to be located slightly below the cursor position at Y = +0.1cm. The fact that the landmark is not clearly visible suggests that the transducer was not held at the optimal angle.

Posterior Wall: B5 is clearly visible from Y = +1.0cm to Y = -1.0cm. Although there is not an echo-free region preceding B5, there is a distinct "dark" to bright transition making it possible to make measurements of B5 with confidence. In this image the intima + media region, which is typically dark, is filled with echoes--some of which are fairly bright. Although there is not a thin, bright line representative of B4, B4 can be identified as the left edge of this echogeneous region from Y = +0.8cm to Y = -1.0cm. These echoes between B4 and B5 and the fact that the distance between B4 and B5 appears greater than usual suggests the presence of material not typically found within the artery wall. For example, the image may indicate some beginning stages of disease.

Anterior Wall: B2 and its characteristic bright to dark transition is clearly visible from Y = +0.6cm to Y = -1.0cm. Measurements of this interface may be made with confidence. There is a distinct, bright line and a dark to bright transition representative of B3 from Y = +0.6cm to Y = 0.0cm. The brightness of this interface compared to typical images of B3 is the result of some apparently highly reflective matter within the intima layer. There is also much echogenic matter between B2 and B3 within the intima + media layer. Measurements for B3 may be made on the right edge of this echogenic layer from Y = 0.0cm to Y = -1.0cm. In this region measurements of B3 are made on the right side of an echo because of the absence of the typical dark to bright transition. The highly reflective nature of the tissues in this wall suggest (as was the case for the posterior wall) the possibility of beginning disease in this artery.

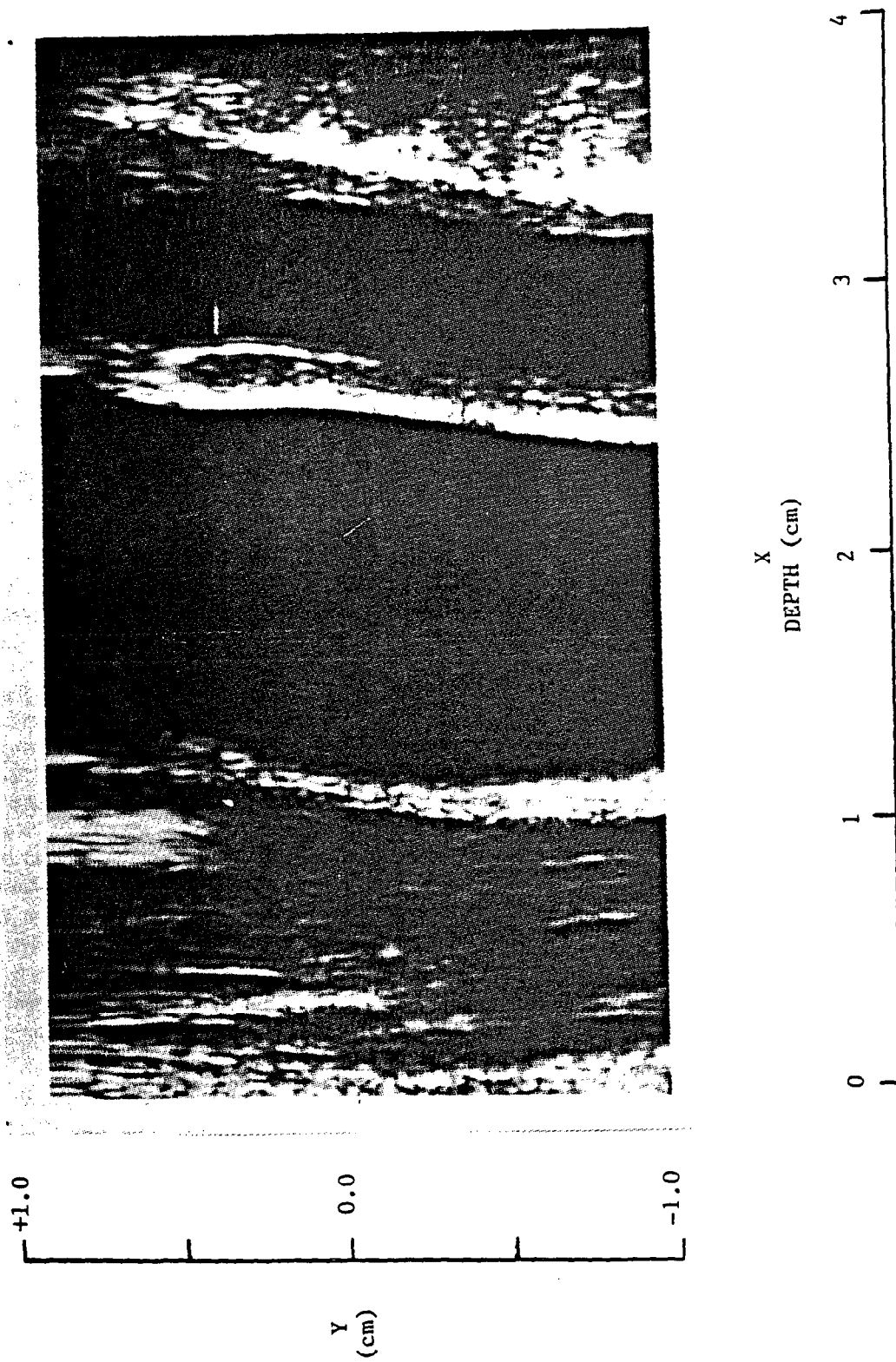
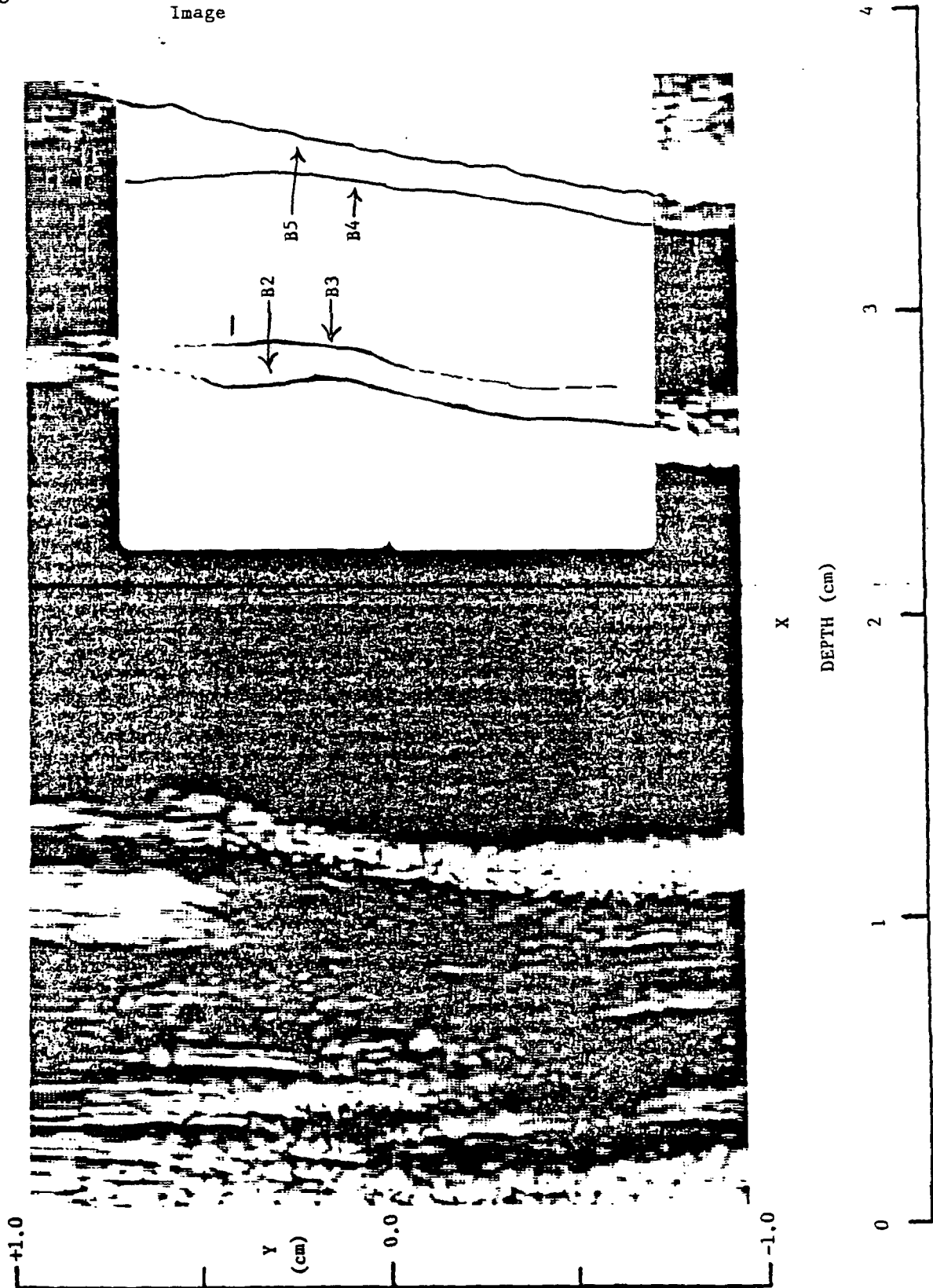


Figure 6.5.G(1) B-mode Image of Right Common Carotid

Figure 6.5.G(2) B-mode Image of Right Common Carotid: Detail of B-mode Image



6.5.8 Exercise for Reading B-Mode Image of Right Internal Carotid:
Figures 6.5.H(1) and 6.5.H(2)

Site: Right Internal Carotid

Anterior Wall Depth: X = 1.7cm (at y = 0.0cm)

Posterior Wall Depth: X = 2.4cm (at y = 0.0cm)

Cursor: The cursor is properly placed at the superior arc of the flow divider located at y = -0.5cm.

Anatomical Landmark: The superior arc of the flow divider is visible and located at y = -0.5cm. This is the proper vertical placement.

Posterior Wall: The internal carotid begins at y = -0.5cm and extends upward. Although the posterior wall is visible from y = -0.5cm to y = 0.0cm the characteristic bright line for B5 is not present. Lowering the monitor brightness may give a smooth dark to bright transition from which a few measurements of B5 may be made. There is no B4 visible within the area of measurement except at the vertical position of the cursor, y = -0.5cm. B4 is visible below the area of measurement because of an apparent lesion which is located just below the tip of the flow divider in the bulb. It should be noted that cases may arise where lesions appear outside the site of measurement as it does in this image.

Anterior Wall: As with B5 there is not a distinct bright line representative of B2. There is a rough boundary which separates the anterior wall from the lumen and measurements of B2 may possibly be made along this interface from y = -0.5cm to y = +0.1cm. These measurements, however, may be of a low confidence level. B3 is not visible in this image of the interval.

Significant Artifact: Speckle adds much texture to both B2 and B5. Both walls appear to be missing above y = 0.0cm. This is because the artery begins to curve away from the skin surface at this point, and sound is greatly attenuated in this region.

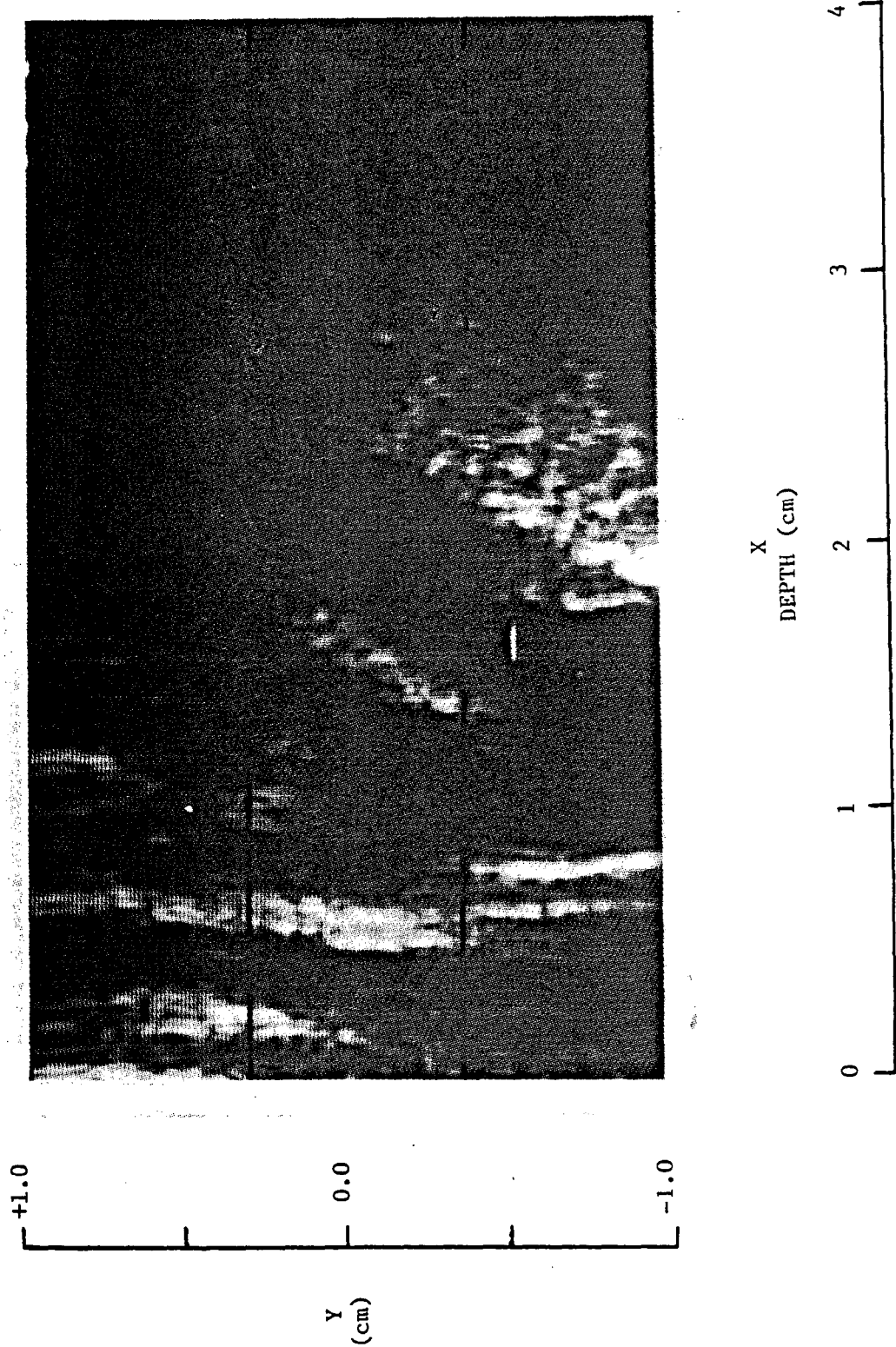
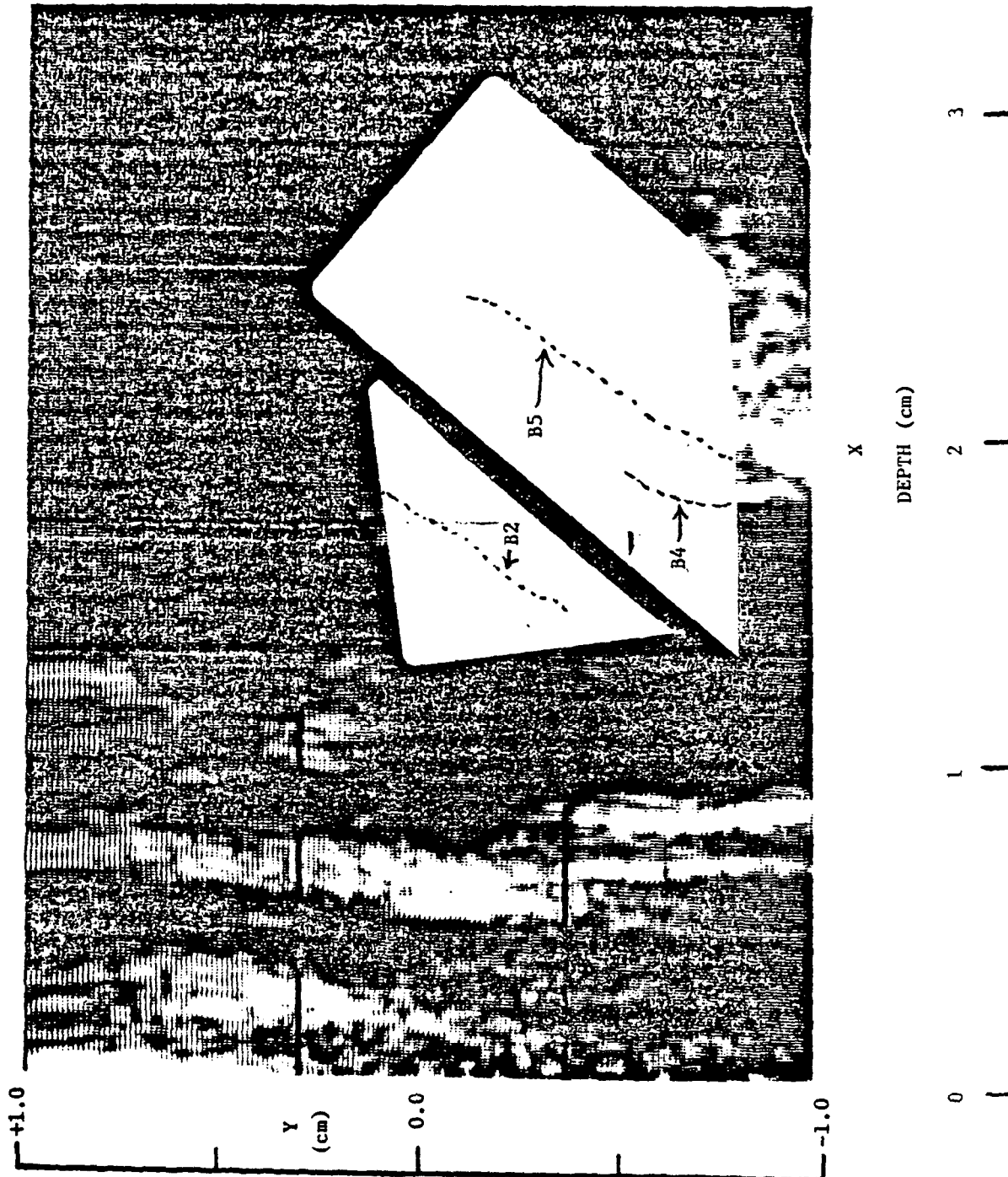


Figure 6.5.H(1) B-mode Image of Right Internal Carotid

Figure 6.5.H(2) B-mode Image of Right Internal Carotid: Detail of B-mode Image



6.5.9 Exercise for Reading B-Mode Image of Left Common
Carotid-Posterior: Figures 6.5.I(1) and 6.5.I(2)

Site: Left Common Carotid-Posterior

Anterior Wall Depth: X = 1.5cm

Posterior Wall Depth: X = 2.5cm

Cursor: The cursor's vertical screen placement is correct at $y = -0.5\text{cm}$.

Anatomical Landmark: The origin of the bulb is visible not in the anterior wall but on the posterior wall. The origin appears to be located at $y = -0.2\text{cm}$.

Posterior Wall: B5 is clearly visible from $y = -0.4\text{cm}$ to $y = +0.4\text{cm}$. Within this range the interface is distinct and continuous, and measurements may be made with confidence. Above the range B5 is less distinct; ($y = +0.4\text{cm}$ to $y = +0.8\text{cm}$) however, measurements may still be made. B4 is also visible, although this boundary is not as distinct. B4 could be identified from $y = 0.0\text{cm}$ to $y = +0.4\text{cm}$.

Anterior Wall: B2 can be identified from $y = -0.5\text{cm}$ to $y = +0.5\text{cm}$. Although there is not a continuous dark band to the right of B2, there is a distinct bright to "dark" transition along the interface and the measurements may be made with a fair amount of confidence. B3 is visible, although not continuous, from $y = -0.7\text{cm}$ to $y = +0.3\text{cm}$. In the middle of the image B2 and B3 appear to be adjacent (no dark band between). Turning down the monitor gain may make it easier to identify B3 at this point.

Significant Artifact: There appear to be gaps in B3, although this is probably not the case. This is probably the result of slight angle changes in the transducer. At the top of the image in the middle of the artery is an echo which suggests that there is some structure within the lumen. This is probably caused by misalignment of the transducer.

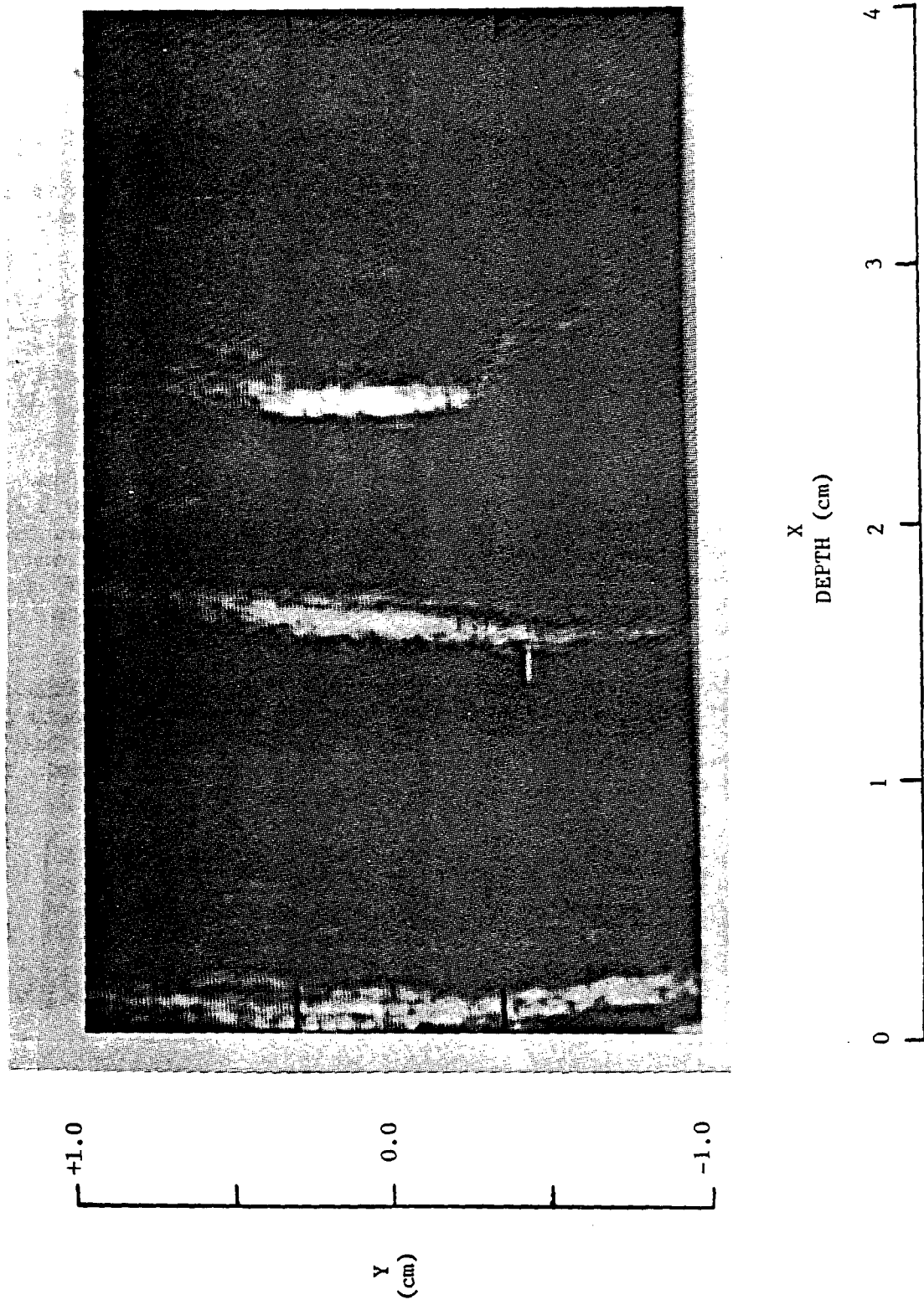
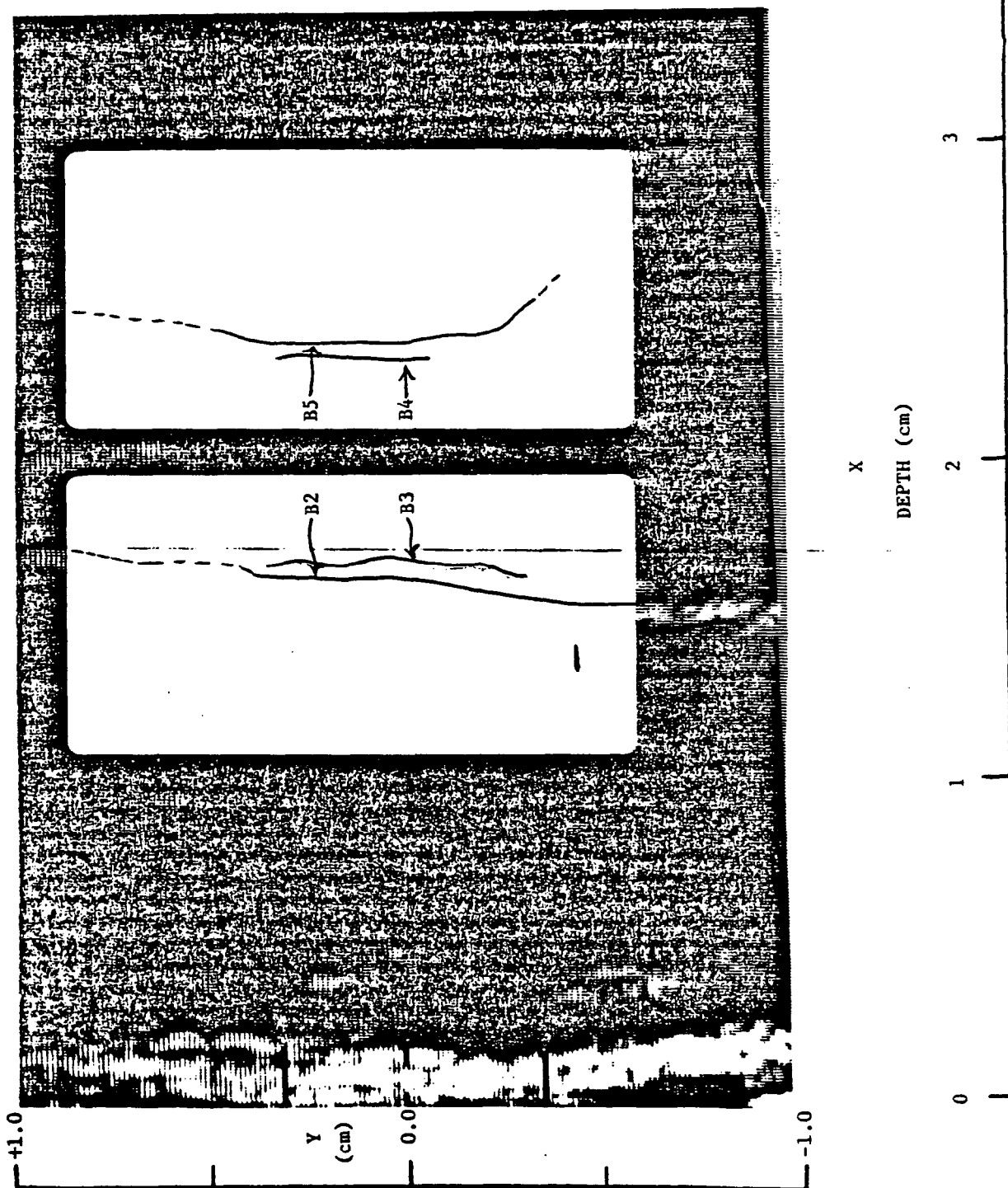


Figure 6.5.I(1) B-mode Image of Left Common Carotid-Posterior

Figure 6.5.I(2) B-mode Image of Left Common Carotid-Posterior: Detail of B-mode Image



6.5.10 Exercise for Reading B-Mode Image of Left Common Carotid-Optimal: Figures 6.5.J(1) and 6.5.J(2)

Site: Left Common Carotid-Optimal

Anterior Wall Depth: X = 1.5cm

Posterior Wall Depth: X = 2.5cm

Cursor: Correctly placed in the lower third of the screen at $y = -0.5\text{cm}$. Ideally positioned in the center of the artery.

Anatomical Landmark: The origin of the bulb is visible on the posterior wall and appears to be located at $y = -0.2\text{cm}$. Ideally it should be placed a little lower ($y = -0.5\text{cm}$); however, the vertical screen placement is adequate for proper measurement of the common carotid artery.

Posterior Wall: B5 is clear and distinct and may be easily identified from $y = +1.0\text{cm}$ to $y = -0.3\text{cm}$. Below this region, from $y = -0.3\text{cm}$ to $y = -1.0\text{cm}$, B5 is slightly visible, and with the aid of low monitor gain, identification of the interface may be made in this area as well. Although there isn't a characteristic dark band to the left of the boundary, B5 is adequately bright and distinct so that confident measurements may be made. B4 is clearly visible and, except for an apparent gap (located at $y = -0.3\text{cm}$), it is smooth and continuous. Confident measurements may be made of B4 from $y = +1.0\text{cm}$ to $y = -0.6\text{cm}$. The echoes which appear within the media suggest that the sonographer's gain may have been relatively high. (Structure within the media is being picked up by the ultrasound system because of the higher gain.)

Anterior Wall: A thin bright line is visible for B2 from $y = +0.6\text{cm}$ to $+0.1\text{cm}$ and again from $y = -0.2\text{cm}$ to $y = -0.5\text{cm}$. Above, below, and in between these two regions the location of B2 is unclear. Because of the apparent "smear" of B2, measurements of the interface may be made more confidently by lowering the monitor gain. Although B3 appears jagged and discontinuous, measurements may be made with a fair amount of confidence from $y = +0.6\text{cm}$ to $y = -0.5\text{cm}$.

Significant Artifact: The apparent gaps in B2, B3 and B4 are probably the result of slight angle changes between the transducer beam and the artery wall.

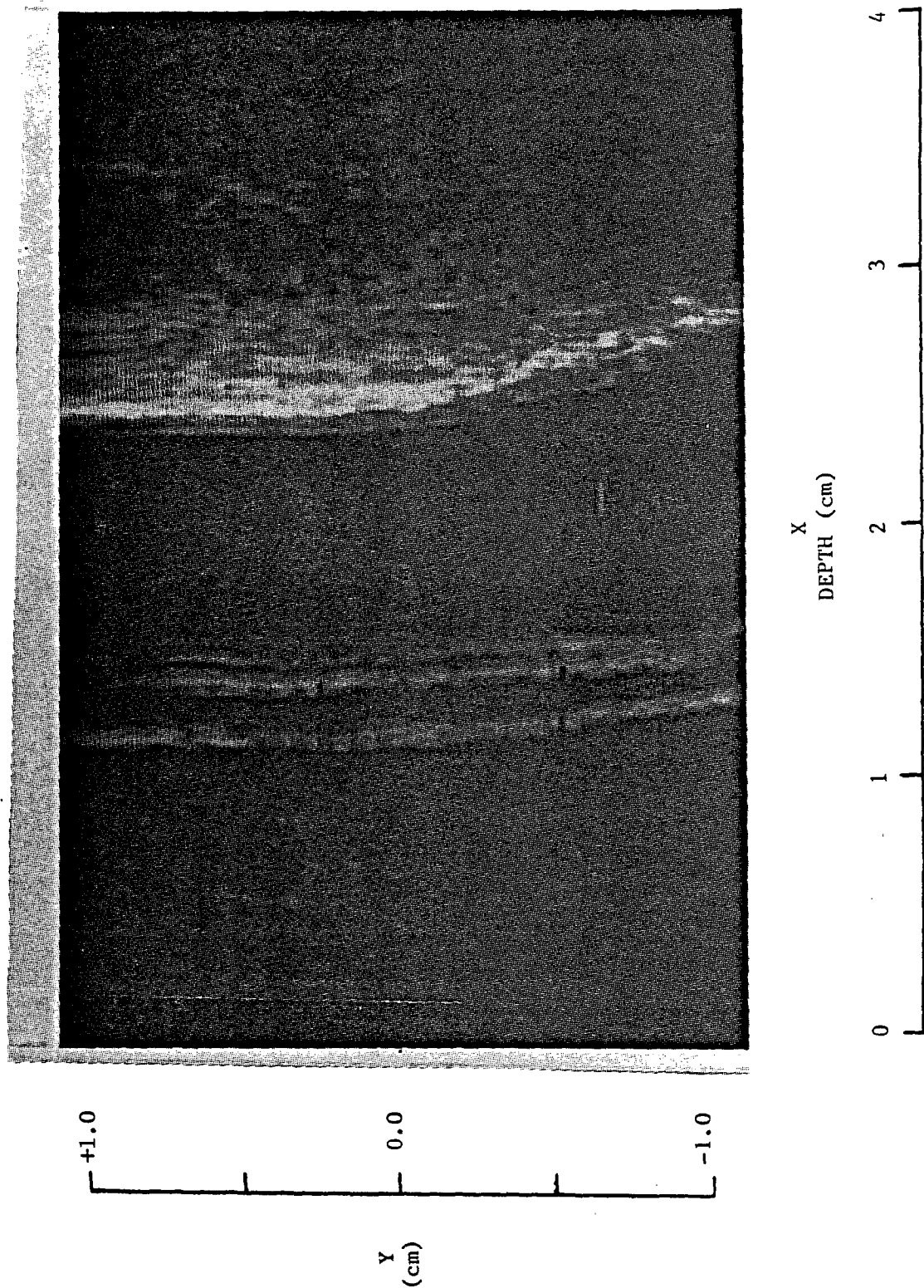
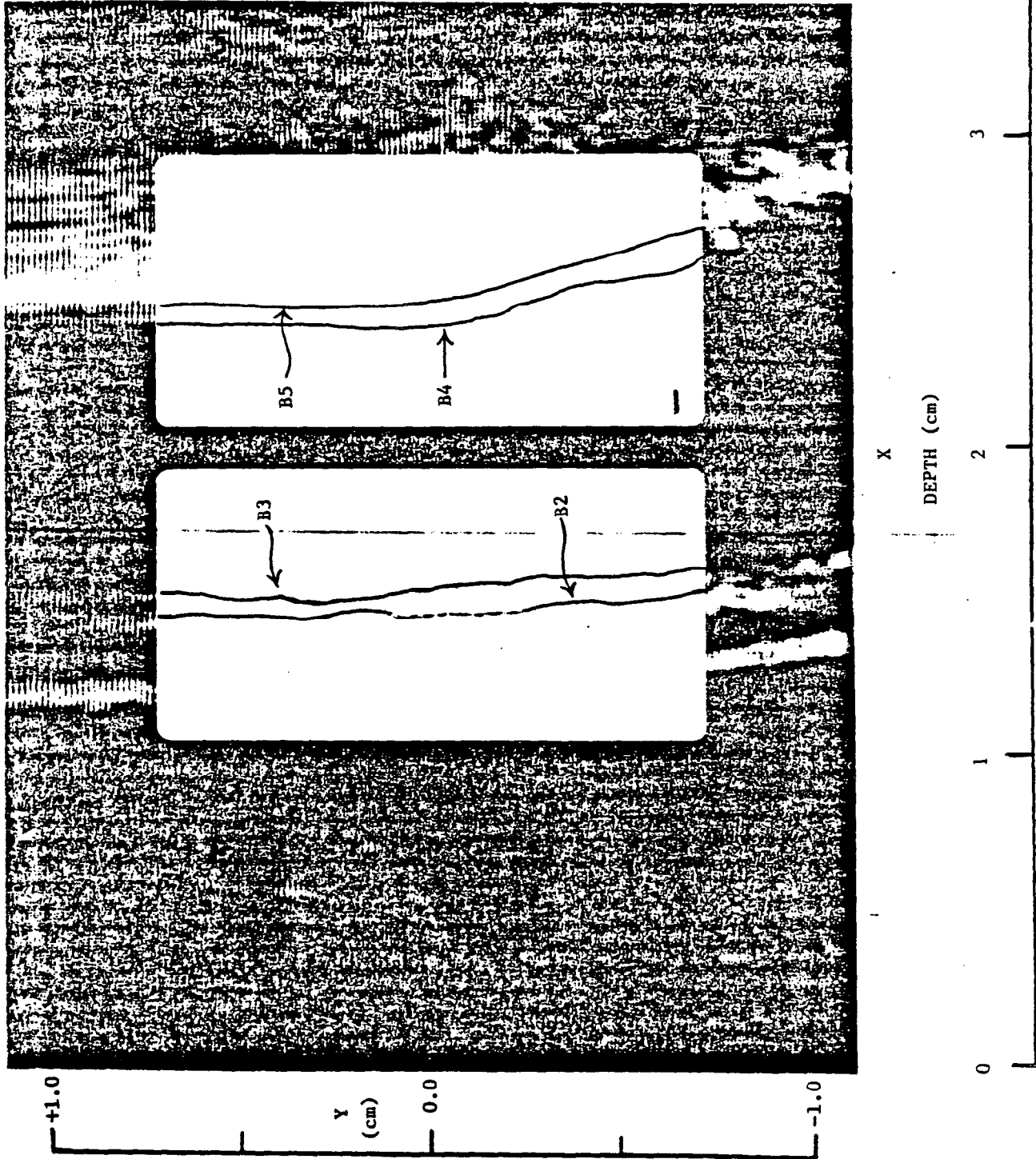


Figure 6.5.J(1) B-mode Image of Left Common Carotid-Optimal

Figure 6.5.J(2) B-mode Image of Left Common Carotid-Optimal: Detail of B-mode Image



6.5.11 Exercise for Reading B-Mode Image of Left Carotid Bulb:
Figures 6.5.K(1) and 6.5.K(2)

Site: Left Carotid Bulb

Anterior Wall Depth: X = 0.8cm

Posterior Wall Depth: X = 1.8cm

Cursor: The cursor is correctly placed at $y = -0.4\text{cm}$. Anatomically, it is positioned at the superior arc of the flow divider. The cursor's vertical position on the screen is ideal since it locates the area of measurement in the middle third of the screen.

Anatomical Landmark: The tip of the flow divider is clearly visible and is located at $y = -0.4\text{cm}$.

Posterior Wall: B5 is not very distinct; however, turning down the monitor brightness may aid in making measurements from $y = -0.3\text{cm}$ to $y = +0.5\text{cm}$. B4 is not visible in this image.

Anterior Wall: B2 can be fairly well identified at the point of a bright to dark transition from $y = -1.0\text{cm}$ to $y = +0.6\text{cm}$. As with B5, turning down the brightness may cause B2 to appear smoother and more distinct and allow measurements to be made with a greater degree of confidence. B3 can not be seen in this image.

Significant Artifact: Speckle as well as the curvature of the bulb add apparent texture to both B2 and B5.

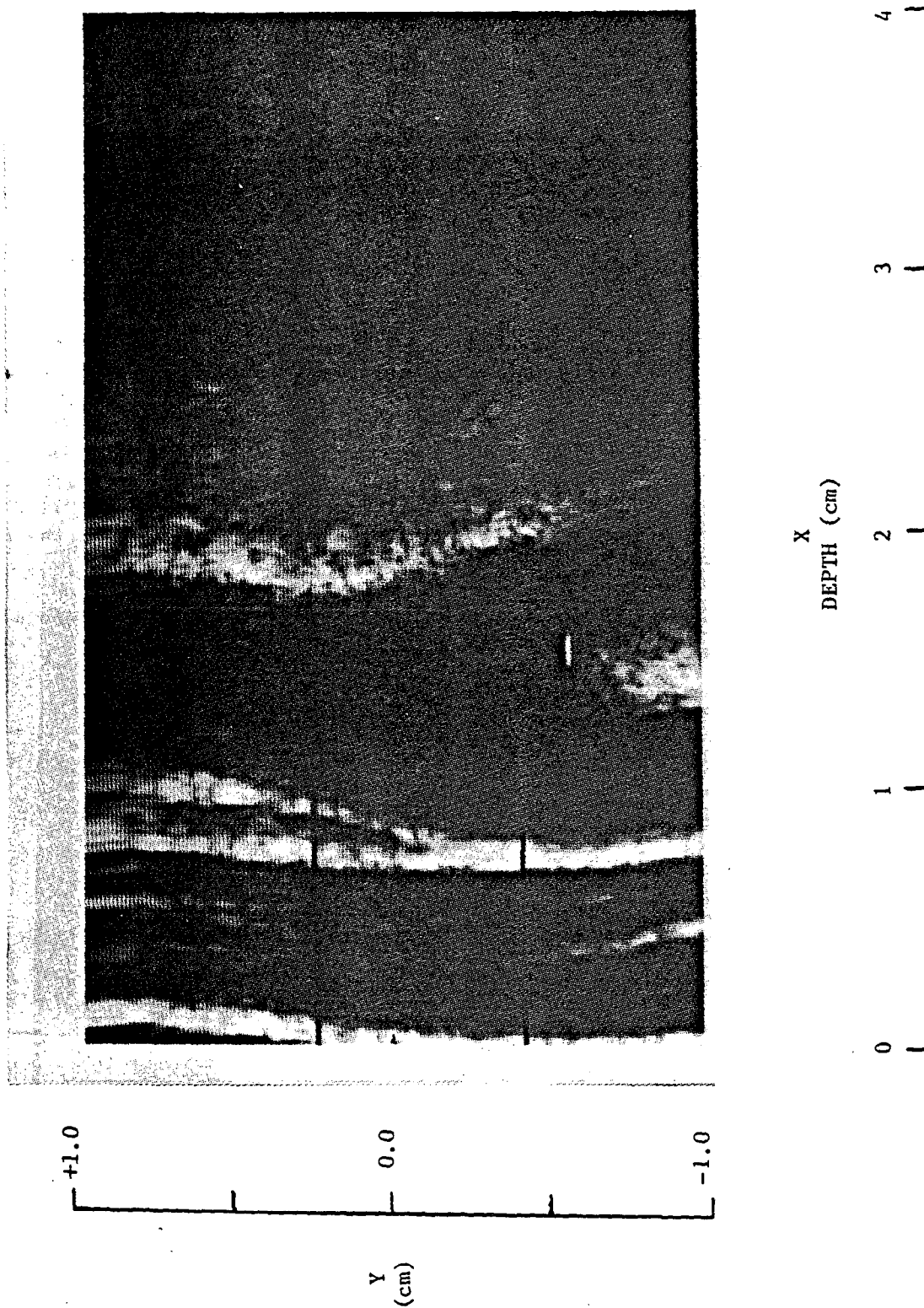
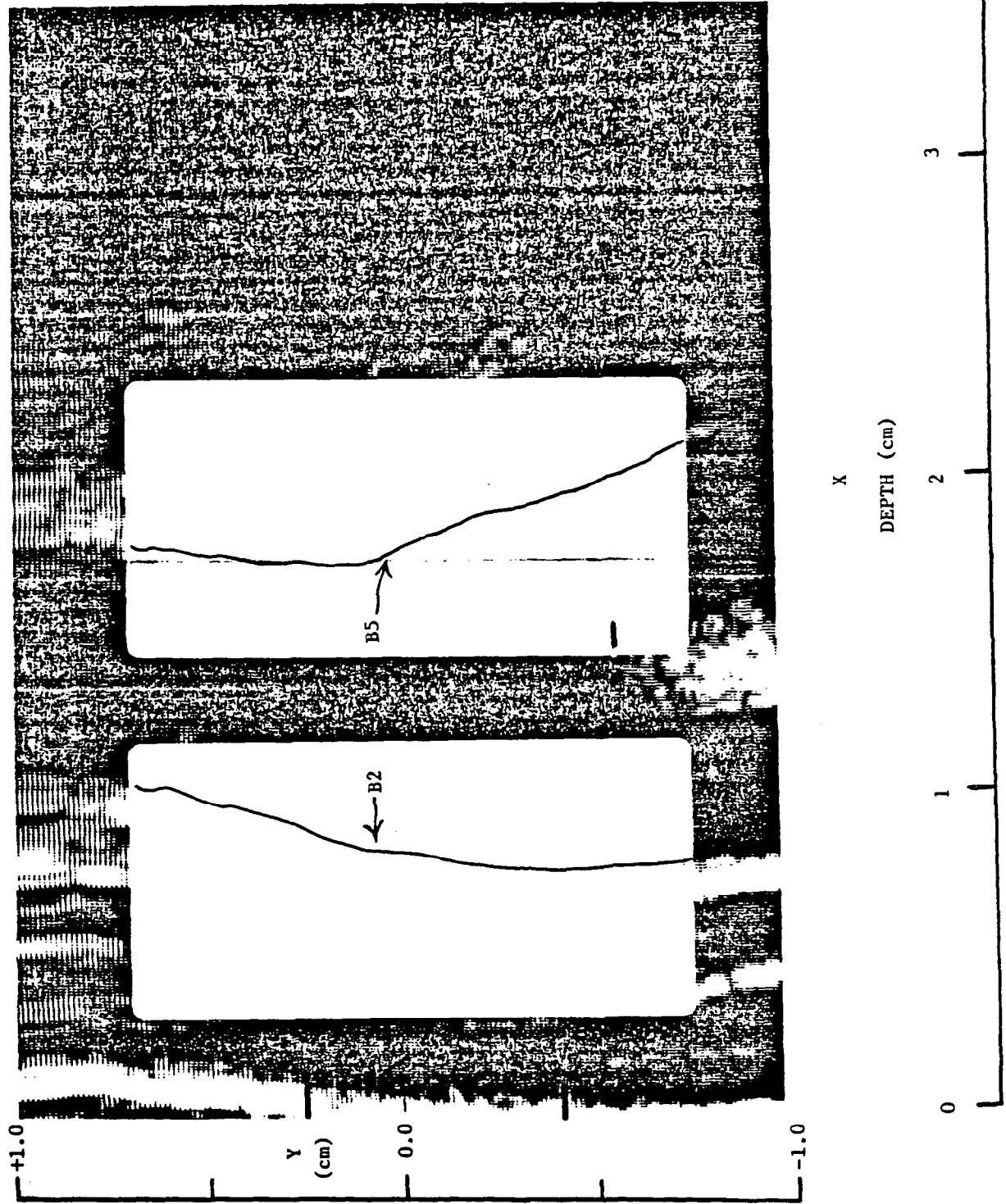


Figure 6.5.K(1) B-mode Image of Left Carotid Bulb

Figure 6.5.K(2) B-mode Image of Left Carotid Bulb: Detail of B-mode Image



6.5.12 Exercise for Reading B-Mode Image of Left Carotid Bulb:
Figures 6.5.L(1) and 6.5.L(2)

Site: Left Carotid Bulb

Anterior Wall Depth: X = +0.5cm

Posterior Wall Depth: X = +2.2cm

Cursor Placement: The cursor is located at a correct vertical position of y = -0.5cm, at the tip of the flow divider.

Anatomical Landmark: The tip of the flow divider is clearly visible and is located at Y = -0.5cm and horizontally at X = 2.0cm.

Posterior Wall: B5 can be measured with relative confidence along two different intervals: from Y = +1.0cm to Y = +0.3cm and from Y = -0.1cm to Y = -0.8cm. Measurement along these intervals is aided by turning down monitor brightness. In the center of the image, from Y = +0.2cm to Y = -0.1cm, the posterior wall is not visible because of an artifact known as shadowing. B4 is visible from Y = +0.2cm to Y = +0.7cm. Although there is not a distinct, thin echo for B4, the band of low level echoes preceding B5 suggests the presence of material different from the lumen and it is possible to measure B4. The overall image gain appears low, and because these low level echoes are visible it suggests the presence of something abnormal (i.e., beginning lesion, fatty streak etc.). In the lower portion of the image, B4 is not clearly visible.

Anterior Wall: There is a thin, bright echo followed by a slightly visible bright to dark transition representing B2. By turning down the monitor brightness, this bright to dark transition may be more visible and B2 may be identified from Y = +1.0cm to Y = -0.7cm. As with the posterior wall, the typically dark band between 2 & 3 (or 4 & 5 on the posterior wall) contains some low level echoes suggesting the presence of matter not normally visible within this intima + media layer. Even though these low level echoes are present, a dark to bright transition for B3 is still slightly visible from Y = +1.0cm to Y = +0.2cm. In the center of the image from Y = +0.2cm to Y = -0.1cm, an apparent lesion and its echogenic substance make it difficult to visualize a dark to bright transition for B3. In this area B3 should be marked just to the right of the lesion as this is a good approximation of the intima-blood interface. Below the point Y = -0.1cm B3 cannot be visualized.

Significant Artifact: This image is a good example of an artifact known as shadowing. The posterior wall appears to have a large gap in it making it impossible to measure B4 and B5 in that particular area. Shadowing is typically the result of highly reflective or absorptive tissues through which very little or no sound passes. The effect is a blocking out or shadowing of any subsequent tissues in that path of the sound. In this case, the lesion on the anterior wall has apparently reflected (or absorbed) most of the sound energy so that no sound reaches the posterior wall. Therefore, neither the posterior wall nor the tissue following it are visible. Shadowed areas often indicate the presence of possible lesions preceding them, but nothing can be concluded about the shadowed tissues.

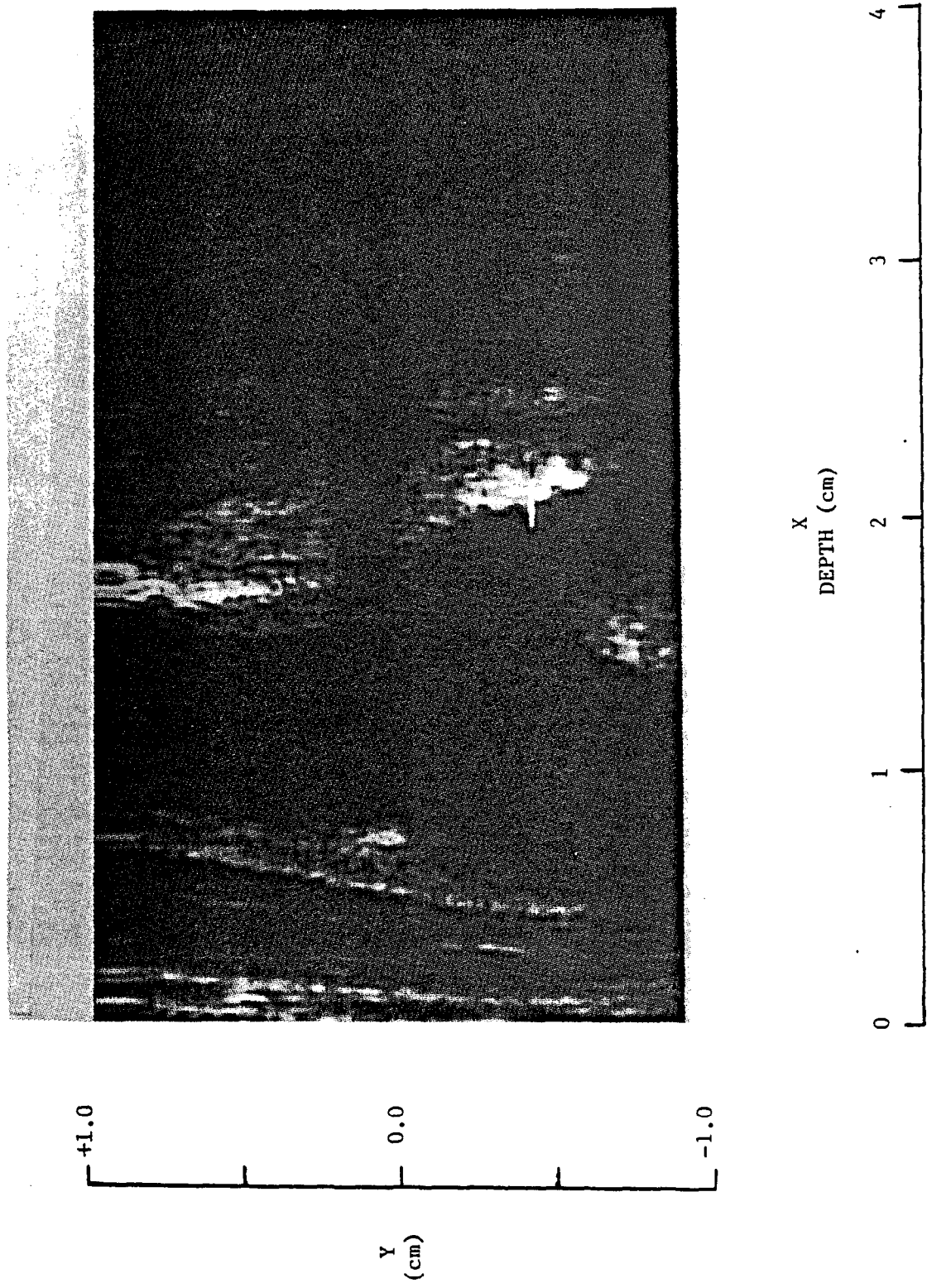
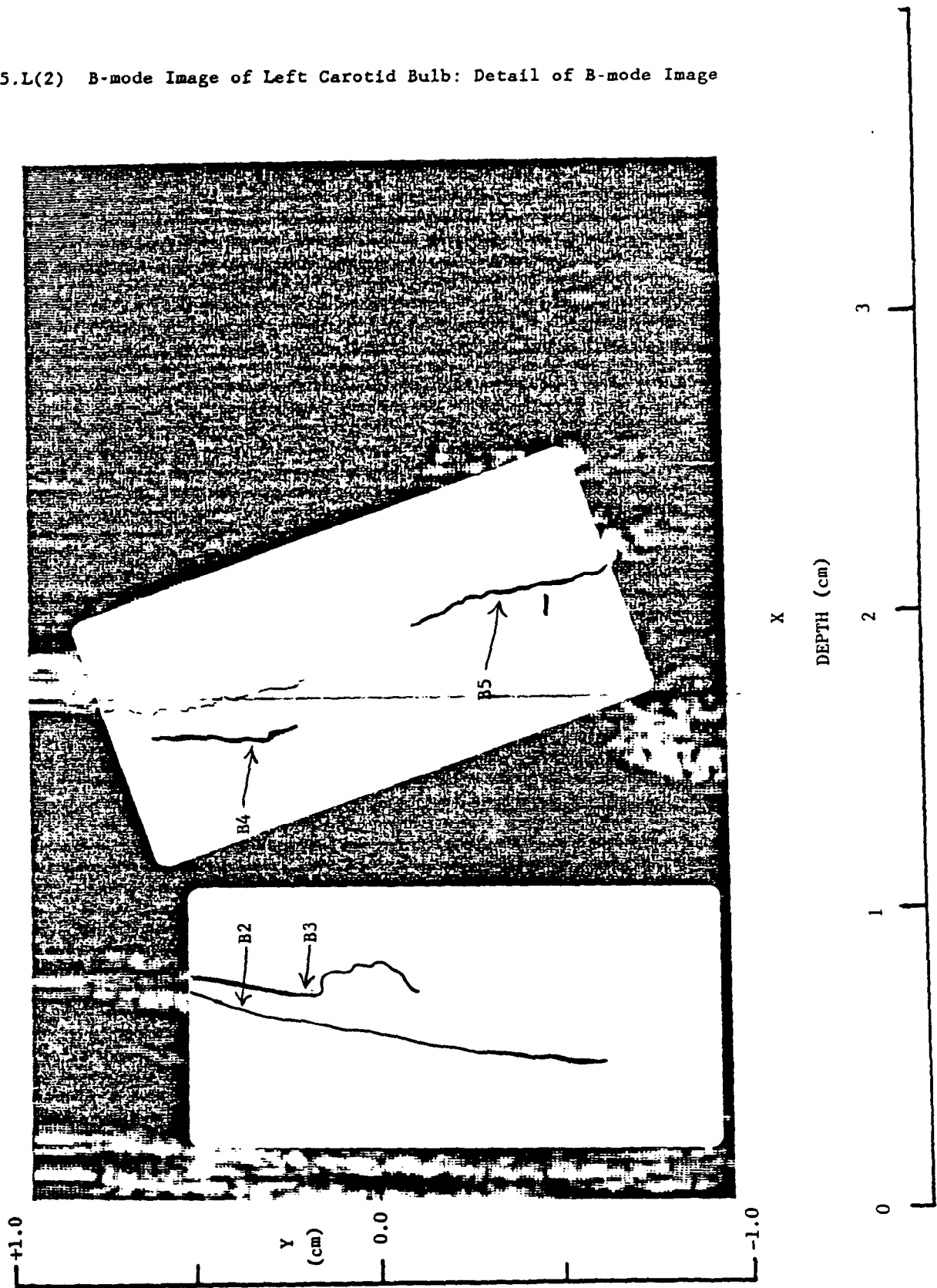


Figure 6.5.L(1) B-mode Image of Left Carotid Bulb

Figure 6.5.L(2) B-mode Image of Left Carotid Bulb: Detail of B-mode Image



6.5.13 Exercise for Reading B-Mode Image of Left Carotid Bulb:
Figures 6.5.M(1) and 6.5.M(2)

Site: Left Internal Carotid Artery

Anterior Wall Depth: X = 1.6cm

Posterior Wall Depth: X = 2.7cm

Cursor Placement: The cursor is improperly placed. It should be placed at the superior arc of the flow divider which is located at $y = +0.4\text{cm}$.

Anatomical Landmark: The tip of the flow divider is clearly visible at $y = +0.4\text{cm}$. This is the proper vertical screen placement.

Posterior Wall: B4 is visualized from $y = -0.5\text{cm}$ to $y = 0.0\text{cm}$. The dark band following B4 is distinct and therefore permits B5 to be easily identified from $y = -0.5\text{cm}$ to $y = +0.4\text{cm}$. Lowering the monitor brightness will eliminate the fuzziness in the dark band from $y = -0.5\text{cm}$ to $y = -0.1\text{cm}$ making it even easier to identify B5.

Anterior Wall: B3 is not easily identified. Although some diffuse patches appear just to the left of the artery lumen, there is no distinct dark band following B2. Therefore, B3 could not be identified with much confidence. It should be noted, however, that turning down the monitor brightness may eliminate some of the diffuseness leaving brighter portions of B3 which may then be identified. B2 is easily identified from $y = -0.3\text{cm}$ to $y = +0.4\text{cm}$. Just above and below this range it may be identified fairly well by turning down the monitor brightness.

Significant Artifact: The weak echoes appearing within the lumen around $X = 2.0\text{cm}$ are artifact resulting from multiple reverberations between the two bright lines located at $X = 1.3\text{cm}$ and $X = 2.7\text{cm}$.

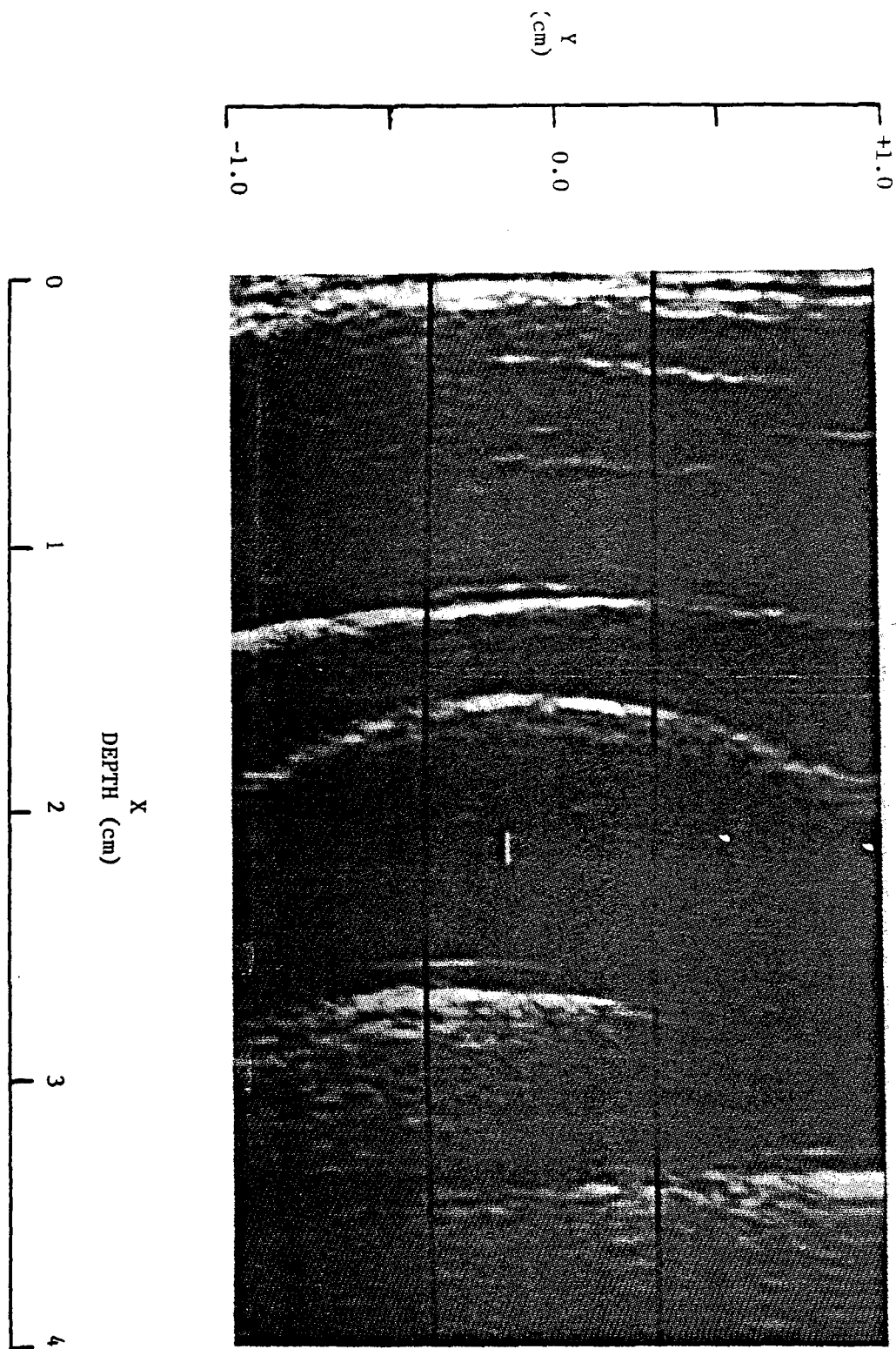
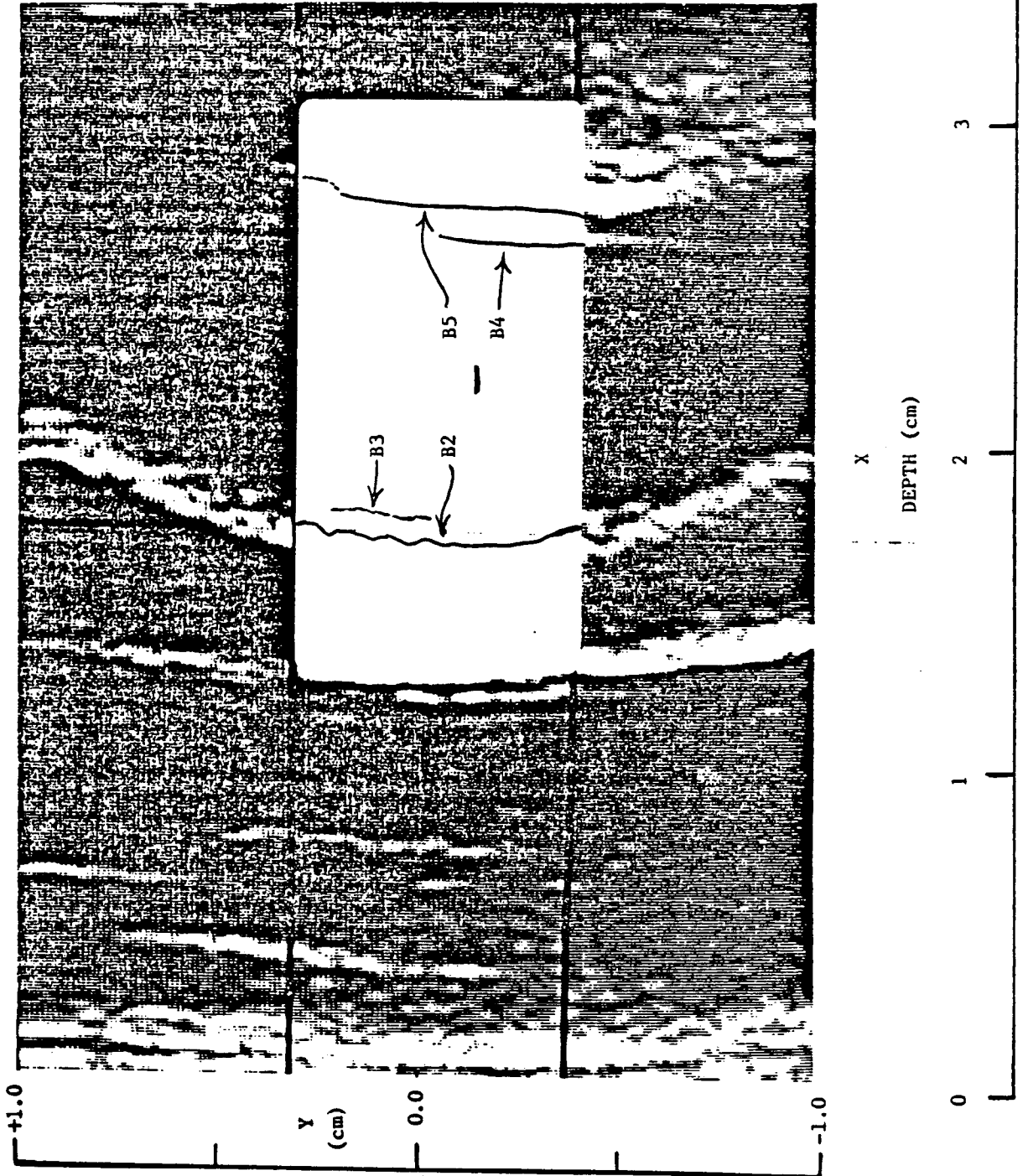


Figure 6.5.M(1) B-mode Image of Left Internal Carotid

Figure 6.5.M(2) B-mode Image of Left Internal Carotid: Detail of B-mode Image



6.6 Calibration of Image Pixel Size

At the beginning of each participant study, a calibration frame is read. An example is shown in Figure 6.6.A.

The length of the cursor line in millimeters is given on the upper right portion of the image. By successively placing the cross-hairs at first the left and then the right ends of the cursor, the number of pixels in the image corresponding to 20 mm is determined. Typically, the calibration factor is one pixel = 0.067 mm. This factor is automatically calculated in the computer and used in computing arterial wall dimensions.

6.7 Selection of Image Frames

Twenty-four frames of each view at each arterial site are stored on optical disk. The frame to be read is selected by the reader as the systolic frame (largest lumen diameter) which best visualizes the four principal boundaries. These boundaries are then marked as described in the next section. Be certain to use wall motion as a tool in convincingly identifying these arterial wall boundaries.

6.8 Placement of Crosshairs on Principal Boundaries

A crosshair is used on each of the identifiable boundaries to mark its location at 11 specific locations as shown in Fig. 6.8.A. The coordinates of these locations are stored in the central computer and used to compute dimensions of arterial lumens and wall layers. A maximum of 44 locations is recorded if all boundaries are clearly visible. In many cases, between 25 and 35 locations are the number actually marked, due to lack of sufficient information in the image.

Based upon the discussion in section 6.4., if a sonographer has made every effort to visualize the four boundaries being measured, missing data is generally (the shadowing artifact being the exception) an indication of the absence of disease within the arterial walls. Whenever data are missing due to shadowing, this should be noted in the comments discussed in the next section. An example of shadowing is given in figure 6.5.M.

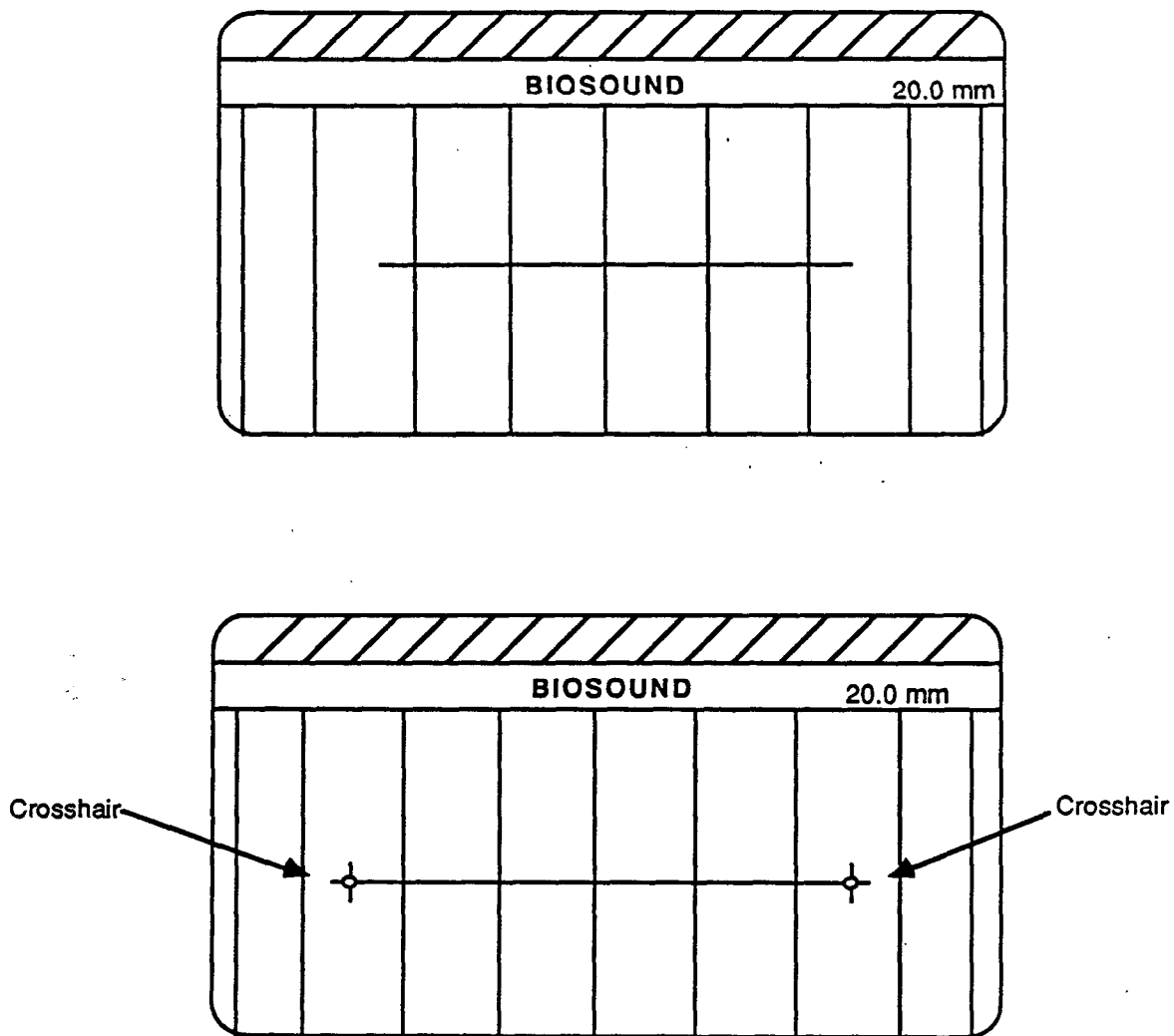


Figure 6.6.A Biosound Calibration Frame for Determination of Image Pixel Size

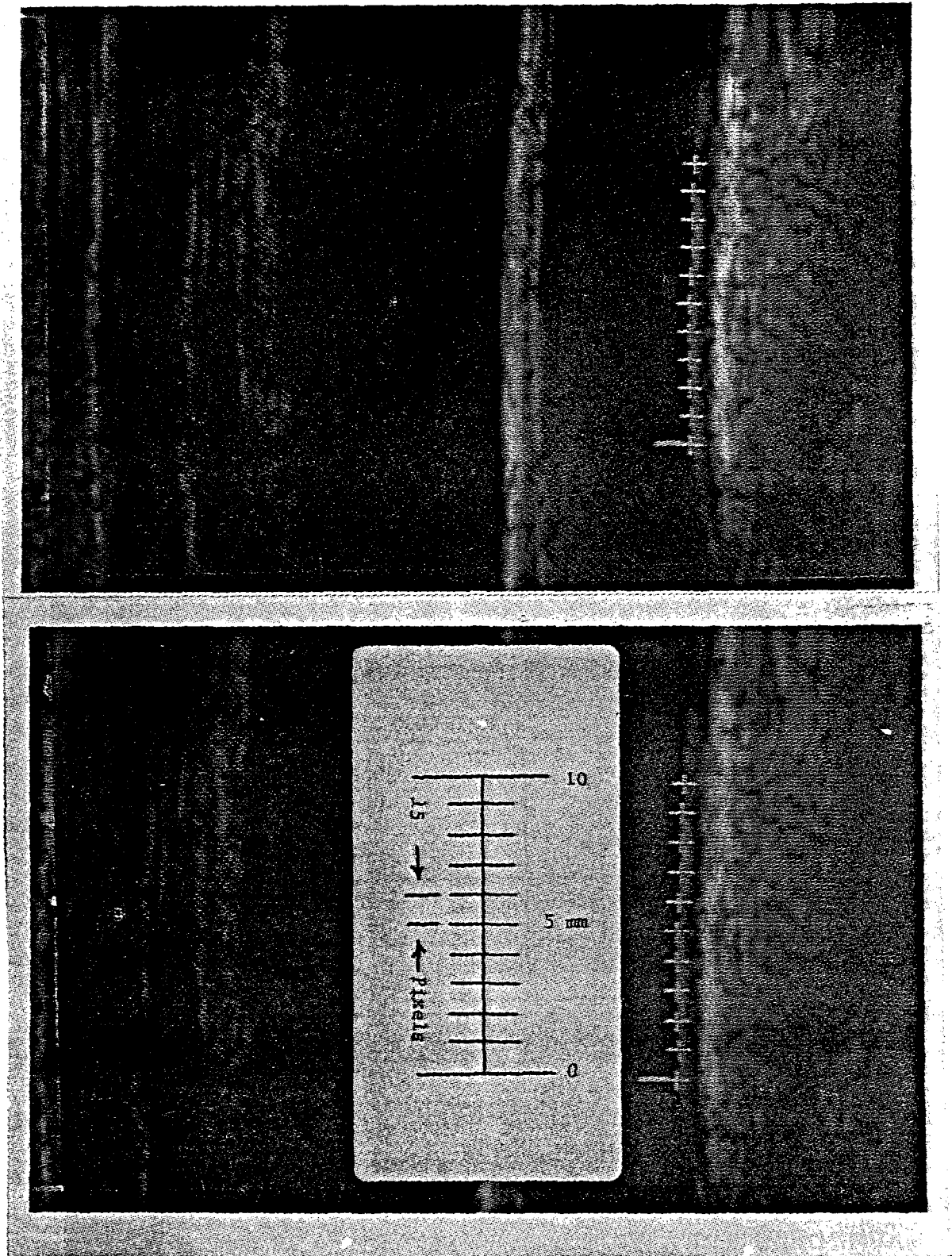


Figure 6.8.A Placement of Crosshairs on B-mode Image Boundaries

6.9 Subjective Comments on the B-Mode Image Frames

Following each frame selected for measurement from the optical disc, readers record the following information: (to be stored along with other computer data on each frame.)

1. Their reader identification number
2. Presence of lesions (within the measurement area)
3. Presence of shadowing (within the measurement area)
4. Alert value (lumen diameter < 2 mm) present
5. Quality of each interface
 - 0 - not readable
 - 1 - poor
 - 2 - fair
 - 3 - good
 - 4 - excellent

The menu is shown below:

Reader Number _____
 Lesion? Y or N _____ Shadow? Y or N _____
 Alert Value? Y or N _____
 Quality of interfaces: _____
 Correct? Y or N _____

(Any information entered from the menu may be corrected if the response is NO; a YES response routes this information to computer memory.)

This information that is input by the reader is shown in Figure 6.9.A along with other data that is stored in the computer.

6.10 Procedure for Reporting Alert Values

Procedures for reporting possible alert values to the Ultrasound Director at the field centers are initiated when the minimum residual lumen in the carotid artery is ≤ 2 mm. Identification of these possible alert values is carried out by the sonographers performing the scans at the field centers or by the readers at the Ultrasound Reading Center. When a field center sonographer suspects one or more sites on the carotid artery meet the possible alert value criterion, the back-up copy of the participant's tape is sent to the field center's Ultrasound Director for reading, in addition to the regular data transfer procedures to the Ultrasound Reading Center.

When an Ultrasound Reading Center reader measures or suspects that the distance between boundaries 3 and 4 is ≤ 2 mm (readings at the URC are limited to ARIC protocol sites), the chief reader is notified immediately to visually confirm the reading. The alert value variable in the database (see Section 6.9) is recorded as "Yes" for storage in the ultrasound database. An electronic mail message is sent to the field center the same day identifying the ARIC participant and the site(s) in the carotid artery in which a possible alert value(s) has been measured or is suspected. The participant's ARIC ID and the date of the E-mail alert value transmission to the field center are logged in the URC Alert Value Log for future reference.

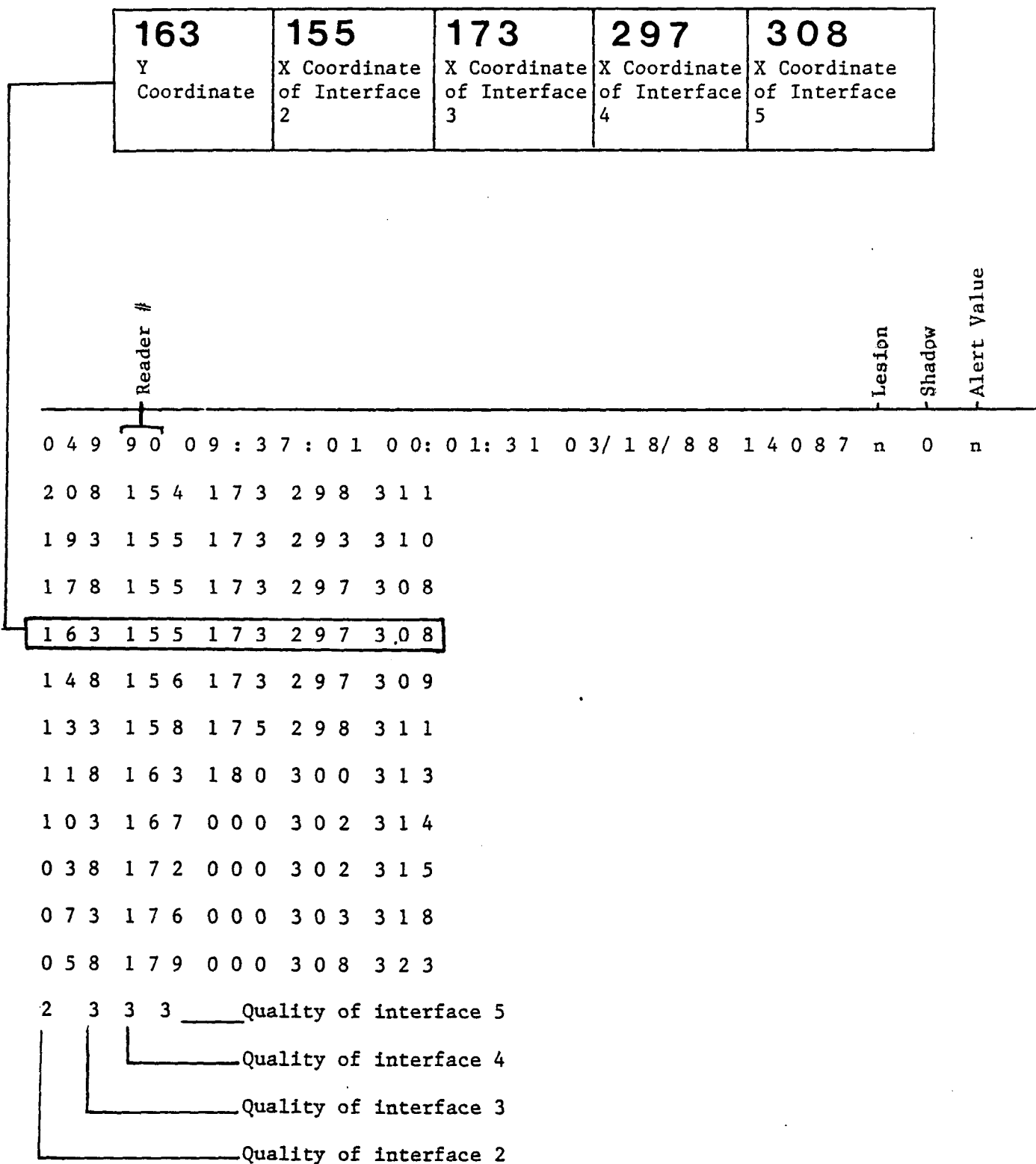


Figure 6.9.A B-Mode Image Data Stored in Computer

Upon receipt of an E-mail message of a possible alert value, the procedures in the field center become identical to those followed if an alert value is suspected by the sonographer. The resolution of possible alert values is the function of the field centers; at the recommendation of the field center Ultrasound Director in accordance with local community standards, a statement documenting the possible abnormal findings of the ultrasound scan may be included in the Summary of Results for ARIC Participants and their Physicians. Field centers keep a log of actual alert values.

7. REFERENCES

1. F.W. Kremkau and J.W. Taylor, "Artifacts in Ultrasound Imaging," J. Ultrasound Med. 5: 227-237 (1986).
2. P. Pignoli, et. al., "Intimal Plus Medial Thickness of the Arterial Wall: a direct measurement with ultrasound imaging", Circulation 74: 1399-1406 (1986).

REVIEW

Artifacts in Ultrasound Imaging

Frederick W. Kremkau, PhD, Kenneth J. W. Taylor, PhD, MD

Ultrasound imaging artifacts of acoustic origin relating to resolution, propagation path, and attenuation are reviewed. Lateral and axial resolution limitations are artifactual in nature since a failure to resolve means a loss of detail and two adjacent structures may be visualized as one. Apparent resolution close to the transducer (speckle) is not directly related to tissue texture but is a result of interference effects from the distribution of scatterers in the tissue. Reverberation produces a set of equally spaced artifactual echoes distal to the real reflectors. The mirror image artifact is the presentation of objects that are present on one side of a strong reflector, appearing on the other side as well. Shadowing and enhancement are useful artifacts for determining the nature of masses. Enhancement results from low attenuation objects in the sound path while shadowing results from strongly reflecting or strongly attenuating objects. Additional artifacts include section thickness, refraction, multipath, side lobe, grating lobe, focal enhancement, comet tail, ring down, speed error, and range ambiguity. (Key words: ultrasonography; artifacts; resolution; shadowing; enhancement; reverberation)

The word *artifact* comes from the Latin *arte* (by skill) and *factum* (to do). Webster's Ninth New Collegiate Dictionary states that the earliest recorded use of this word in English occurred in 1821. Definitions include 1) a characteristic product of human activity, and 2) a product of artificial character due to an extraneous agency. The use of the word in this review relates to the second definition. Imaging artifacts are display phenomena not properly representing the structures to be imaged. They are of various types, as follows:

1. acoustic: error in presentation;
2. optical illusion: error in perception;
3. anatomic: error in interpretation (often called a pitfall);
4. other: electrical noise, dust in photographic system, etc.

In this review, only artifacts of acoustic origin are

Received February 11, 1985, from the Department of Diagnostic Radiology, Yale University School of Medicine, New Haven, Connecticut. Revised manuscript accepted for publication September 3, 1985.

Address correspondence and reprint requests to Dr. Kremkau: Center for Medical Ultrasound, Bowman Gray School of Medicine, Winston-Salem, NC 27103.

Table 1. Ultrasound Imaging Artifacts of Acoustic Origin

Resolution Group

1. Axial Resolution
2. Lateral Resolution
3. Speckle
4. Section Thickness

Propagation-Path Group

1. Reverberation
2. Refraction
3. Multipath
4. Mirror Image
5. Side Lobe
6. Grating Lobe

Attenuation Group

1. Shadowing
2. Enhancement
3. Refraction (Edge) Shadowing
4. Focal Enhancement

Miscellaneous Group

1. Comet Tail
 2. Ring Down
 3. Speed Error
 4. Range Ambiguity
-

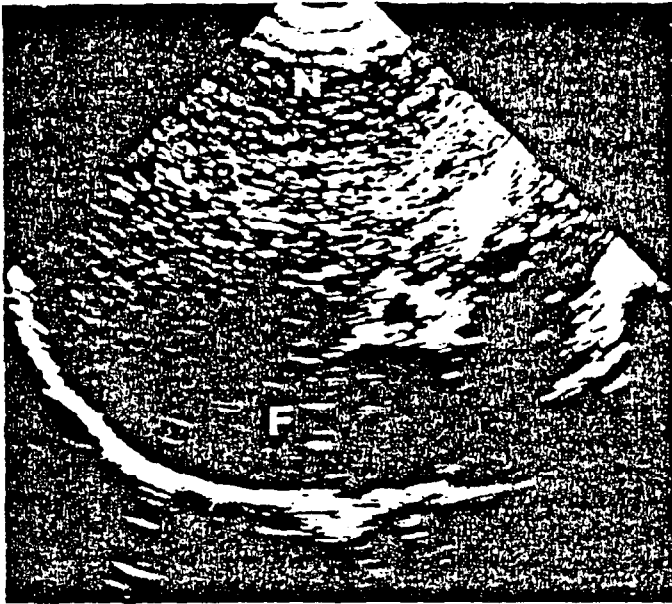


Figure 1 (*left*). Sagittal scan of a normal liver. Lateral resolution is degraded in the far zone (F). Focal banding (B) is seen in the focal region. Apparent resolution in the near zone (N) is partially a result of acoustic speckle. (Courtesy of J.J. Sivo, Yale-New Haven Hospital)

Figure 2. Dermoid cyst in the female pelvis. The boundary between lipid and non-lipid regions is presented well axially in A (*below, left*). In B (*below, right*), the same boundary appears thicker when imaged laterally with the patient erect. (Courtesy of T.S. Richman, Yale University)



discussed. These acoustic artifacts cause errors in presentation of anatomic structures. Some are useful and desirable while others are not. For example, enhancement beyond an echogenic fluid collection permits its true cystic nature to be appreciated. Automatic correction of this artifact would preclude perception of this important information and is, therefore, not desirable. The unde-

sirable artifacts that hinder correct interpretation must be avoided or at least recognized as such in order to make the correct diagnosis.

Acoustic artifacts in ultrasound imaging occur as presentations on the display that, with respect to the anatomy in question, are added (not real), are missing, or are of improper location, brightness, shape, or size. They result when the assumptions

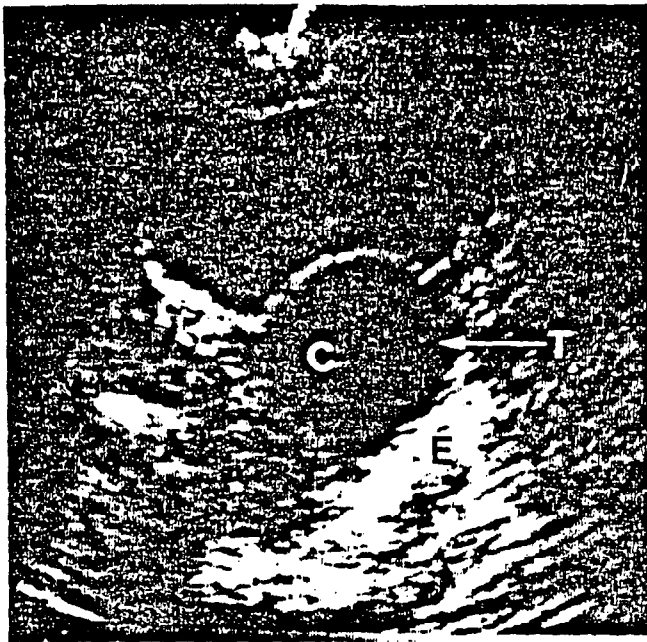


Figure 3 (left). A pelvic cyst (C) showing internal section-thickness artifact (T) and distal enhancement (E). (Courtesy of J.J. Sivo, Yale-New Haven Hospital)

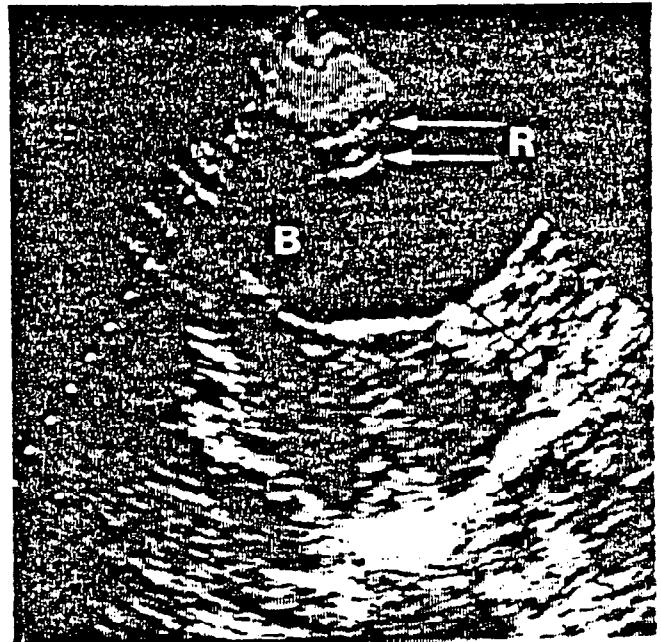


Figure 4 (right). Reverberation (R) and section-thickness artifact (T) in the bladder (B). (Courtesy of J.J. Sivo, Yale-New Haven Hospital)

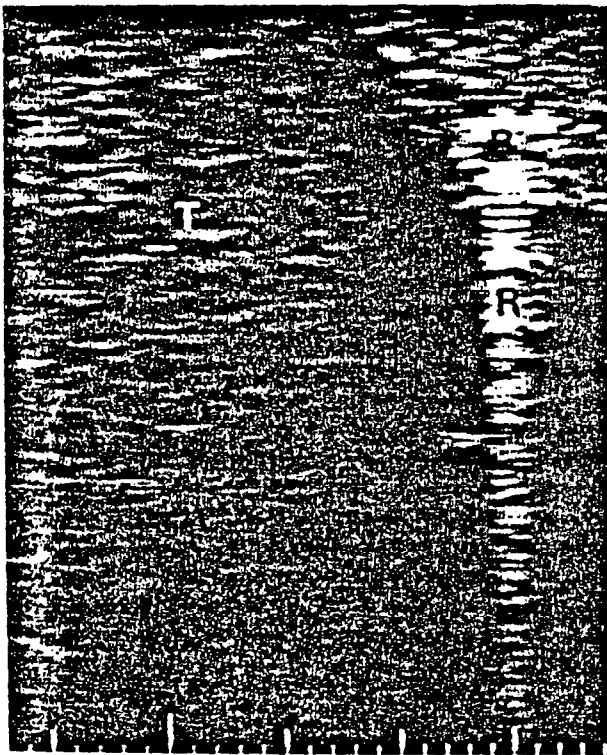


Figure 5 (left). Short-range reverberation (R) from an air gun BB (B) adjacent to the testicle (T). (Courtesy of A.T. Rosenfield Yale University)

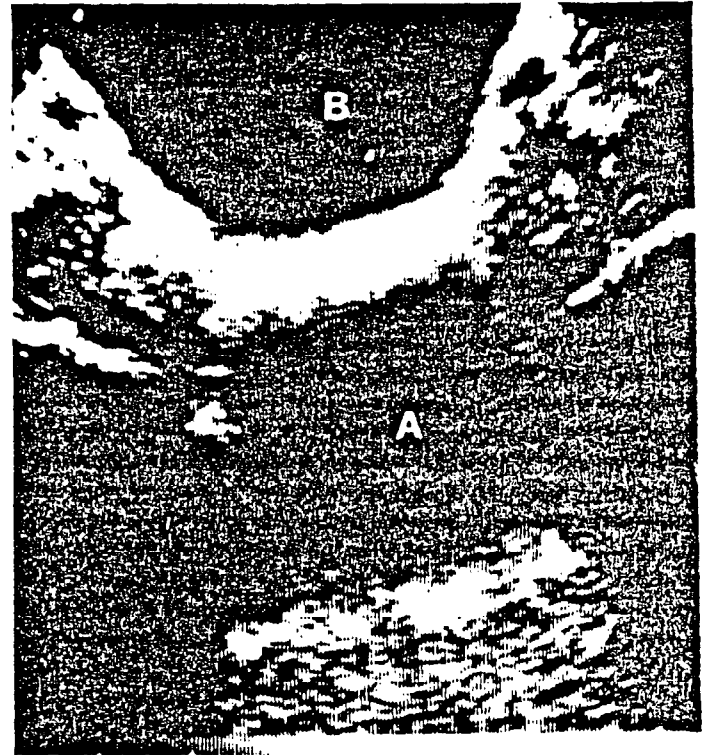


Figure 6 (right). Long-range reverberation causes bladder (B) to be imaged a second time (A).

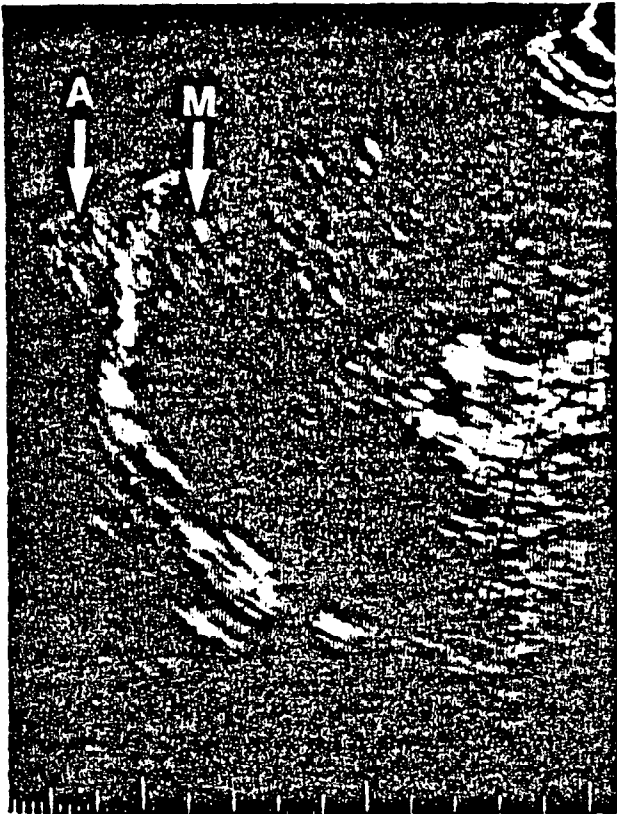


Figure 7. An echoic mass (M) in the liver is also artifactually represented (A) superior to the diaphragm. (Courtesy of J.J. Sivo, Yale-New Haven Hospital)

made by the ultrasound imaging instrument are incorrect and lead to errors in imaging. These assumptions include:

1. sound travels in straight lines;
2. echoes originate only from objects located on the transducer axis;
3. intensity of returning echoes is directly related to the scattering strength of imaged objects; and
4. distance is proportional to the round-trip travel time—13 microseconds per centimeter of depth.

Some artifacts are produced by improper equipment operation (e.g., improper transducer location or orientation information sent to the display) or settings (e.g., incorrect receiver compensation setting). Some are caused by improper scanning technique (e.g., allowing patient or organ movement during scanning with a static imaging instrument). These could be included in category 4 of the list above. Others are inherent in the ultrasound diagnostic method (such as categories 1 and 2 in the list above) and can occur even with proper equipment and technique. The acoustic artifacts reviewed here are of that nature. They are listed in table 1, grouped as they are considered in this review. The physical principles underlying the occurrence of

these artifacts are presented elsewhere,¹ as are discussions of acoustic artifacts.¹⁻⁴

RESOLUTION GROUP

Spatial resolution limitations are artifactual in nature, since they cause closely spaced objects to appear merged together and tiny objects to be presented larger than they are. A sagittal scan of a normal liver is shown in figure 1. Axial resolution is seen to be relatively constant with depth. However, lateral resolution varies with depth, being optimum in the focal region of the transducer. Axial resolution is equal to half the pulse length and lateral resolution is equal to the pulse width (beam width) in the image plane. Since pulse width is normally larger than pulse length, axial resolution is better than lateral (fig. 2).

The apparently excellent resolution close to the transducer is artifactual in nature. This parenchymal echo pattern, normally interpreted to be "tissue texture," does not represent a one-to-one correspondence of scatterers to brightness dots, but rather patterns of constructive and destructive interference of returning echoes from a scatterer distribution in the interrogated tissue volume. This interference pattern, called acoustic speckle,⁵⁻⁹ is a major source of ultrasound image degradation. It can be viewed as a form of acoustic noise. Lack of correlation between apparent and actual resolution in an image has been shown to be caused by speckle.¹⁰ Smith and Lopez have shown that detection of high-contrast and low-contrast objects is limited by spatial resolution and image speckle, respectively.¹¹ Morrison et al. have described and explained speckle motion in real-time imaging.¹² This motion bears no simple relation to tissue or transducer motion and may be very misleading. Digital and photographic averaging¹³ and deconvolution¹⁴ have been used to reduce speckle and improve images.

The section thickness artifact within a pelvic cyst and the urinary bladder is shown in figures 3 and 4. This weakly echoic region might suggest the presence of solid material but is more likely artifact. It results from the finite width of the imaging pulse in the direction perpendicular to the scan plane. This produces an imaged section of tissue (through the scanning process) with some thickness, but the echoes in that slice are compressed into an infinitely thin slice for presentation. The artifactual region in this scan represents echoes received from the edge of the interrogated slice either toward or away from the viewer. Scattering from the cyst or bladder boundary there has been received and placed on the image (as if within the cyst or bladder). Goldstein and Madrazo described this artifact and demonstrated its effects in gallbladder, cysts, and ascites.¹⁵ Filling in of images of cysts^{16,17} and cardiac septal defects¹⁸ and mimicking of gall-

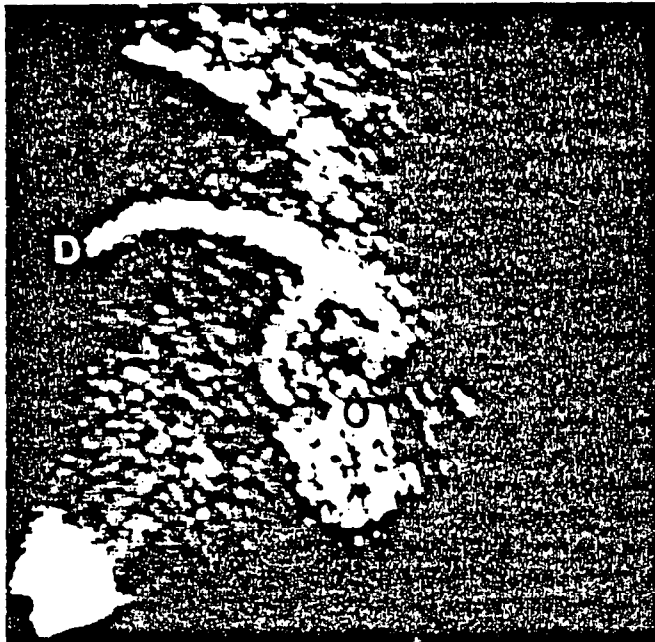
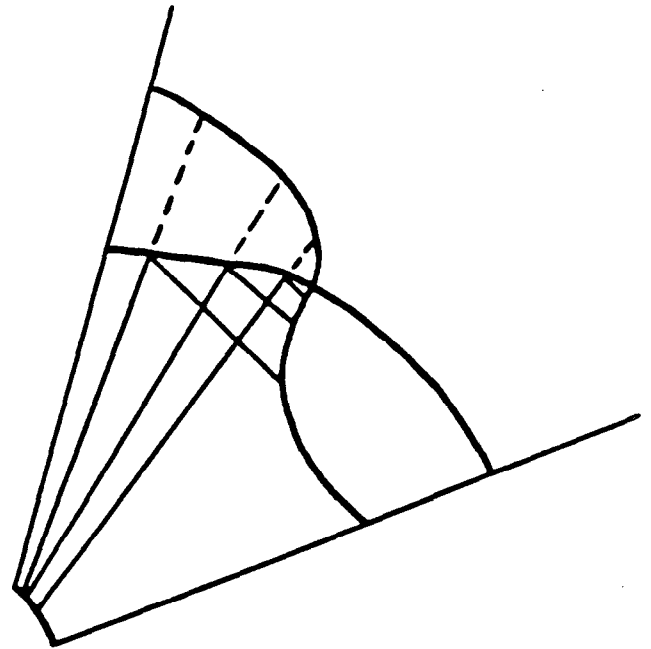


Figure 8. A (left), an unusual presentation of mirror-image artifact around the diaphragm (D). The shape of the artifact (A) is not the same as that of the object (O) (probably bowel). The explanation of this result is shown in B (right). (Courtesy of J.J. Sivo, Yale-New Haven Hospital)



bladder sludge¹⁹ have been attributed to this artifact.

PROPAGATION-PATH GROUP

If two or more reflectors are encountered in the sound path, multiple reflections (reverberation)

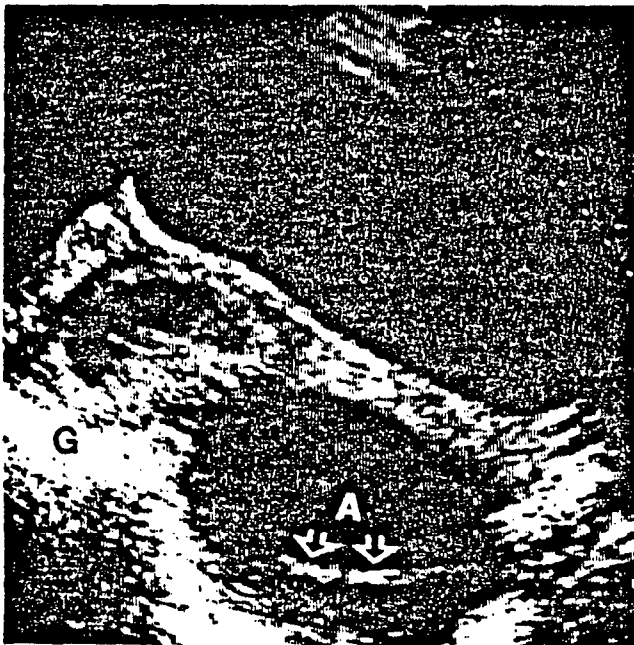


Figure 9. Side lobe artifact (A) appears in a scan of a corpus luteal cyst but not in other scans of the same cyst. The reflector generating this artifact is likely bowel gas (G). (Courtesy of A. Carter, Yale University)

will occur. These may be sufficiently strong to be detected by the instrument and to cause confusion on the display. An example of this artifact in the urinary bladder is shown in figure 4. The internal echoes presented should not be there. They represent subsequent (later, presented deeper) echoes from traversing the path between two reflectors several times.¹ This results in additional reflectors that are not real being placed on an image. They will be placed behind the second real reflector at separation intervals equal to the separation between the first and second real reflectors. Each subsequent reflection is weaker than prior ones, but this will be at least partially compensated for by the compensation function (TCC) of the receiver. The first of the two reflectors is usually the transducer face. An exception to this, reverberation from within metal objects^{20,21} (fig. 5), is quite pronounced and makes them easy to locate and identify. They usually produce a series of closely spaced echoes because of their small dimensions and high sound speed. This has been called the "comet-tail artifact" and is discussed in the "Miscellaneous Group" section. An extreme example of reverberation is shown in figure 6, where the urinary bladder is imaged twice.

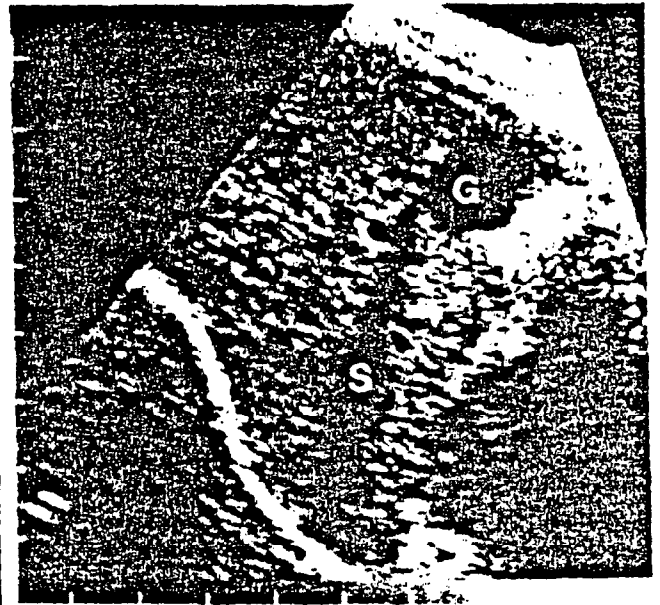
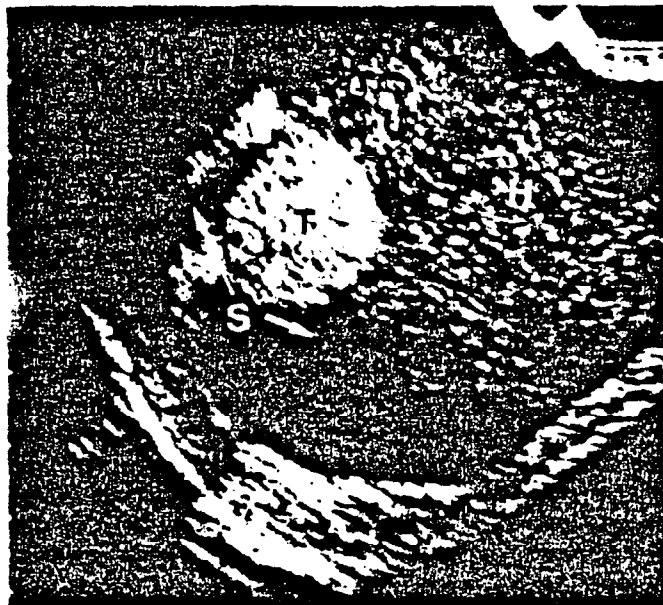
Refraction can cause a reflector to be improperly positioned on the display. The change in direction of sound as it crosses a boundary where a speed change occurs causes lateral error in reflector positioning.¹ Such improper lateral repositioning of structures has been demonstrated in phantoms.²² Several effects of in vivo refraction have been reported.²³⁻²⁹



Figure 10 (left). Shadowing (S) from a gallstone (G) and enhancement (E) from the gallbladder. (Courtesy of J.J. Sivo, Yale-New Haven Hospital)

Figure 11 (below, left). Scattering from particles in hemothecce (H) simulates a solid mass surrounding the testicle (T). Shadowing from the testicle (or enhancement from hemothecce) indicates the cystic nature of this collection.

Figure 12 (below, right). Edge shadowing (S) from the gallbladder (G). (Courtesy of J.J. Sivo, Yale-New Haven Hospital)



The term, multipath, describes the situation in which the paths to and from a reflector are different.¹ The longer path that the sound takes traveling to or from a reflector results in an axial error in reflector positioning (increased range). Refraction and multipath positioning errors are normally relatively small and contribute to general degradation of the image rather than to gross errors in structure location.

The mirror-image artifact³⁰ is most commonly seen around the diaphragm^{31,32} although it occasionally occurs elsewhere.³³ Since the air in the lungs acts as a total reflector of sound, imaging superior to the diaphragm³⁴ is not expected. Yet tissue appears to be routinely imaged above the di-

aphragm. This is because the sound is reflected off the diaphragm on its way to another reflector and back. The instrument assumes a straight line path and places the reflector superior to the diaphragm.¹ An echoic mass correctly located in the liver and also artifactually presented superior to the diaphragm is shown in figure 7. An example of a more unusual case of mirror image in which the artifactual object looks substantially different than the real one is given in figure 8.

Side lobes (from single-element transducers) and grating lobes (from arrays), beams in addition to the primary sound beam, cause objects that are not directly in front of the transducer to be displayed incorrectly in lateral position (fig. 9).^{1,4,35}

ATTENUATION GROUP

Shadowing is the reduced amplitude of echoes caused by intervening structures with high attenuation.³⁶ A pronounced shadow distal to a gallstone is shown in figure 10. The stone shows brightly, indicating a strong reflection. This, in addition to the likely larger absorption in the stone, causes the sound passing through it to be weak. This results in weak echoes (dark presentation) of tissues distal to the stone.³⁷ The greater the amount of the beam cross-section attenuated, the greater the shadowing. Therefore, the location of the attenuating object relative to the focus determines how much shadowing occurs for a given object.³⁸⁻⁴⁰ Stone shadowing has been discussed extensively.⁴¹⁻⁴⁴ Loss of femur shadowing between 20 and 32 weeks' gestation is suggestive of osteogenesis imperfecta.⁴⁵

Enhancement is the increased relative amplitude of echoes caused by an intervening structure of low attenuation. Enhancement distal to the gallbladder is shown in figure 10; an example of enhancement distal to a pelvic cyst is given in figure 3. As with shadowing, small cyst location relative to the focus is important in producing observable enhancement.¹⁷

Shadowing and enhancement help to determine the cystic nature of echogenic fluid collections (fig. 11).

Shadowing from the edge of a curved object can



Figure 13. A case of reverberation mimicking enhancement. An anechoic mass is located at the diaphragm. The apparent enhanced transmission distal to the mass (into the lung) is a result of two reverberations within the anechoic mass. (Courtesy of S.R. Schwimer, Lebovic and Schwimer, P.C.)

occur as a result of refraction.⁴⁶⁻⁴⁸ In figure 12, such edge shadowing from the gallbladder is shown. The shadow results from reduced intensity as the beam spreads after refraction through a curved surface.⁴⁷ Edge enhancement (also due to refraction) can also occur,⁴⁷ although edge shadowing is the more common occurrence.

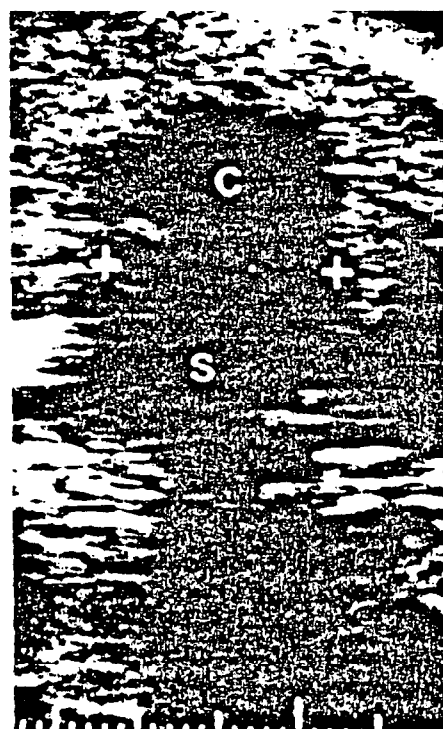
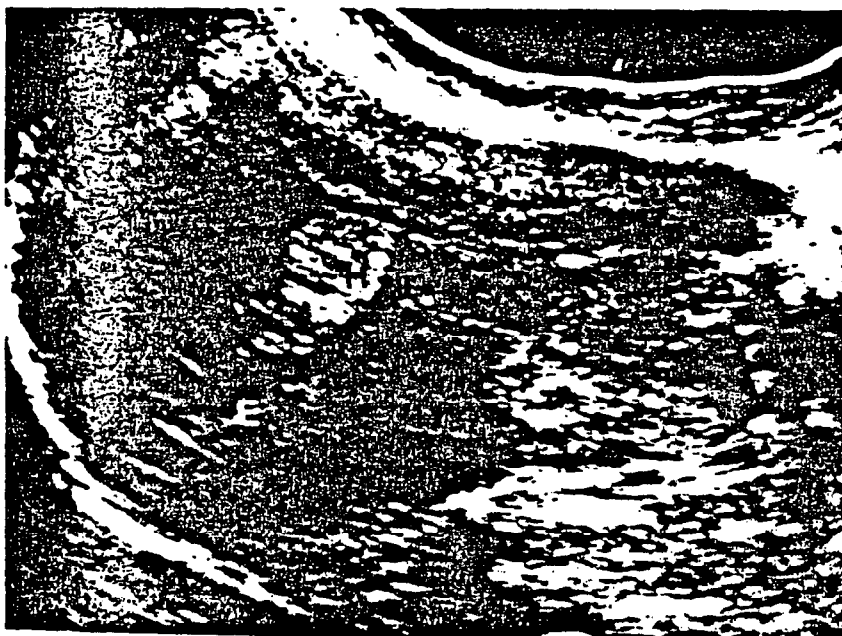


Figure 14 (*left*). Hyperechoic hemangioma (H) with distal enhancement (E). (Reprinted with permission from Taylor KJW: Atlas of Ultrasonography. New York, Churchill-Livingstone, 1985, ch 2)

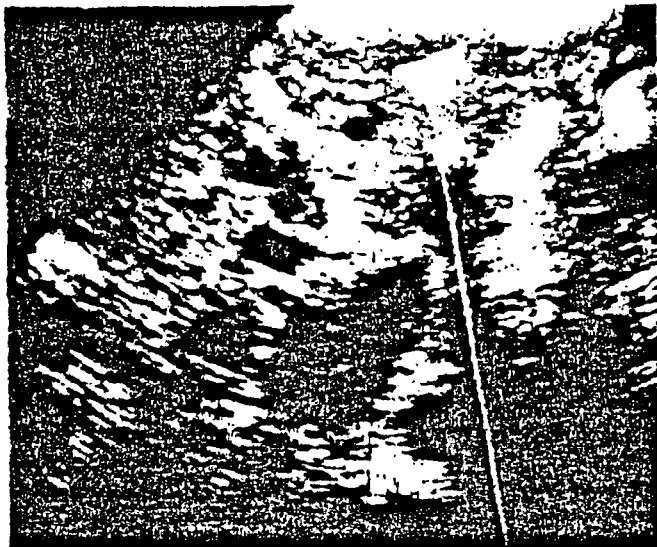
Figure 15 (*right*). Anechoic breast carcinoma (C) with distal shadowing (S).



Figure 16 (left). Comet tail from the diaphragm.

Figure 17 (below, left). Ring down from air in the bile duct. (Reprinted with permission from Taylor KJW: Atlas of ultrasonography. New York, Churchill-Livingstone, 1985 ch 2)

Figure 18 (below, right). Adrenal myelolipoma with 11-cm axial dimension on ultrasound scan. The distal diaphragm is displaced 2 cm. (Reprinted with permission from Richman TS, Taylor KJW, Kremkau FW: Propagation speed artifact in a fatty tumor (myelolipoma): significance for tissue differential diagnosis. J Ultrasound Med 2:45, 1983)



Increased brightness can also occur in the focal region of the transducer as a result of the higher intensity present there. Such banding or focal-region "enhancement" (not strictly enhancement according to the definition presented above) is seen in the liver in figure 1. In extreme cases of this, a non-existent mass might be suspected.

Apparent enhancement can occur where unexpected. The liver and an anechoic mass within or adjacent to the diaphragm are shown in figure 13. Enhancement appears to be present in the lung. On closer inspection it is seen that this apparent enhanced transmission is, rather, presentation of two reverberations from within the anechoic mass. The strong echo from the air boundary superior to the diaphragm appears distal to the mass (as it should). This boundary is then imaged two more times (superior to the diaphragm) as a result of reverberation.

All four combinations of high and low echogeni-

city and high and low attenuation in lesions (resulting in distal shadowing and enhancement, respectively) occur. This is because absorption is the dominant contributor to attenuation in tissues (scattering is a minor contributor). Thus, scattering level (echogenicity) and attenuation are not correlated. High echogenicity with shadow (gallstone) and low echogenicity with enhancement (gall-bladder) are shown in figure 10. These are the commonly occurring combinations. Examples of high echogenicity with enhancement (low absorption hemangioma) and low echogenicity with shadowing (high absorption breast carcinoma) are given in figures 14 and 15. In these cases it is clear that attenuation and echogenicity are uncorrelated.

MISCELLANEOUS GROUP

An example of a particularly well-localized "enhancement" phenomenon which has been termed

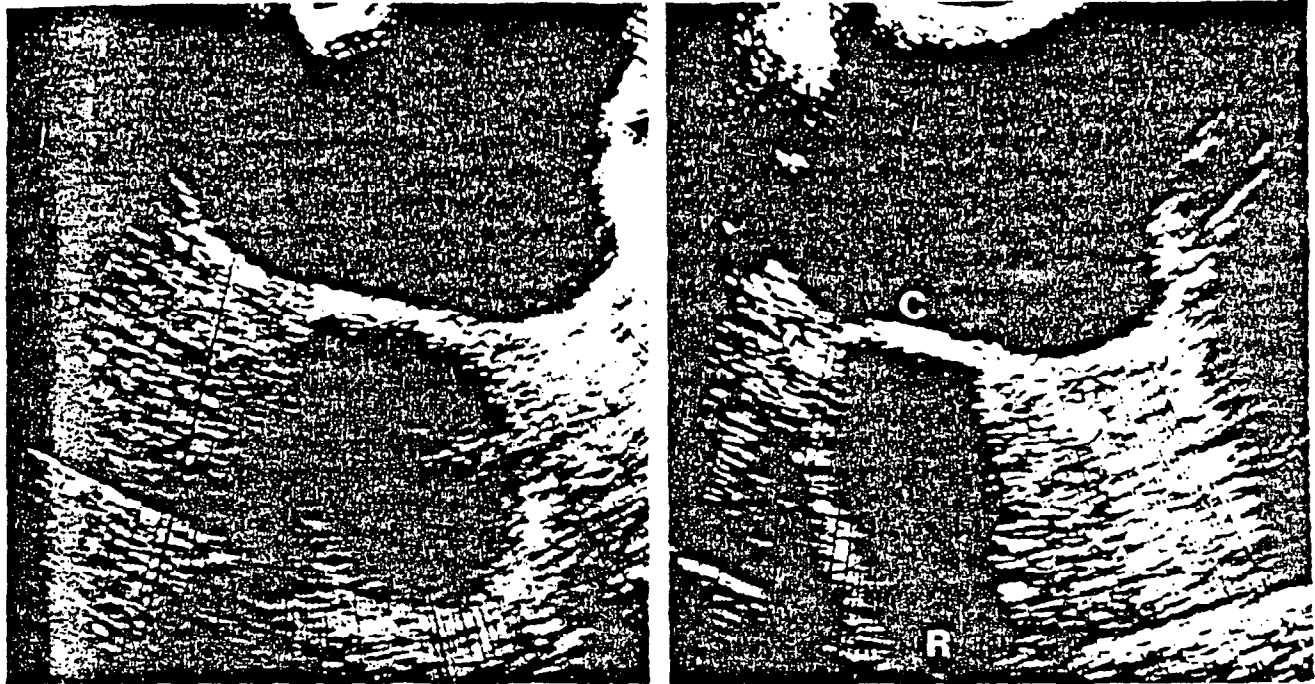


Figure 19. *A* (left), Apparent pelvic collection. *B* (right), a second view of the collection shown in *A* that indicates its artifactual nature. The distended urinary bladder compresses the empty rectum and completely fills the pelvis (the patient had a hysterectomy). The outer margin of the patient (determined by measurement) is indicated by the arrows. The coccyx (*C*) produces a distal shadow. Reverberation (*R*), i.e., a second image of the coccyx, and enhancement from increased gain (TGC) on the second round-trip fill in the shadow posteriorly. The combination of shadowing, reverberation, and enhancement produces the convincing but totally artifactual mass seen in *A*. (Reprinted with permission from Taylor KJW: Atlas of Ultrasonography. New York, Churchill-Livingstone, 1985, ch 2)

comet-tail artifact is shown in figure 16.^{49,50} It appears to be a series of closely spaced discrete echoes similar to the short-range reverberation in figure 5. The example in figure 17 appears to be fundamentally different from this. Discrete echoes cannot be identified because they are too close to-

Table 2. Artifacts Listed by Manifestation

Added Objects	Missing Objects	Incorrect Object Brightness
Speckle	Resolution	Shadowing
Section Thickness		Enhancement
Reverberation		
Mirror Image		
Comet Tail		
Ring Down		
Incorrect Object Location	Incorrect Object Size	Incorrect Object Shape
Refraction	Resolution	Resolution
Multipath	Refraction	Refraction
Side Lobe	Speed Error	Speed Error
Grating Lobe		
Speed Error		
Range Ambiguity		

gether, rather, a continuous emission of sound from the origin may be occurring. The mechanism for such a continuous effect (termed ring-down artifact⁵¹) is not well understood but may be caused by a resonance phenomenon associated with gas bubbles.⁵¹

Propagation speed error^{52,53} occurs when the assumed value for propagation speed by the instrument is incorrect. If the actual speed is greater than that assumed, the calculated distance to a reflector is too small and the display will place the reflector too close to the transducer. If the actual speed is less, the reflector will be displayed too far from the transducer. A recent report has shown that at least some of this artifact is due to refraction.²⁵ Refraction and propagation speed error can also cause a structure to be displayed with incorrect size and shape. An example of these effects is shown in figure 18, where an adrenal myelolipoma measuring 9 cm in diameter on a computed tomographic (CT) scan appears larger on an ultrasound scan because of the low sound speed within it.

In ultrasound imaging, it is assumed that for each pulse produced, all reflections are received before the next pulse is sent out. If this is not the case, ambiguity can result.⁵⁴ This is because the instrument calculates the distance to a reflector from the echo arrival time assuming that all echoes were

Table 3. Artifacts and Their Causes

Artifact	Cause
Axial Resolution	Pulse Length
Lateral Resolution	Pulse Width
Speckle	Interference
Section Thickness	Pulse Width
Reverberation	Reflection
Refraction	Refraction
Multipath	Reflection
Mirror Image	Reflection
Side Lobe	Side Lobe
Grating Lobe	Grating Lobe
Shadowing	Attenuation
Enhancement	Attenuation (low)
Refraction Shadowing	Refraction
Focal Enhancement	Focusing
Comet Tail	Reverberation
Ring Down	Resonance
Speed Error	Speed Error
Range Ambiguity	High Pulse Repetition Frequency

generated by the last emitted pulse. The maximum depth to be imaged unambiguously by an instrument determines its maximum pulse repetition frequency. In dynamic imaging, the maximum depth imaged unambiguously (cm) multiplied by the lines per frame and by frame rate (frames per second) cannot exceed 77,000. Otherwise, distant reflectors will be placed at distances too close to the transducer. This observation has been reported in echocardiography.⁵⁵

CONCLUSION

We conclude with an interesting and sobering case. In figure 19A, a pelvic collection in a patient in whom we were searching for an abscess is shown. This pelvic collection is completely artifactual! Another view with the distended urinary bladder completely filling the pelvis (the patient had a hysterectomy) is shown in figure 19B. The coccyx (C) produced a distal shadow. Reverberation in the bladder images the coccyx a second time (R). Distal filling (in figure 19A) occurs this time because time-gain-compensation has over-increased the gain (relatively low attenuation in the urine). This deceiving image resulted from the combination of three artifacts—shadowing, reverberation, and enhancement. The artifactual mass is totally located outside the patient, whose outer margin is indicated by the arrows in figure 19B.

In this review we have discussed 18 ultrasound imaging artifacts of acoustic origin. They are listed in Table II according to the ways in which they are manifested. Explanations of how these artifacts occur are listed in Table III. In some cases, artifact names are identical to their causes.

Some artifacts are useful in interpretation and diagnosis (e.g., shadowing and enhancement), while some can cause confusion and error (e.g., section thickness and reverberation). A proper understanding of artifacts and how to deal with them when encountered enables sonographers and sonologists to use them in diagnosis while avoiding the pitfalls which they can cause.

REFERENCES

1. Kremkau FW: Diagnostic Ultrasound: Principles, Instrumentation and Exercises, 2nd ed. Orlando, Grune & Stratton, 1984
2. Taylor KJW: Atlas of Ultrasonography, 2nd ed. New York, Churchill-Livingstone, 1985, ch 2
3. Taylor KJW, Jacobson P, Talmont CA, et al: Manual of Ultrasonography, New York, Churchill-Livingstone, 1980, ch 3
4. Laing FC: Commonly encountered artifacts in clinical ultrasound. *Sem Ultrasound* 4:27, 1983
5. Burckhardt CB: Speckle and ultrasound B-mode scans. *IEEE Trans Sonics Ultrasonics* 25:1, 1978
6. Abbott JG, Thurstone FL: Acoustic speckle: theory and experimental analysis. *Ultrason Imag* 1:303, 1979
7. Jaffe CC, Harris DJ: Sonographic tissue texture: influence of transducer focusing pattern. *AJR* 135:343, 1980
8. Wells PNT, Halliwell M: Speckle in ultrasonic imaging. *Ultrasonics* 19:225, 1981
9. Wagner RF, Smith SW, Sandrik JM, et al: Statistics of speckle in ultrasound B-scans. *IEEE Trans Sonics Ultrasonics* 30:156, 1983
10. Flax SW, Glover GH, Pelc NJ: Textural variations in B-mode ultrasonography: a stochastic model. *Ultrason Imag* 3:235, 1981
11. Smith SW, Lopez H: A contrast-detail analysis of diagnostic ultrasound imaging. *Med Phys* 9:4, 1982
12. Morrison DC, McDicken WN, Smith DSA: A motion artefact in real-time ultrasound scanners. *Ultrasound Med Biol* 9:201, 1983
13. Sommer FG, Sue JY: Image processing to reduce ultrasonic speckle. *J Ultrasound Med* 2:413, 1983
14. Dickinson RJ: Processing of ultrasound images to reduce speckle. In: McAvoy BR (ed): 1982 IEEE Ultrasonics Symposium Proceedings. New York, Institute of Electrical and Electronics Engineers, Inc., 1982, p 655
15. Goldstein A, Madrazo BL: Slice-thickness artifacts in gray-scale ultrasound. *JCU* 9:365, 1981
16. Carson PL, Oughton TV: A modeled study for diagnosis of small anechoic masses with ultrasound. *Radiology* 122:765, 1977
17. Jaffe CC, Rosenfield AT, Somer G, et al: Technical factors influencing the imaging of small anechoic cysts by B-scan ultrasound. *Radiology* 135:429, 1980
18. Jaffe CC, Atkinson P, Taylor KJW: Physical parameters affecting the visibility of small ventricular septal defects using two-dimensional echocardiography. *Inv Radiology* 14:149, 1979
19. Fiske CE, Filly RA: Pseudo-sludge: a spurious ultrasound appearance within the gallbladder. *Radiology* 144:631, 1982
20. Wendell BA, Athey PA: Ultrasonic appearance of metallic foreign bodies in parenchymal organs. *JCU* 9:133, 1981
21. Schwartz DB, Zweibel WJ, Zagzebski J, et al: The use of real-time ultrasound to enhance fetoscopic visualization. *JCU* 11:161, 1983
22. Madsen EL, Zagzebski JA, Ghilardi-Netto T: An anthropomorphic torso section phantom for ultrasonic imaging. *Med Phys* 7:43, 1980
23. Buttery B, Davison G: The ghost artifact. *J Ultrasound Med* 3:49, 1984
24. Bonhof JA, Bonhof B, Linhart P: Acoustic dispersing lenses cause artifactual discontinuities in B-mode ultrasonograms. *J Ultrasound Med* 3:5, 1984

ARTIFACTS IN ULTRASOUND IMAGING — VOLUME 5, APRIL 1986

25. Mayo J, Cooperberg PL: Displacement of the diaphragmatic echo by hepatic cysts: a new explanation with computer simulation. *J Ultrasound Med* 3:337, 1984
26. Savakus AD, Shung KK, Miller NB: Distortions of ultrasonic field introduced by the rib cage in echocardiography. *JCU* 10:413, 1982
27. Muller N, Cooperberg PL, Rowley VA, et al: Ultrasonic refraction by the rectus abdominis muscles: the double image artifact. *J Ultrasound Med* 3:515, 1984
28. Sauerbrei EE: The split image artifact in pelvic sonography: the anatomy and physics. *J Ultrasound Med* 4:29, 1985
29. Shung KK, Fei DY, Bronez MA: Effects of atherosclerotic lesions on ultrasonic beam and CW Doppler signals. *JCU* 13:11, 1985
30. Gardner FJ, Clark RN, Kozlowski R: A model of a hepatic mirror-image artifact. *Med Ultrasound* 4:19, 1980
31. Lewandowski BJ, Winsberg F: Echographic appearance of the right hemidiaphragm. *J Ultrasound Med* 2:243, 1983
32. Wittich G, Czembirek H, Tscholakoff D: Retrocaval pseudolymphoma: clinical impact of the mirror artifact. *J Ultrasound Med* 1:173, 1982
33. Golding RH, Li DKB, Cooperberg PL: Sonographic demonstration of air-fluid levels in abdominal abscesses. *J Ultrasound Med* 1:151, 1982
34. Fried AM, Cosgrove DO, Nassiri DK, et al: The diaphragmatic echo complex: an in vitro study. *Invest Radiol* 20:62, 1985
35. Laing FC, Kurtz AB: The importance of ultrasonic side-lobe artifacts. *Radiology* 145:763, 1982
36. Mitchell SE, Gross BH, Spitz HB: The hypochoic caudate lobe: an ultrasonic pseudolesion. *Radiology* 144:569, 1982
37. Sommer FG, Taylor KJW: Differentiation of acoustic shadowing due to calculi and gas collections. *Radiology* 135:399, 1980
38. Jaffe CC, Taylor KJW: The clinical impact of ultrasonic beam focusing patterns. *Radiology* 131:469, 1979
39. Taylor KJW, Jacobson P, Jaffe CC: Lack of an acoustic shadow on scans of gallstones: a possible artifact. *Radiology* 131:463, 1979
40. Filly RA, Moss AA, Way LW: In vitro investigation of gallstone shadowing with ultrasound tomography. *JCU* 7:255, 1979
41. Carroll BA: Gallstones: in vitro comparison of physical, radiographic, and ultrasonic characteristics. *AJR* 131:223, 1978
42. Rubaltelli L, Talenti E, Rizzato G, et al: Gas-containing gallstones: their influence on ultrasound images. *JCU* 12:279, 1984
43. Parulekar SG: Ultrasonic detection of calcification in gallstones: "the reverberation shadow". *J Ultrasound Med* 3:123, 1984
44. King W, Kimme-Smith C, Winter J: Renal stone shadowing: an investigation of contributing factors. *Radiology* 154:191, 1985
45. Chervenak FA, Romero R, Berkowitz RL, et al: Antenatal sonographic findings of osteogenesis imperfecta. *Am J Obstet Gynecol* 143:228, 1982
46. Sommer FG, Filly RA, Minton MJ: Acoustic shadowing due to refractive and reflective effects. *AJR* 132:973, 1979
47. Robinson DE, Wilson LS, Kossoff G: Shadowing and enhancement in ultrasonic echograms by reflection and refraction. *JCU* 9:181, 1981
48. Ueda M, Ishii Y, Tabei M: Computer simulation of artifacts in B-mode images. In: McAvoy BR (ed). 1983 IEEE Ultrasonics Symposium Proceedings. New York: Institute of Electrical and Electronics Engineers, Inc., 1983, p 718
49. Ziskin MC, Thickman DI, Goldenberg NJ, et al: The comet tail artifact. *J Ultrasound Med* 1:1, 1982
50. Thickman DI, Ziskin MC, Goldenberg NJ, et al: Clinical manifestations of the comet tail artifact. *J Ultrasound Med* 2:225, 1983
51. Avruch L, Cooperberg PL: The ring-down artifact. *J Ultrasound Med* 4:21, 1985
52. Richman TS, Taylor KJW, Kremkau FW: Propagation speed artifact in a fatty tumor (myelolipoma): significance for tissue differential diagnosis. *J Ultrasound Med* 2:45, 1983
53. Pierce G, Golding RH, Cooperberg PL: The effects of tissue velocity changes on acoustical interfaces. *J Ultrasound Med* 1:185, 1982
54. Goldstein A: Range ambiguities in real-time ultrasound. *JCU* 9:83, 1981
55. Gomberg J, Andrews G, Power J, et al: Range-gated ambiguity as a cause of artifacts in real-time echocardiography. *J Ultrasound Med* 1 (Suppl):120, 1982

LABORATORY INVESTIGATION

ATHEROSCLEROSIS

Intimal plus medial thickness of the arterial wall: a direct measurement with ultrasound imaging

PAOLO PIGNOLI, M.D., ELENA TREMOLI, PH.D., ANDREA POLI, M.D., PIERLUIGI ORESTE, M.D., AND RODOLFO PAOLETTI, M.D.

ABSTRACT A study in vitro of specimens of human aortic and common carotid arteries was carried out to determine the feasibility of direct measurement (i.e., not from residual lumen) of arterial wall thickness with B mode real-time imaging. Measurements in vivo by the same technique were also obtained from common carotid arteries of 10 young normal male subjects. Aortic samples were classified as class A (relatively normal) or class B (with one or more atherosclerotic plaques). In all class A and 85% of class B arterial samples a characteristic B mode image composed of two parallel echogenic lines separated by a hypoechoic space was found. The distance between the two lines (B mode image of intimal + medial thickness) was measured and correlated with the thickness of different combinations of tunicae evaluated by gross and microscopic examination. On the basis of these findings and the results of dissection experiments on the intima and adventitia we concluded that results of B mode imaging of intimal + medial thickness did not differ significantly from the intimal + medial thickness measured on pathologic examination. With respect to the accuracy of measurements obtained by B mode imaging as compared with pathologic findings, we found an error of less than 20% for measurements in 77% of normal and pathologic aortic walls. In addition, no significant difference was found between B mode-determined intimal + medial thickness in the common carotid arteries evaluated in vitro and that determined by this method in vivo in young subjects, indicating that B mode imaging represents a useful approach for the measurement of intimal + medial thickness of human arteries in vivo.

Circulation 74, No. 6, 1399-1406, 1986

EXPERIMENTAL STUDIES on nonhuman primates¹ and on human subjects²⁻⁴ indicate that atherosclerotic lesions may progress without a reduction in luminal size because of dilatation of the arterial wall. The correct estimation of the size of atherosclerotic lesions therefore requires the simultaneous measurement of arterial wall thickness and residual luminal size. Atherosclerotic lesions in peripheral and carotid arteries are generally evaluated by the measurement of luminal size by invasive methods such as contrast angiography or by noninvasive ultrasound techniques. Gross and microscopic pathologic examination allows measurement of arterial wall thickness in tissue specimens only.

In our laboratory the measurement of the intimal + medial thickness has been attempted by the use of the noninvasive technique of B mode real-time imaging. This approach is currently used to measure organ dimensions^{5,6} as well as atherosclerotic lesions.⁷ A multicenter validation trial is now being conducted to determine the accuracy of B mode imaging vs that of angiography and histology.⁸ However, the potential of B mode imaging for direct measurement (i.e., not that from residual luminal size) of arterial wall thickness has not been assessed as yet.

In a previous study⁹ we found a significant correlation between results of gross pathologic evaluations and measurements by B mode imaging of arterial wall thickness. This study, however, was conducted on a limited number of normal or moderately diseased arterial segments.

The objectives of this study were (1) to determine the anatomic structures involved in ultrasound energy reflection in the arterial wall, (2) to determine the accuracy of intimal + medial thickness measurements by B mode imaging by comparison with findings of gross and microscopic pathologic examinations in nor-

From the Institute of Pharmacological Sciences, E. Grossi Paoletti Center for the Study of Metabolic Diseases, and Department of Surgery, Merate Hospital (Ussl 14), Merate (COMO), and the Institute of Pathology, Ente Ospedaliero Niguarda Ca Grande, Milan.

Supported by grants 83.02766.56 and 83.00553.57 of the National Research Council of Italy (CNR) and of the Italian Ministry for Education (Ministero della Pubblica Istruzione) 1983/1984.

Address for correspondence: Paolo Pignoli, M.D., Institute of Pharmacological Sciences, University of Milan, Via A. del Sarto 21, 20129 Milan, Italy.

Received Feb. 11, 1985; revision accepted Aug. 14, 1986:

PIGNOLI *et al.*

mal and pathologic arterial segments, and (3) to assess the feasibility of the measurement of intimal + medial thickness of arterial walls not only *in vitro* but also *in vivo* in human subjects.

The investigations were carried out *in vitro* with specimens of human aortas and common carotid arteries and *in vivo* in common carotid arteries of normal human subjects.

Materials and methods

Selection and procession of autopsy material. Abdominal aortas and common carotid arteries were removed at autopsy from 18 male subjects (age range 20 to 74 years), 12 to 20 hr after death.

Processing of aortic tissue. Aortic tissue was processed as previously described.⁹ Briefly, after longitudinal opening, rectangular strips (2 × 4 cm) of washed aortic tissue were longitudinally distended with a Plexiglas holder and fixed with formalin (10% for 10 hr). The segments to be studied were held in place with two metallic pins.

Processing of the common carotid artery. Common carotid arteries from young subjects (age range 20 to 25 years) were cannulated and perfused under pressure (90 mm Hg) with 10% buffered formalin for 10 hr.² After ultrasound interrogation, arteries were longitudinally opened and processed for gross and microscopic examination.

For experiments *in situ* common carotid arteries were cannulated during autopsy (24 to 30 hr after death) with a Foley catheter (Rusch-Gold Balloon catheter, SILKOLATEX, West Germany) and flushed under pressure (= 120 mm Hg) with saline. The arteries were processed as described for aortic tissue.

Gross and microscopic pathologic evaluation and classification. The specimens were cut longitudinally between two metallic pins previously fixed 10 mm apart to define the segment of interest. After ultrasound interrogation the specimens were stained for 12 hr in a supersaturated Sudan IV 38% isopropyl alcohol solution¹⁰ and then washed for 1 hr. After lipid staining, gross pathology of the artery was evaluated by a Zeiss operative microscope at 10× magnification. The media was differentiated from the adventitia on the basis of the color and consistency. The calibration of the ocular graduate scale to be used for thickness measurements was performed with a Zeiss test microobject. The resolution of the microscope was 20 paired lines per millimeter. After gross pathologic evaluation the specimens were cut, decalcified with a Standard Cal Ex Solution (Fisher Inc.) for 4 hr, and embedded in paraffin after dehydration. The histologic slices were stained with Verhoeff-Van Gieson and with hematoxylin-eosin stains and evaluated by optical microscopy.

Each sample was classified into one of two arbitrarily defined categories (A or B) on the basis of gross and microscopic characteristics. Class A included aortic segments that were macroscopically normal or had fatty streaks. Microscopically these samples showed homogenous intima with varying amounts of intimal thickening, intimal fibrosis, internal elastic lamina fragmentation, and duplication. The arterial segments included in class B showed a fibrous/muscular cap with a lipid and/or necrotic core. Microscopically, the intima showed focal areas of fibrotic smooth muscle cell proliferation, microcalcification, and necrosis.

The intimal + medial thickness of the arterial specimens was determined by gross pathologic and histologic examination. The thickness of adventitia and of the overall complex intima +

media + adventitia was measured by gross pathologic evaluation, whereas the intimal and the medial thicknesses were determined by histologic examination only.

Ultrasound instrumentation. A high-resolution small-part real-time scanner (Biosound, Biodynamics Inc, Indianapolis) was used. This instrument generates a wide-band ultrasonic pulse with a midfrequency of 8 MHz. The measured pulse length at 6 dB is 0.5 μsec, corresponding to an axial resolution of approximately 385 μm for an ultrasonic speed of 1540 m/sec. The reported¹¹ dynamic range is at least 70 dB. The lateral resolution is 0.5 mm. A standard 15 inch television monitor allowed magnification of the objects by 10×. Marker lines were present on the display for depth measurements, which were performed with a mechanical caliper.

Experiments *in vitro* were carried out by placing the aortic tissue specimens in a Plexiglas tank filled with water at room temperature (22° to 25° C). A mechanical system allowed optimal positioning of the ultrasound incident beam with respect to the area under evaluation. The intimal surface was exposed to the incident incoming pulse. Common carotid arteries were perfused with saline under pressure and ultrasound interrogation was carried out along their longitudinal axes. For each carotid artery four longitudinal measurements were obtained by rotating (90 degree increment) the vessels along the axis.

Experiments *in situ* were performed on common carotid arteries during autopsy (n = 3). B mode evaluations were carried out *in situ* on the same carotid arteries with and without the tissues located between the outer side of the vessels and the ultrasound probe (skin, subcutaneous tissue, and muscles). Scans were carried out in the anteroposterior and laterolateral planes of the lower and higher third of the common carotid arteries. After ultrasound interrogations the carotid arteries were removed and processed.

Experiments *in vivo* were carried out in 10 young subjects (age range 20 to 29 years) with no clinical sign of atherosclerotic disease.

The subjects were kept supine with the head slightly extended. Two longitudinal scans were performed in the anteroposterior and coronal planes of the lower and higher third of the right and left common carotid arteries. In both studies *in vitro* and *in vivo* only the far (deeper) wall image was evaluated.

Identification of the anatomic structures generating the B scan pattern. To define the anatomic structures generating the B scan pattern 10 of the 116 aortic specimens (five from class A and five from class B) were examined in dissection experiments. A 1.5 to 2.0 mm deep excision of the intima was performed in five class B arteries. These specimens were then interrogated by ultrasound and evaluated by microscopy. The findings on the B scan images obtained in the region of the inlay were compared with the structural changes induced by dissection in the arterial wall. To define the anatomic structures generating the outer line, arterial segments with and without the adventitia and the periarterial tissues were interrogated by ultrasound and evaluated by light microscopy.

Quantitative ultrasound and pathologic measurements were also made to determine the correlation between the B mode image and the anatomic structures. The distance separating the inner and outer lines shown in figure 1 was measured in 45 class A aortic specimens and defined as the B mode image of intimal + medial thickness. Without prior knowledge of ultrasound data, gross pathologic and histologic evaluations of the different tunicae were performed in all the aortic specimens (45 class A and 49 class B), and the results were correlated with those obtained by B mode imaging of the intimal + medial thickness.

To ensure that B mode, gross pathologic, and histologic evaluations were performed in the same location, the following criteria were used. (1) From each arterial specimen a segment

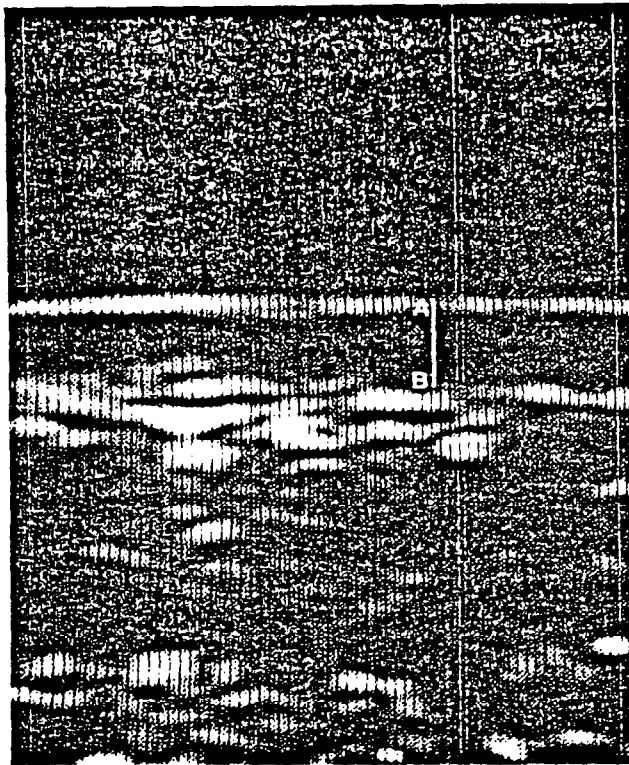


FIGURE 1. The typical B scan pattern (the double line pattern) of a normal class A arterial wall. The A to B line represents the distance between the inner and the outer echogenic lines and corresponds to the B mode image of intimal + medial thickness.

showing homogenous thickness was selected, and a distance of 10 mm was delimited with two metallic pins. This procedure was undertaken to avoid the error that might result from making measurements with the three methods at slightly different points. (2) B mode and gross pathologic evaluations were carried out in the middle of the segment under study, which was identified by the metallic pins. (3) Histologic measurements were obtained in the middle of longitudinal sections identified by the holes left by the pins.

The overall error in the identification of the site at which the different measurements (B mode, histologic, and gross pathologic) were made was estimated to be ± 0.5 mm. For all the aortic specimens showing a characteristic B scan pattern (45 class A and 49 class B), the absolute and percent differences between results of B mode and gross pathologic evaluations of intimal + medial thickness were determined.

Intimal + medial thickness values obtained *in vitro* in common carotid arteries with B mode imaging were compared with those determined *in vivo* in common carotid arteries of young living subjects.

Statistical analysis of the experimental data. The data are expressed as the mean \pm SD. Statistical analysis was carried out by paired two-tailed *t* test. Correlation coefficients were calculated by plotting the values obtained with B mode imaging against those obtained by pathologic techniques.

Results

Gross pathologic and histologic evaluations of aortic specimens and common carotid arteries. One hundred sixteen aortic segments were studied. Fifty of the 116

segments (43%) were grouped in class A (macroscopically normal or with fatty streaks), whereas 66 (57%) were grouped in class B (aortic segments with atherosclerotic lesions). Histologic evaluations of these segments showed that intimal thickness of class A and class B arteries was 0.25 ± 0.12 and 1.11 ± 0.27 mm, respectively, whereas intimal + medial thickness was 1.03 ± 0.27 and 1.72 ± 0.71 mm, respectively. Results of gross pathologic evaluations were comparable (class A intimal + medial thickness 1.13 ± 0.26 mm and class B 1.93 ± 0.84 mm). The mean intimal + medial thickness measured by histologic examination of common carotid arteries *in vitro* ($n = 44$) was 0.48 ± 0.06 mm. The gross pathologic evaluation resulted in comparable data (0.50 ± 0.06 mm).

The typical B mode image of the arterial wall and its prevalence in class A and class B aortic specimens. In all the class A and in 85% of class B aortic specimens a similar B scan pattern was found. This pattern was characterized by two parallel echogenic lines separated by an hypoechoic or anechoic space (figure 1). This B scan pattern was defined as the "double line pattern." The inner (luminal) line was generally more regular, smooth, and thin than the outer one. In 20% class B

PIGNOLI *et al.*

aortic segments (12 of 61) the double line pattern was absent, whereas it was present but more complex in 9% and in 31% of class A and B aortic segments, respectively. The characteristic double line pattern was found in the far wall of all the common carotid arteries evaluated *in vitro* (figure 2).

Identification of the structures generating the double line pattern. Five class B aortic specimens were prepared to identify the structures generating the inner echogenic line of the double line pattern. A small portion of the arterial wall was excised from the luminal side. The excision was found, by light microscopy, to be confined within this tunica. In these specimens the intimal/medial transition and the more peripheral layers were unchanged (figure 3). The B scan image generated by the five dissected arteries showed the disappearance of the inner line at the level of the inlay. This finding demonstrates that the inner line is generated by the intimal surface. In all of the five class A arteries the adventitia was completely removed from the media as confirmed by histologic examination (figure 4). The B scan image of each of these specimens showed the disappearance of the outer line in the region without adventitia, indicating that this line was generated by the adventitia.

To determine the anatomic structures delimited by the inner and the outer lines of the double line pattern, the distance between these two lines was measured

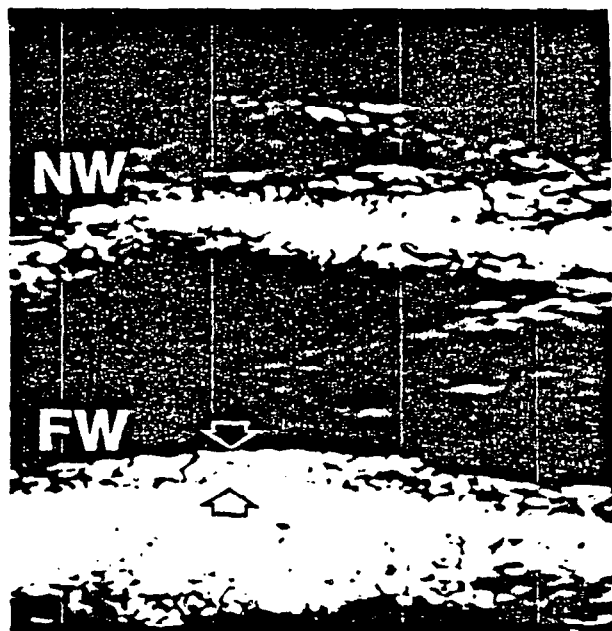


FIGURE 2. B mode image of a water pressure-perfused normal longitudinally scanned human common carotid artery *in vitro*. NW = near wall; FW = far wall. The double line pattern within black and white arrows is visible only on the FW.

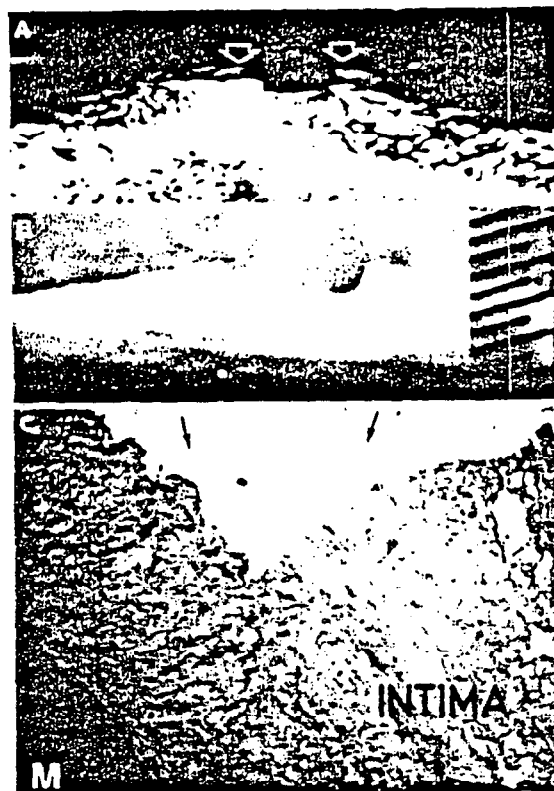


FIGURE 3. B mode image of a class B arterial wall with an inlay of dissected intima. Space between long bars in panel B is equal to 1 mm. The magnification of panels B and C is twice and 20-fold, respectively, that of A. M = media. Arrows are pointed opposite the bottom of the inlay.

with the use of B mode imaging. Values for intimal + medial thickness determined by B mode imaging were correlated with histologic and gross pathologic thickness values for the different tunicae. The B mode measurements of intimal + medial thickness showed a significant correlation with values obtained by gross pathology and by histology in both class A and class B aortic samples (figure 5). In contrast, B mode intimal + medial thickness values appeared to correlate less well with the values for other components of the vessel wall, alone or in combination (intima + media + adventitia and adventitia alone as measured by gross pathology and intima and media measured by histology; figure 6).

It should also be noted that evaluations of intimal + medial thickness by B mode imaging and gross pathologic examination did not significantly differ in either class A or class B aortic samples (class A: B mode intimal + medial thickness, 1.22 ± 0.37 vs 1.13 ± 0.26 by gross pathology, NS; class B: B mode, 2.06 ± 1.02 vs 1.93 ± 0.84 by gross pathology, NS).

Accuracy of B mode measurements. To determine the

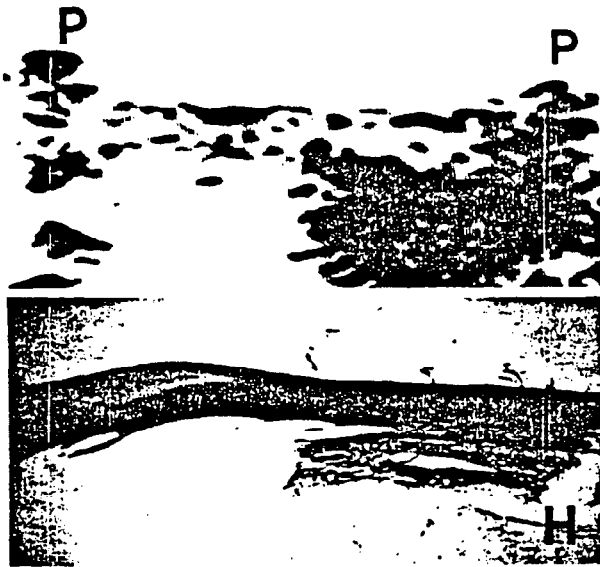


FIGURE 4. B mode image (top) and histologic section (bottom) of a class A arterial wall with a region without adventitia (wa). Magnification in both images ($\times 10$). P = pin; H = hole.

absolute and percent error in B mode measurements of aortic tissue specimens in vitro vs an accepted reference standard (results of gross pathologic examination), the absolute and percent differences between intimal + medial thickness values obtained by the two methods were evaluated. The absolute difference between B mode and gross pathologic findings was 0.19 ± 0.23 mm and the percent difference was $11.5 \pm 10.4\%$ for the whole group of aortic specimens ($n = 94$).

The accuracy of the determinations in class A samples was significantly different from the accuracy in class B samples (absolute error 0.12 ± 0.09 and 0.25 ± 0.30 mm for class A and B samples, respectively, $p < .001$), whereas percent error ($10.9 \pm 7.7\%$ and $11.9 \pm 11.4\%$ for class A and B, respectively) was similar.

In addition, the absolute and the percent differences were significantly lower when the ultrasound images were typical as opposed to complex (absolute error 0.12 ± 0.09 and 0.47 ± 0.38 mm for typical and complex ultrasound images, respectively; percent error $8.8 \pm 5.7\%$ and $22.1 \pm 16.0\%$ for typical and complex ultrasound images, respectively).

Common carotid intimal + medial thickness: comparison between measurements in vitro in situ and those in vivo. The mean intimal + medial thickness in common carotid arteries ($n = 44$) as evaluated in vitro by B mode imaging was 0.52 ± 0.08 . This value did not differ significantly from those found on histologic and pathologic examinations.

To assess whether intimal + medial thickness measured in vitro in arterial specimens was similar to that in situ, experiments were carried out during autopsy on carotid arteries that had been cannulated and flushed with saline. For this purpose common carotid arteries were cannulated with an inflatable balloon catheter, and the position of the balloon was verified on the monitor of the instrument. The catheter was kept in the same position during all the experiments, working as a position marker. A clip was placed on the anterior wall of the artery, just over the balloon, to allow the correct identification of the scanning plane after the excision of the artery.

Measurements of intima + media in situ obtained with intact superficial tissues yielded values not significantly different from those obtained in exposed carotid arteries (1.11 ± 0.14 and 1.08 ± 0.19 mm for in situ and exposed arteries, respectively, $n = 3$; absolute error $5.25 \pm 1.65\%$). Thickness data obtained in vitro in pressure-fixed vessels on the arterial segment identified by the balloon and the clip were 10% lower than those obtained in situ or in the exposed arteries (0.99 ± 0.29 mm, $n = 3$). This difference could be attributable to an effect of fixation.

B mode experiments to evaluate intimal + medial thickness of common carotid arteries in 10 living subjects showed that the double line pattern was present at the far wall of all the common carotid arteries considered ($n = 20$). B mode intimal + medial thickness measured in vivo was 0.53 ± 0.05 mm ($n = 20$). No significant difference was found between the mean values in common carotid arteries evaluated in vitro and in vivo by B mode imaging.

Discussion

Our investigations show that a characteristic B mode image is consistently generated in vitro at the far wall level by most arterial walls (100% of class A and 85% of class B arteries).

It is relevant to note that, most likely due to the different order in which the interfaces of the intima/lumen and media/adventitia are exposed to the incoming ultrasound beam, the B mode images of the near (more superficial) and far (deeper) walls are different. Our experiments were performed only on far walls because they could be more constantly and repeatably visualized, and therefore our conclusions can be applied only to far walls.

The characteristic B scan pattern of class A arterial walls shows two parallel echogenic lines separated by a relatively hypoechoic space (the double line pattern) (figure 1). A similar acoustic behavior of the arterial

PIGNOLI *et al.*

wall has been previously reported *in vitro*^{9, 12-20} and *in vivo*^{21, 22} in normal and diseased human carotid arteries. In experiments in which a dissection confined to the intima was produced in class B aortic specimens the luminal intimal transition was profoundly modified, but the intimal medial transition remained unmodified (figure 2). The inner line change found on the B mode image must be caused by an alteration in the generating structure: this line can thus be identified as the luminal/intimal transition. These experiments were performed only in class B arteries, since the intimal thickness of class A specimens did not allow a careful dissection. On the other hand, the removal of the adventitia from the media resulted in the disappearance of the outer line, indicating that the adventitia was responsible for the echoes representing this line.

Since the time-gain compensation setting of the in-

strument may influence the appearance of the hypo-echoic space between the two lines, the double line pattern of each arterial specimen was evaluated over a large range of time-gain compensation settings. In our experience, however, the typical double line pattern was easily recognizable in the same class A arterial specimens over a large range of time-gain settings. Thus, a time-gain compensation in the usual range does not appreciably influence the distance between the two echogenic lines.

In class B arteries, however, even with optimal adjustment of the time-gain compensation setting, high-amplitude echoes were frequently present between the inner and outer lines. In 12 of 61 arterial specimens (19.7%) these echoes, sometimes followed by acoustic shadows, did not allow the identification of the typical double line pattern.

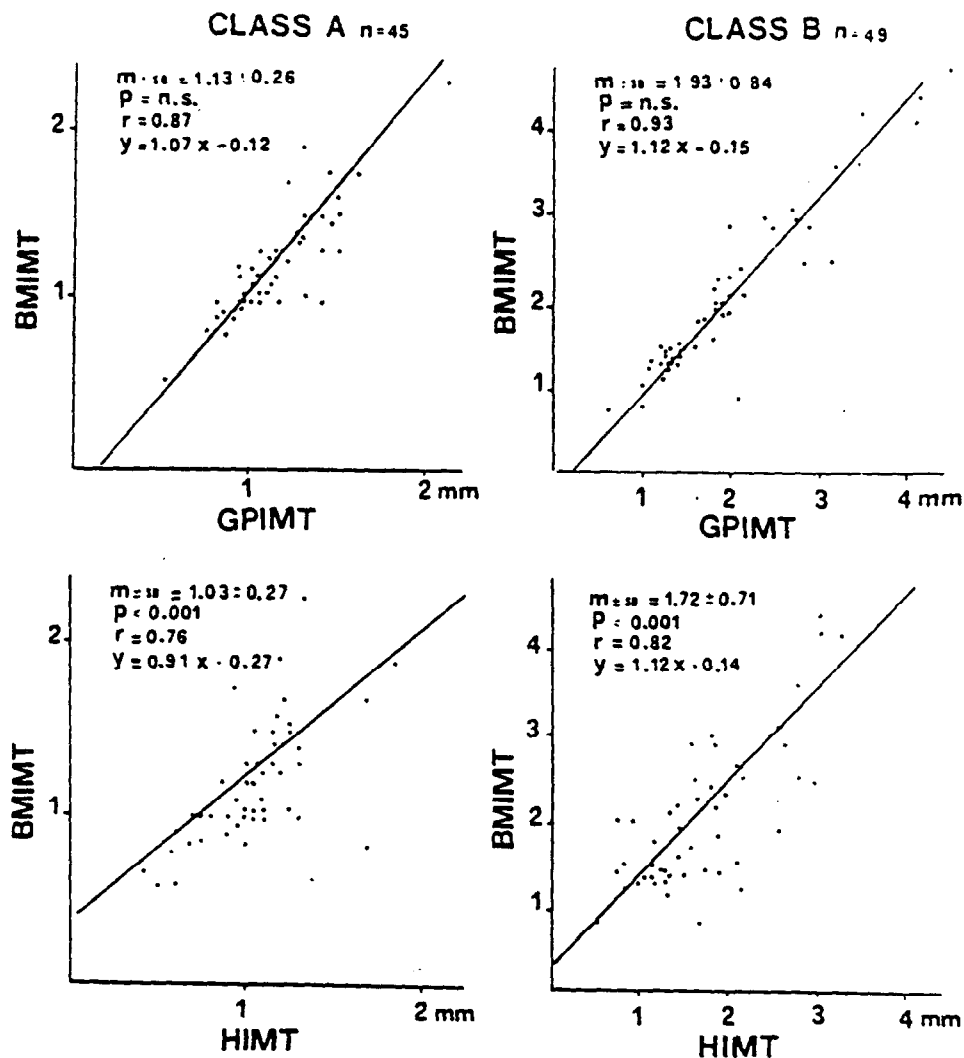


FIGURE 5. Correlation of intimal + medial thickness measured with B mode imaging (BMIMT) and that evaluated by histology (HIMT) in class A and B arterial specimens. The correlation coefficients and the regression lines are shown. GPIMT = intimal + medial thickness measured by gross pathology.

LABORATORY INVESTIGATION-ATHEROSCLEROSIS

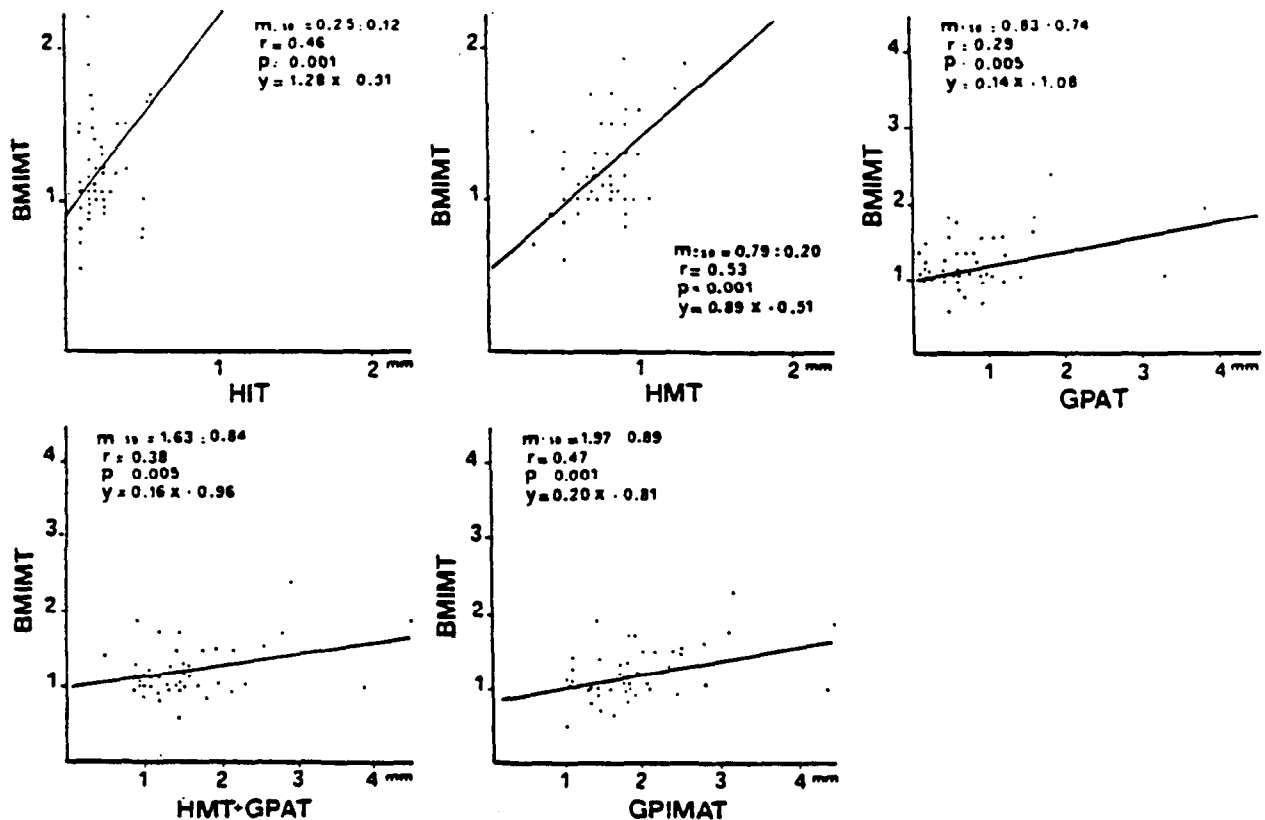


FIGURE 6. Correlation of B mode intimal + medial thickness (BMIMT) with intimal thickness (HIT) and medial thickness (HMT) measured by histology and with intimal + medial + adventitial (GPIMAT) and adventitial thickness (GPAT) measured by gross pathology. The combination of medial thickness measured by histology and adventitial thickness evaluated by gross pathology (HMT + GPAT) is also correlated with B mode intimal + medial thickness. All these measurements were carried out in class A aortic specimens. The correlation coefficients and the regression lines are shown.

In class A and B aortic specimens a good correlation between gross pathologic and histologic intimal + medial thickness ($r = .77$) was found. In addition, these data were very similar to those obtained by B mode imaging. The difference between intimal + medial thickness measured by B mode imaging and gross pathology was not statistically significant, indicating that B mode measurements represent the distance between the luminal surface and the inner part of the adventitia. This distance represents the intimal + medial thickness (figure 1). In contrast, the difference between B mode intimal + medial thickness and that measured by histology in class A and B specimens was highly significant ($p < .001$). This discrepancy was due to artifacts introduced during procession of tissue for histologic evaluation.^{2, 21}

The B mode image pattern may be complicated by the presence of additional echoes between the two echogenic lines and/or by a fuzzy appearance or discontinuities in the outer line. The B mode image was complex in 15 of 61 class B (25%) and in four of 45 class A (9%) specimens and these arterial wall mea-

surements were less accurate. The absolute and percent errors in B mode measurements, as compared with gross pathologic findings, in class A and B arteries with a complex ultrasound image were significantly different from those for arterial specimens with a typical ultrasound picture.

Therefore, evaluation of intimal + medial thickness can be carried out more precisely in the early stages of atherosclerotic disease, when other available methods (Doppler ultrasound and contrast angiography) cannot be used. All the normal young subjects studied in vivo and most of the patients with angiographically and surgically proven atherosclerotic lesions had the characteristic double line pattern at the level of the common carotid artery. The results of experiments in situ indicate that the presence of superficial tissues does not influence the B mode image of the arterial wall or the thickness of the intima + media. In addition, B mode measurements of intimal + medial thickness of common carotid arteries obtained in vivo were almost identical to those obtained in vitro with both B mode imaging and histologic techniques. We may therefore

conclude that the results *in vitro* reported in this study can be extended to conditions *in vivo*.

The present study demonstrates that: (1) a characteristic B mode image (the double line pattern) is consistently generated *in vitro* by the far walls of most of the arteries, (2) the distance between the transducer-facing edges of the inner and outer lines of the B mode image correlates with and does not differ significantly from the intimal + medial thickness, (3) regarding the accuracy of B mode imaging, a percent error of less than 20% has been found in 77% of the arterial specimens of both classes (normal and pathologic), and (4) the accuracy of B mode imaging depends on the presence of a typical B scan image. In 85% of class B arterial specimens a characteristic B mode image was found and in 59% of specimens of the same class the image was typical and easy to interpret.

We conclude that B mode imaging represents a useful tool for the detection and monitoring of changes in intimal + medial thickness, allowing the evaluation of changes in the arterial wall in areas without localized plaques. At the present time, it is difficult to determine whether this information will be of clinical relevance. It is possible that early changes in vascular thickness will later result in atheroma; they could on the other hand evolve only in a diffuse intimal thickening and have no hemodynamic relevance. It is also not known whether a relationship exists between the morphologic changes in the vessel wall detected by our method (thickening) and local damage to the endothelial layer, which can induce alterations of potential clinical relevance. The noninvasive nature of this new approach is a recommendation for its use in the pre-clinical diagnosis and follow-up of patients with atherosclerosis.^{24, 25}

We thank Prof. C. R. Sirtori for helpful discussion and criticism in preparing the manuscript. Prof. Romeo Pozzato, Chairman and Professor of Forensic Medicine, University of Milan, Milan, and Prof. T. Longo, Professor of Surgery, University of Milan, Milan, are also acknowledged.

References

- Bond MG, Adams MR, Bullock BC: Complicating factors in evaluating coronary artery atherosclerosis. *Artery* 9: 21, 1981
- Zarins K, Zatina MA, Glagov S: Correlation of postmortem angiography with pathologic anatomy: quantitation of atherosclerotic lesions. In Bond MG, Insull W, Glagov S, Chandler AB, Cornhill JF, editors: *Clinical diagnosis of atherosclerosis*. New York, 1983, Springer Verlag, p 283
- Roberts WC: The coronary arteries in coronary heart disease: morphologic observations. *Pathobiol Annu* 5: 249, 1975
- Wissler RW: Principles of the pathogenesis of atherosclerosis. In Braunwald E, editor: *Heart disease: a textbook of cardiovascular medicine*. Philadelphia, 1984, Saunders, p 1183
- Stegall HG: Ultrasonic measurements of organ dimensions. In Reneman RS, editor: *Cardiovascular applications of ultrasound*. Amsterdam, 1974, North Holland Publishing Co., page 150
- Ohkawai H, Nitta SI, Tanaka M, Dunn F: *In vivo* measurement of thickness or of speed of sound in biological tissue structures. *IEEE Trans Sonic Ultrasonic SU-30*: 231, 1983
- Insull W Jr: Universal reference standards for measuring atherosclerosis lesions. The quest for the "gold standard." In Bond MG, Insull W, Glagov S, Chandler AB, Cornhill JF, editors: *Clinical diagnosis of atherosclerosis. Quantitative methods of evaluation*. New York, 1983, Springer Verlag, p 283
- Berson AS: Ultrasound B scan assessment program. *Atherosclerosis Rev* 10: 169, 1983
- Pignoli P: Ultrasound B-mode imaging for arterial wall thickness measurement. *Atherosclerosis Rev* 12: 177, 1984
- Sheenan DC, Hrapchak BB: Theory and practice of histotechnology. St. Louis, 1980, The CV Mosby Co, p 206
- Biodynamics Inc: *Biosound instructions manual*. Indianapolis, 1981
- Murakami R: Analytical and experimental determination of acoustic reflecting characteristics of normal aortic walls, thesis. University of Washington, Seattle, 1973
- Beretsky I: Detection and characterization of atherosclerosis in a human arterial wall by raylographic technique, an *in vitro* study. In White D, Brown R, editors: *Ultrasound in medicine*. New York, 1977, Plenum Press, vol 3B, p 1597
- Barber FE: Scattering from arterial tissues by ultrasonic microprobe. In White D, Brown R, editors: *Ultrasound in medicine*. New York, 1977, Plenum Press, vol 3B, p 1979
- Greenleaf JF, Duck FA, Samyoo WF, Johnson SA: Ultrasonic data acquisition and processing system for atherosclerotic tissue characterization. 1974 Ultrasonics Symposium Proceedings. IEEE Catalog No. 74CH0896-ISU, 1974
- Hartley DJ, Strandness DE Jr: The effects of atherosclerosis on the transmission of ultrasound. *J Surg Res* 9: 575, 1969
- Rooney JA, Gammel PM, Hestenes JD, Chin HP, Blankenhorn DH: The use of ultrasonic spectroscopy to characterize calcified lesions. *IEEE Trans Sonics Ultrasonics SU-28*: 291, 1981
- Rooney JA, Gammel PM, Hestenes JD, Chin HP, Blankenhorn DH: Velocity and attenuation of sound in arterial tissue. *J Acoust Soc Am* 71: 462, 1982
- Geleskie JV, Shung KK: Further studies on acoustic impedance of major bovine blood vessel walls. *J Acoust Soc Am* 71: 467, 1982
- Wolverson M, Bashiti H, Sundaram M, Heiberg E, Grider R: Ultrasonic tissue characterization of atheromatous plaques using a high resolution real time scanner. Presented at the 25th Scientific Session, American Institute of Ultrasound in Medicine, New Orleans, Sept. 15-19, 1980
- Zwiebel WJ: High resolution B mode and Duplex carotid sonography. In Zeiwbel WJ, editor: *Introduction to vascular ultrasonography*. New York, 1982, Grune & Stratton, p 103
- James EM, Earnest IV G, Forbes DF, Houser OW, Folger WN: High resolution dynamic ultrasound imaging of the carotid bifurcation: a prospective evaluation. *Radiology* 144: 853, 1982
- Bahr GF, Bloom G, Friberg U: Volume changes of tissues in physiological fluids during fixation in osmium tetroxide or formaldehyde and during subsequent treatment. *Exp Cell Res* 12: 342, 1957
- Bond MG, Riley WA, Barnes RW, Kaduck JM, Ball MR: Validation studies of a noninvasive real time B scan imaging system. In Berson AS, Budinger IF, Ringquist I, Mock MB, Watson JT, Powel RS, editors: *Noninvasive techniques for assessment of atherosclerosis in peripheral, carotid and coronary arteries*. New York, 1982, Raven Press, p 197
- Arteriosclerosis 1981, Report of the Working Group on arteriosclerosis of the National Heart, Lung and Blood Institute. U.S. Department of Health and Human Services, NIH Publication No. 81-2034, July 1981, p 27